Numerical modeling of continental collision and intraplate deformation.

Application to the Cenozoic geodynamic evolution of North Iberia

Ángel Valverde Pérez

- Ph.D. Thesis -

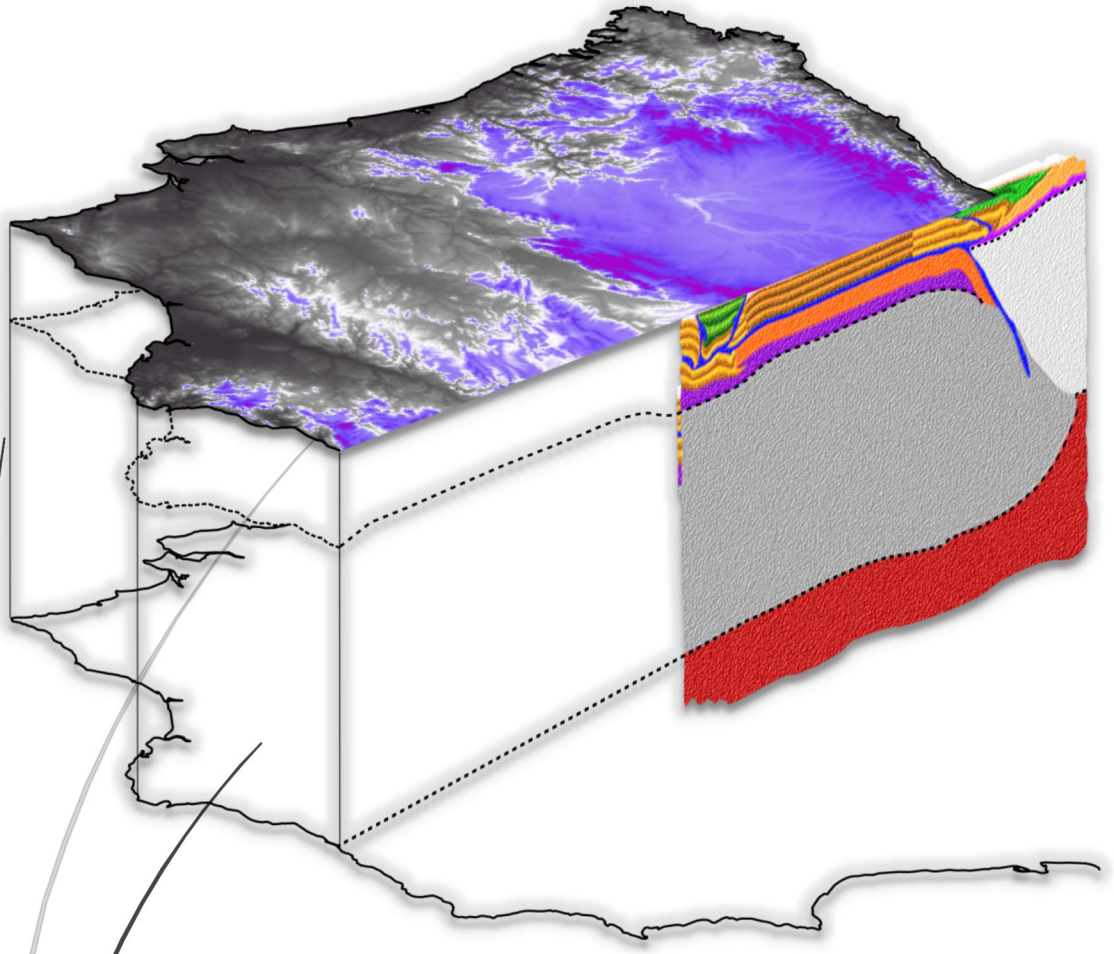

Barcelona, 2020

CSIC
Consejo Superior de Investigaciones Científicas
GEO3BCN
Geosciences Barcelona - CSIC
Universitat de Barcelona

Departament de Dinàmica de la Terra i de l'Oceà
Facultat de Ciènces de la Terra
Universitat de Barcelona

Numerical modeling of continental collision and intraplate deformation. Application to the Cenozoic geodynamic evolution of North Iberia.

Tesis doctoral presentada por Ángel Valverde Pérez al Departament de Dinàmica de la Terra i de l'Oceà de la Universitat de Barcelona para optar al grado de Doctor en Ciencias de la Tierra

Group of Dynamics of the Lithosphere (GDL)
Geociències Barcelona(Geo3BCN)
Consejo Superior de Investigaciones Científicas (CSIC)

Directores:

Dr. Daniel García-Castellanos Dra. Ivone Jiménez-Munt

Tutora:

Dra. Anna Martí Castells

Barcelona, 2020

“Más fácil es cruzar el vasto desierto, descansando durante el camino en los oasis”

Index

Acknowledgments

Corría el año 2015 cuando un joven yo, recién terminado el Master de Meteorología y Geofísica en la Universidad Complutense de Madrid, se le presentó la oportunidad de hacer un doctorado en modelización numérica en Barcelona. Primero me gustaría agradecer por ese empujoncito de mis tutoras de Master: Dra. Ana Negredo y Dra. María Charco por animarme a continuar en la investigación científica.

Y me dije, ¿y porqué no? Porqué no ir a un instituto de investigación puntero en ciencias de la tierra de la ciudad condal, el antiguo instituto Jaume Almera (ICTJA) y ahora Geoscience Barcelona (GEO3BCN), donde aprendería a desarrollarme como científico, a utilizar y desarrollar herramientas avanzadas de programación, a investigar misterios no resueltos por la ciencia, comprender textos científicos y que me brindaría la oportunidad de participar en congresos internacionales. Por todo lo aprendido estos años, y la guía que han sido, mención especial a mis directores de tesis doctoral el Dr. Daniel García-Castellanos y la Dra. Ivone Jiménez-Munt. Gracias por vuestros consejos, la presión que me hizo avanzar hasta el día de hoy, la dedicación y vuestro tiempo. También quiero agradecer a mis tutores el Dr. Joan Manuel Vilaplana (ya retirado) y la Dra. Anna Martí Castells por su apoyo desde la Universidad de Barcelona y por hacer el seguimiento de esta tesis. Quiero destacar también la ayuda imprescindible de la gente del BSC (Barcelona Supercomputer Center) por prestarme uno de los equipos informáticos más potentes y avanzados de Europa.

Así que, en el invierno de 2015 dejo atrás la seguridad que siempre ofrecen unos padres preocupados. A los que tengo que agradecer que siguieran pendientes, que me han apoyado tanto, por sus toques de atención, por esos tuppers de mamá (mamá te quiero, me salvaron la vida), por las ayudas de mi padre con los problemas, por las charlas. A vosotros y más que a nadie os dedico esta tesis, a doña Victoria Pérez Gómez y don Ángel Valverde Dueñas, mis grandes mentores de la vida, espero que esteis orgullosos de donde hemos llegado, después de tantas cosas que hemos vivido. También al resto de mi familia, que me siguen apoyando con sus palabras y mensajes, os quiero.

Y dicen que la familia no se elige, pero los amigos son la familia que sí se puede escoger. No dejé muchos amigos atrás en Madrid, pero los que tenía perduraron, lo cual es de agradecer sabiendo que les veía menos. Aunque sus bromas y mensajes de ánimo los he tenido presente. Mencionar primero a Alberto Jiménez, gracias siempre, por venirte a informática conmigo en el colegio y ayudarme a sentirme más fuerte cada día, a Roberto Domínguez, por todas las charlas, los buenos ratos, las risas y consejos, a Roxana Georgiana, por tu inquebrantable moralidad, lucha y determinación ante todo, que me ha servido de inspiración. También quiero destacar a una fuente de inspiración especial desde la carrera universitaria, corría 2008, que habría hecho yo sin ti, Dra. Pilar Sánchez Sánchez-Pastor, o como yo la llamo Piluky normal con K, que me esforzaba por seguirte el ritmo y terminamos

acabando en el mismo instituto de investigación en Barcelona. Por tantos momentos, viajes, fiestas y sonrisas, por estar ahí en lo bueno y también en lo malo, por hacerme reír y aguantar mis quebraderos, por tantas cosas, un millón de gracias.

Y ya en Barcelona, tierra extraña para mi, no solo tengo que agradecer a mis directores y tutores, sería irrespetuoso no dar las gracias al equipo de GDL (Group of Dynamics of the Lithosphere) que me acogieron como a uno más. Al Dr. Manel Fernàndez por sus consejos sobre algunos aspectos geodinámicos de la península Ibérica , y su buen humor. Al Dr. Jaume Vergés también por su tiempo y ayuda en el estudio de los Pirineos y sus generosas bromas que con gusto recibía. A Marc, por salvarme la vida con las librerías de los innumerables programas que había que instalar. A mi compañero Ajay Kumar, cuyo espíritu y alegría era contagioso. A Mari, por compartir penas y risas, a la a mencionada Pilar con su ayuda y apoyo he podido sobrevivir. Y otras personas del instituto y alrededores que me alegraban los días con sus sonrisas: Xavi en la entrada y a toda esa gente maravillosa de la cafetería de en frente del instituto. Y de esta nueva familia quiero mencionar a tres grandes personas cuya experiencia, sabiduría, y amistad son un tesoro casi mayor que esta tesis:

La Dra. Encarnación Montoya (Encarni, que raro se me hace llamarte de otra forma) que ha sido una salvación, un aire fresco murciano (y sus amigos también) en la ciudad condal, una mujer que admiro y que deseo seguir compartiendo cafés, cervezas, abrazos y charlas, además me debe un baile. El Dr. Jonas B. Ruh, un hombre peculiar, suizo estrambótico, con el que he aprendido científicamente y de la vida (backgammon y petanca sobre todo), también gracias por los momentos, las charlas y deseo que la amistad dure por muchos años.

A la que considero ya como mi hermana mayor, esa que nunca he tenido, que me acogió en su pequeño despacho de la tercera planta, y hemos luchado siempre juntos por un despacho mejor. Por esa chispa que tienes, esa dedicación, desde Antibes en 2015, pasando por Roma, los momentos en Casteldefels y todos los ratos en el despacho. Por todas las frases o perlas que hemos ido soltando a lo largo de estos años, mi primera compañera de salsa y bachata, por las charlas de ciencias, las opiniones encontradas, por tu apoyo siempre. Por ser la mejor "compitrueno" de despacho que uno pueda desear en un doctorado, y que nunca perdamos el contacto. Te lo agradeceré infinitamente Dra. Mireia Peral.

Por último y no menos importante, el programa que he estado usando durante la tesis fue desarrollado en Melbourne, Australia. Allí pasé los tres mejores meses de mi doctorado. Y tengo que agradecer a los doctores Louis Moresi y Rebecca Farrington por acogerme en su equipo y enseñarme durante mi estancia. A todo el equipo que hay detrás de este proyecto llamado Underworld. A mi amiga Roberta Carluccio que gracias a ella mi estancia en Melbourne fue más divertida. Y también agradezco los consejos aportados por el Dr. David Pedreira de la universidad de Oviedo y al Dr. Ernst Willingshofer de la universidad de Utrecht, sin sus consejos mi tesis habría tenido peor calidad sin duda

Funding

This thesis is part of the project MITE (CGL2014-59516) financed by the CSIC. I also thank to the projects AECT-2017-1-0018, AECT-2017-2-00013, AECT-2017-3-0008, AECT-2018-1-0007, AECT-2018-3-0007, AECT-2019-1-0013 and AECT-2019-2-0005 for allowing me to use the computational resources from the RES (Red Española de Supercompatución) and specially to the Barcelona Supercomputing Center (BSC - CNS). This thesis was part of the national founding from the Ministry of Economy and competitiveness: Programa Estatal de promoción de Talento y su Competitividad I+D+i, ayudas para contratos predoctorales para la formación de doctores 2015 (BES - 2015 - 073348).

Notation & Symbols

σ	Tensor de Stress
$T^{(n)}$	Tensor traction and (n)
is	the directional vector
P	Total pressure
P_{li}	Lithostatic pressure
δ_{ij}	Kronecker's delta function
$(II_{\sigma_{ij}})$	Second invariant of deviatoric stress
τ, σ_e	Effective shear stress
ε_{ij}	Cauchy's infinitesimal strain tensor
$\dot{\varepsilon}_{ij}$	Strain Rate tensor
ε_{II}	Second invariant of the strain rate tensor
η	Viscosity
T	Temperature
A_D	Pre-exponential factor
E	Activation Energy
V	Activation Volume
n	Creep exponent or power-law exponent
R	Gas constant
η_{yield}	Nonlinear effective viscosity
τ_y	Yield stress
C_0	Cohesion of materials at confining pressure
μ_f	Frictional coefficient
Z	Depth
ρ	Density
g_i	gravity or i component of gravity
κ	thermal diffusivity
k	thermal conductivity
C_p	Specific heat
H	Heat productions
α	Thermal expansion
β	Thermal compressibility

Summary

This thesis aims at improving the current understanding of the geodynamic controls on tectonic deformation during plate collision, using the Cenozoic evolution of Iberia as a case scenario. Despite the vast efforts during the last decades, there is a limited understanding today about what plate properties control the propagation of tectonic deformation towards the interior of tectonic plates. Meanwhile, the classic enigmas about the timing and the processes involved in the construction of the Iberian topography also persist: What is the origin of the high average elevation of the Iberian Peninsula? What is the quantitative contribution to topography induced by the intraplate tectonics of Iberia? How was this intraplate deformation in the middle of the Iberian microplate triggered?

To answer these questions, I first gathered information about the tectonic events in Iberia during the Cenozoic from previous structural tectonic and geodynamic modelling publications. Continental collision with Eurasia in the north first gave rise to the uprising of the Pyrenean and Basque-Cantabrian chains. Deformation subsequently jumped southwards and formed the elevation of the interior mountain ranges. Meanwhile in the southern margin, the subduction of the Tethys oceanic lithosphere due to the Africa-Iberia convergence gave rise to the Betics and opened the Alborán Sea. The underlaying hypothesis of this thesis is that this succession can be reproduced via a geodynamic model giving the appropriate initial conditions that are in reasonable agreement with the geological setting during the early-Cenozoic Iberia.

To this purpose, we carried out a series of high-resolution mechanical and thermomechanical numerical models with a state-of-the-art code named UNDERWORLD 2.0 (still under development at Univ. Melbourne). We first review fundamental ideas such as the patterns of deformation of the lithosphere predicted for converging continental margins, as well as the elevation of mountain ranges in a continental collision scenario. Then we investigate how the crustal deformation accommodates far from the continental margins, taking into account the

mathematical equations and physical laws that govern the thermal field and rock deformation.

Based on these, a series of mechanical numerical models are developed to explore the possible evolutionary scenarios after a continental collision. Two deformation end member models appear: **double-vergence** and **crustal folding**. While in the first one deformation concentrates near the axial collision zone where the orogen develops, in the second, deformation is transmitted farther from the initial contact between lithospheres. We compare these results with patterns of deformation seen in the Pyrenean mountain range as well as other natural scenarios where cortical folding occurs near a thrust failure like in the Zagros Chain in Iran.

This thesis then focuses on a series of high-resolution 2D numerical models for the North-Central area of the Peninsula. These models aim at linking the Cenozoic evolution of the Cantabrian chain to that of the Central System and the Duero basin. Here, deformation and failure consider creep-like behavior and plasticity in a viscoplastic rheology. We test the hypothesis of the presence of a detachment level within the Variscan basement, at the lower crust, of limited srength and thus capable of transmitting deformation towards the interior, potentially leading to the rise of the Central System. An alternative tested hypothesis is that the entire lithosphere folded in response to the convergence between Iberia and Eurasia.

Finally, we extend these 2D numerical models to the southern margin of Iberia to investigate how the approximation of Africa may have affected the distribution and timing of shortening in the different domains of the microplate, with particular emphasis on the topography and deformation of the Central System and adjacent basins.

Resumen

La presente tesis doctoral aborda el estudio de la evolución geodinámica de sistemas de colisión continental, usando como escenario de referencia la microplaca de Iberia durante el Cenozoico (últimos 65 millones de años). Pese al enorme esfuerzo acumulado por la comunidad geológica en este ámbito, los enigmas clásicos sobre la cronología y los procesos involucrados en la construcción del relieve y el subsuelo ibéricos persisten: ¿Cuál es el origen de la elevada topografía media de la Península? ¿Cómo ha sido construida su actual topografía como resultado de la peculiar posición de la microplaca tectónica de Iberia entre África y Eurasia?

Para abordar estas preguntas, he recopilado información de estudios previos sobre episodios tectónicos desde el Cretácico Superior hasta la actualidad con especial atención a los intervalos relacionados con el choque continental con Eurasia que dio lugar al levantamiento de la cadena Pirenaica y Vasco-Cantábrica, la posterior elevación de las cadenas montañosas del interior y la posterior evolución del margen sur en relación con la aproximación entre África e Iberia.

Para encontrar los mecanismos responsables de esta evolución, he diseñado una serie de modelos numéricos de alta resolución que simulan en 2D la deformación de la litosfera en límites de placa convergentes, utilizando uno de los programarios más evolucionados de la geodinámica internacional (*Underworld* 2.0; Univ. Melbourne). Este volumen empieza por tanto explicando las ecuaciones matemáticas y leyes físicas que gobiernan el modelo numérico, las relaciones entre los parámetros físicos y su importancia y sus limitaciones.

Así, se han realizado una serie de modelos numéricos sintéticos en esta tesis para identificar los posibles escenarios evolutivos tras un choque continental donde aparecen dos modelos de deformación: **doble vergencia** y **plegamiento cortical**. Mientras que en el primero la deformación se concentra en torno a la zona de colisión donde se desarrolla un orógeno mediante fallas que buzan hacia la zona axial, en el segundo se transmite la deformación más lejos de la zona de

colisión. Estos modelos sintéticos explican algunos rasgos de la deformación de la Cordillera Pirenaica y de la cadena de montañas de Zagros en Irán.

Seguidamente, muestro otra serie de modelos numéricos termodinámicos 2D para la zona Norte-Centro de la Península. En este caso, los modelos tratan de explicar la evolución cenozoica de la cadena Cántabra junto con el Sistema Central y la cuenca del Duero en función de la viscoplasticidad adoptada para la roca. Se pone a prueba un hipotético nivel de despegue entre el basamento Varisco y la corteza superior que hubiera permitido transmitir esfuerzos hacia el interior formando el Sistema Central y la posibilidad de que toda la litosfera sufriera un plegamiento en respuesta a la compresión. Finalmente, estos modelos numéricos 2D se extienden hasta el sur Peninsular, examinando el papel de la frontera entre las litosferas Africana e Ibérica en la formación del Sistema Central y las cuencas adyacentes.

Chapter 1

Introduction

Deep processes of the Earth are studied by indirect methods, such as the study of seismic wave velocity, the magnetic record in the seafloor, or the interpretation of manifestations in the surface topography. An extremely valuable technique that has helped comprehending the mechanics of these unreachable internal phenomena of the dynamics of the Earth has been the use of analogue and numerical models. Sir James Hall did the first analog models in 1815 (Schellart, 2002) and over the decades, analog modeling underwent a breakthrough. Similarly, the boom of computing in the 80s and the standarisation of parallel computing in this century has led to the widespread application of numerical models to the field of geodynamics.

Geoscience without numerical modeling is nowadays unthinkable. To better understand the complexity of the Earth as a dynamic system, many concepts in geoscience and mathematics must be combined. Initial analog and analytical models were not enough to expand the knowledge beyond the first order behaviors of the Earth. To satisfy that necessity and gain a better understanding of the Earth's dynamics and evolution, major efforts have been done in numerical simulations, specially from the 1960s.

In parallel, during the last decades, computing technology has developed exponentially enabling a breakthrough in modeling techniques. The numerical

models themselves have improved in their methods for solving the equations or laws integrated into their code, minimizing the calculation time and increasing the efficiency of computer resources. This has allowed identifying the main processes and parameters of the physical-chemical equations governing the deformation of the lithosphere.

However, it is important to recall that numerical solutions applied to geodynamic problems are approximate solutions which inherent errors and limitations in spatial resolution. While models can be tested against the analytical solutions of the governing equations, they also must be stable, keeping errors minimized, and converging to a suitable solution. In other words, a model has to be accurate and reliable. The approximations are applied to small domains (numerical grids) so the numerical solution provides results at discrete locations in space and time. Enhancing the model spatial and time resolution can become a double-edged sword for the geodynamic modeler, increasing computation time and introducing numerical instabilities in areas of high contrast of a mechanical parameter.

Nevertheless, geodynamic computer modeling has permitted to investigate short time scales inquiries such as laboratory experiments with magma samples to study the **rheology** of the Earth's interior under high pressures and temperatures, to processes that take millions of years to evolve, such as the **plate kinematics** or the relief **erosion**. In the last decades, proliferation of numerical modeling techniques applied to geodynamics has allowed researchers to investigate and understand processes that cannot be experimentally assessed in a systematic way in situ, such as studying the whole structure of a volcano, plate dynamics, mantle processes, lithosphere subductions, etc.

Computer geodynamic models numerically resolve the equations associated to physical-mathematical models of mantle and lithospheric deformation. Because most geodynamic processes cannot be reproduced in their spatial and time scales in laboratory, computer simulations acquire a particular relevance in this discipline. Results from these models must be compared with data that are often sparse, both in space and time. Numerical models improve with time when we understand more about the causes that generate the processes to be solved, the events that trigger

it, the physical laws that govern it, or the best computer techniques and greater calculation capacity. The previously made interpretations by other studies should be integrated and updated when models become more sophisticated.

During the last decades, numerical models for understanding the geodynamic evolution of the Earth has led to new fields of studies. Bullard et al., in 1965, were the first authors to use rigorous computational methods for determining the relative positions of the continents around the Atlantic before **Pangea supercontinent** breakup (Late Triassic - Early Jurassic). Since then, great achievements have been made with numerical modeling over time. To cite some of them: In 1970 when Minear & Toksöz developed the first 2D numerical subduction model. The first attempt in 3D modelling of mantle convection was done in 1985 by Baumgardner. Beaumount et al. (1992) and Willet et al. (1993), started to replicate how an orogen evolve in a compressional scenario using mechanical models. Computer models have validated the link between the Earth's geodynamo to convection in the outer core (Glatzmaiers & Roberts, 1995). Over the last decades, there have been numerous studies trying to understand how orogens evolve and link to natural examples, incorporating more complex rheologies depending on strain weakening, pressure, and temperature, studyig as well, what parameter or parameters control the evolution of mountain ranges (e.g.; Willet, 1999; Beaumont et al., 2000; Pfiffner et al., 2000; Brun et al., 2002; Cloetingh et al., 2002; Capitanio & Goes, 2006; Gerya et al., 2009; Duretz et al., 2013; Jamieson & Beamount, 2013; Burov et al., 2014; Vogt et al., 2017).

This advance in numerical modeling over the years has allowed us to comprehend more and more how the Earth works not only on a global scale but also on a regional or local scale. As knowledge advances parallel with technology and derived resources, hence there are study areas explained by multiple theories over time. Such is the case for the evolution of the Iberian microplate. Still is an open problem in geoscience of what are the causes for the topography evolution of Iberia and the geodynamic and tectonic changes of it.

1.1 Background

The main geological scenario that will be used to compare the modeling results of this thesis is the Iberian microplate. The tectonic deformation of Iberia is the result of a complex motion of the Iberian microplate, relative to the Eurasia and Africa plates, that started in Late Cretaceous times. At this time, the Iberian microplate was characterized by a shallow marine environment with almost its western half part emerged above sea level, known as the Iberian Massif. The Iberian domain was caught amid the convergence between Africa and Eurasia plates since ca. 83.5 Ma (see reconstruction of Iberia at 70 Ma; Figure 1.1).

Numerous tectonic reconstructions of the Alpine-Mediterranean region have been proposed since Cretaceous times (Rosenbaum et al., 2002; Andeweg, 2002;

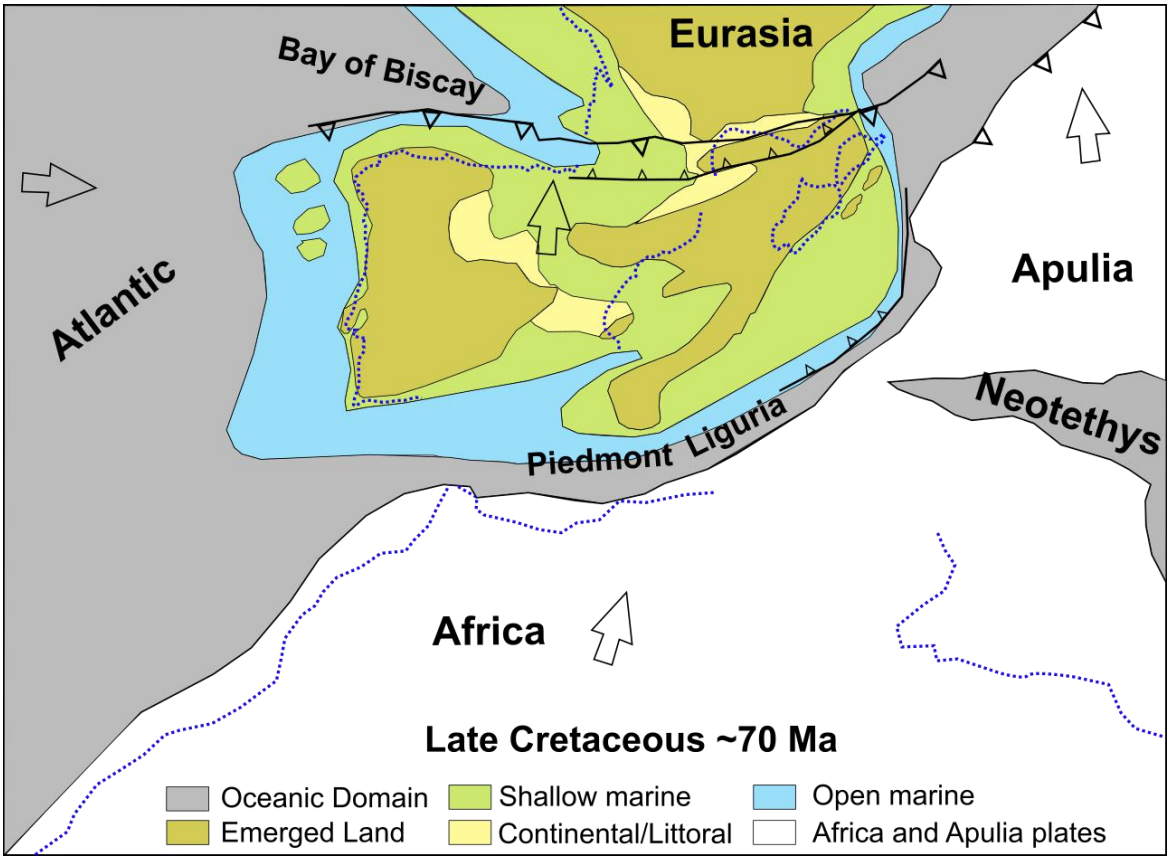

Figure 1.1. Combining the paleo-tectono-geological reconstruction for the Iberian microplate in the Late Cretaceous from Andeweg Thesis (2002) with paleogeographic reconstruction from Stampfli & Hochard (2009), accounting to the plate motions at ca. 70Ma. Blue dashed lines correspond to nowadays coastlines.

Schettino & Turco, 2011; Macchiaveli et al., 2017; van Hinsbergen et al., 2019). Rosenbaum et al. (2002a) reconstruct the North Atlantic and West Mediterranean domains by plate kinematics using ***PLATYPLUS*** software, i.e., relative motions between Iberia, Africa and Europe using previous published data and applying motion files by interpolating rotation parameters since 175 Ma until present. Andeweg described the evolution of the Iberian microplate in the last 65 My, and focusing in uplifting and filling of the sedimentary basins, taking into account the evolution of the sedimentary basins.

Schettino & Turco (2011) used magnetic anomalies from the ocean seafloor and on-land geologic evidence to generate the tectonic history of the western Tethys since Late Triassic. They focused in the eastward prolongation of the Pangea breakup combined with the subduction of the paleo-Tethys ocean. Similarly, Macchiavelli et al. (2017) employed a new analysis of the magnetic southern North Atlantic anomaly data, to constrain the kinematics of the Iberian plate during the last 83 My. A new study from van Hinsbergen et al. (2019) uses ***Gplates*** program but they are focused in the evolution of the Mediterranean region from 240 Ma until present (Figure 1.2).

The present crustal and upper mantle of the Iberian plate is the result of the relative movement of Iberia between Europe and Africa, and the accommodation of the deformation not only at the boundaries (e.g., Pyrenees, Betics), but also in the interior of Iberia (e.g., Iberian Ranges, Central System). The evolution of Iberia over the last 65 million years, the intraplate deformation and its relationship to the anomalous high average elevation of Iberia of around 660 m (Casas-Sainz & de Vicente, 2009) has sparked various theories for their possible explanation. Some researchers propose that tectonic deformation (Garcia-Castellanos et al., 2012) is sufficient to explain this elevation or a buoyancy respond high temperature/low-density layer in the sublithospheric mantle (Carballo et al., 2015). Different mechanisms have been proposed as responsible for the elevation formation of Iberia: 1) A relative uniform uplift of the Iberian craton (e.g., Vázquez & Hoehne, 1992); 2) Tilting of the entire plate towards the west during the Quaternary (e.g., Solé Sabarís, 1983); 3) Lithospheric folding, causing differential vertical motions

(e.g,, Cloetingh et al., 2002; de Vicente et al., 2007); 4) crustal shortening related to Africa-Eurasia convergence combined with lateral crustal density variation (Vergés & Fernàndez, 2006); and 5) thermal anomalies originated in the mantle that would uplift the whole Iberia in the last 30 million years (Conway-Jones et al., 2019).

The relative movements between the plates resulted in the subduction of the Iberian micro-continent below the Eurasian plate along the Pyrenees and the subduction under the African or Nubian plate during the Cenozoic (e.g., Vergés & Fernández, 2012; Platt et al., 2013; Casciello et al., 2015) (Figure 1.2). Most of the shortening has been accommodated in the northern and southern boundaries of the Iberian plate, however, it is still under debate the quantity, when and how long they lasted (Banks & Warburton, 1991; Muñoz, 1992; Stampfli et al., 2002; Rosenbaum, 2012a; Vergés & Fernàndez, 2012; Quintana et al., 2015; Macchiavelli et al., 2017). Based on plate kinematics reconstruction, Rosenbaum et al. (2002a) estimated the maximum convergence between the Iberian and Eurasian plate of about 200 km in the eastern part of the Pyrenean Chain over the last 83 My. Teixell (1998), using geological cross sections for crustal shortening along the Pyrenees gave different values; 100 km in the western part, 125 km in Central and 150 km in the east. To the west, the convergence raised the Cantabrian Mountain range, where most of the studies agree with the total shortening of around 80 and 100 km, although some discrepancies appear between the upper crust and the lower crust (Banks & Warburton, 1991; Gallastegui, 2000; Pedreira et al., 2015). In the south, based on crustal restoration of the Internal Betics, the convergence between Africa and Iberia is estimated around 300 km (Platt et al., 2003; Vergés & Fernàndez, 2006). The evolution of the Africa-Iberia boundary is more complex, with several stages of compression and extension, that makes complicated to specify the total shortening, reaching a total of up to 165 km (Banks and Warburton, 1991). Other authors proposed different shortening values for the south margin, for example, 145 km from Quintana et al. (2015) or between 122.5-260.5 km from Platt et al. (2003). All these shortening amounts must fit, in turn, with the geodynamic models for the evolution of the Western Mediterranean. Vergés and Fernàndez (2012)

propose a double subduction with the NW-dipping subduction in the Algerian margin segment and SE-dipping in the Betics margin segment of SE Iberia since latest Cretaceous times. During the subduction of this Tethys oceanic domain the Gibraltar arc started to form becoming caught between the converging Africa and Iberia after 8 Ma (e.g., Casciello et al., 2015).

Numerical modeling has contributed to roughly understand the general evolution of the Iberian microplate. Based on results from thermomechanical modeling of lithospheric deformation, Cloetingh et al. (2002) proposed that the tectonic deformation of Iberia was controlled by a folding-like response of the Iberian plate in response to horizontal stresses related to the Africa and Eurasia plate kinematics. Carballo et al. (2015) jointed modeling results of gravity, topography, geoid, heat flow and mantle seismic data and related the lithospheric and mean elevation to mantle composition and buoyancy induced by low-velocity/high temperature/low density layer in the sublithospheric mantle. Recently, Conway-Jones et al. (2019) also suggest that the high topography of Iberia is supported by a thermal anomaly of the upper mantle. But there are still several unknowns related to the geodynamic evolution of the Iberian microplate: a) How does the shortening propagate and distribute throughout the entire Iberian microplate? Where and when the Europe-Africa convergence accommodates? b) What mechanical properties control the intraplate Cenozoic deformation of Iberia? c) What is the structure and rheology of the crust and how inherited structures from past events influence on the deformation patterns? d) What is the origin of the high average altitude of the Iberian Peninsula relative the Eurasian continent? (Figure 1.3) Is it just the result of the Africa-Europe convergence, or a thermal mantle anomaly, or a combination of both?

A)

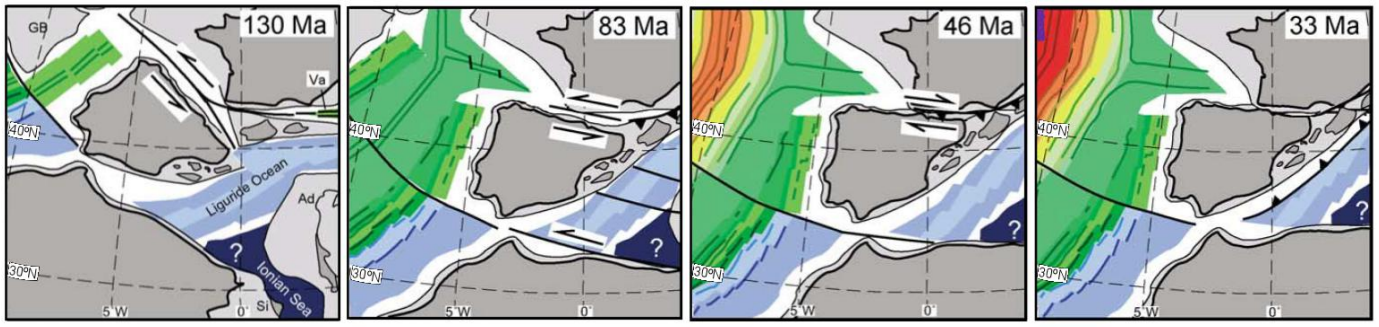
130 Ma
83 Ma
46 Ma
33 Ma
GB
Va
Ad
Liguride Ocean
Ionian Sea
40°N
30°N
5°W
0°

B)

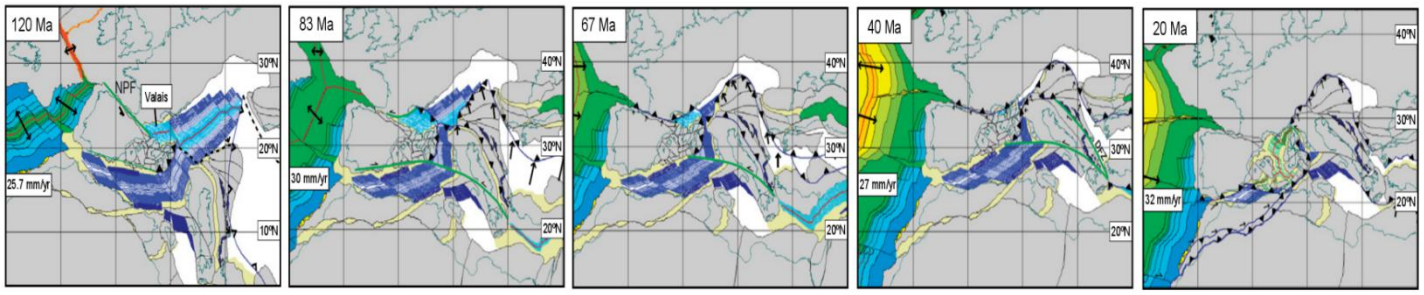
120 Ma
83 Ma
67 Ma
40 Ma
20 Ma
NPF
Valais
25.7 mm/yr
30 mm/yr
27 mm/yr
32 mm/yr

C)

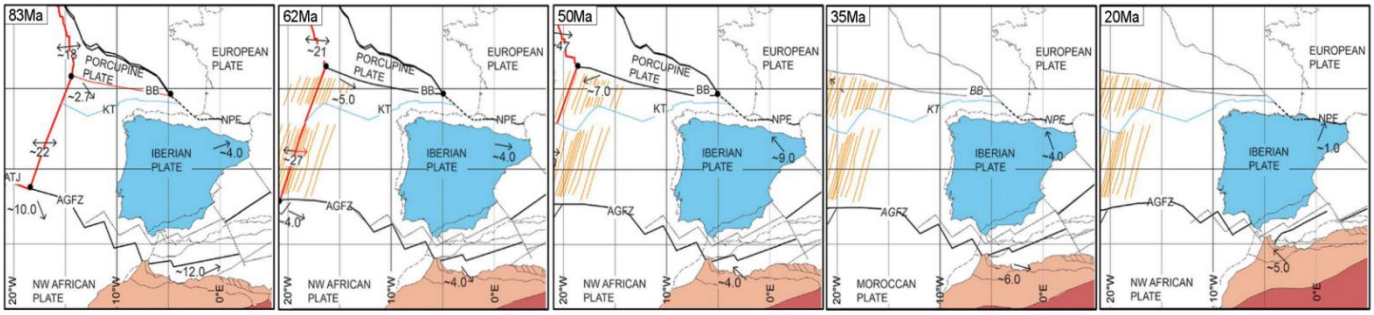
83Ma
62Ma
50Ma
35Ma
20Ma
EUROPEAN PLATE
PORCUPINE PLATE
IBERIAN PLATE
NW AFRICAN PLATE
MOROCCAN PLATE
BB
KT
NPE
AGFZ
ATJ

D)

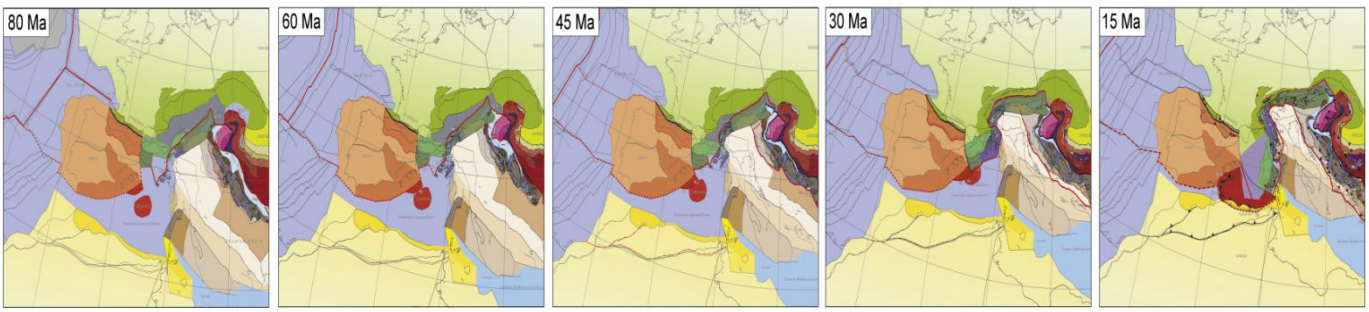
80 Ma
60 Ma
45 Ma
30 Ma
15 Ma

E)

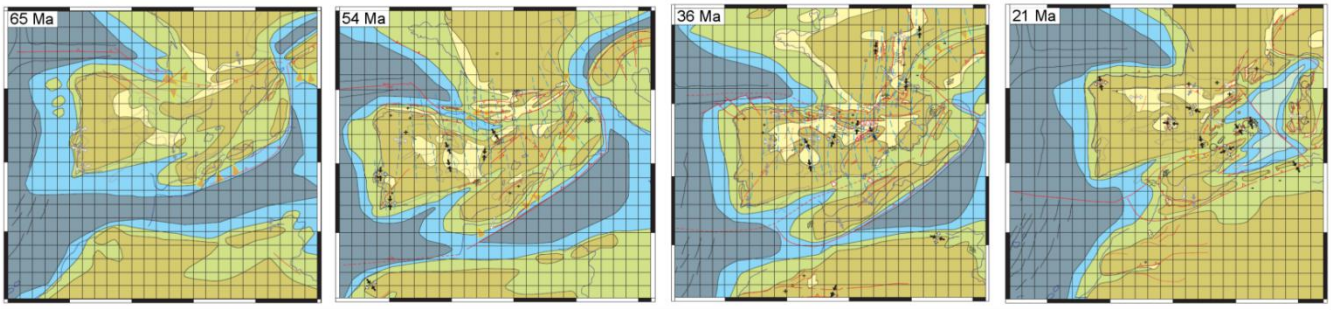
65 Ma
54 Ma
36 Ma
21 Ma

Figure 1.2. Complementary reconstructions for the eastern Atlantic and western Mediterranean modified from: A) Rosenbaum et al. (2002) highlighted with their kinematic reconstruction the Iberia rotation during the late Cretaceous, the strike slip movement of Iberia and Europe and the convergence of Africa with a subduction trench dipping to the N - NW direction beneath Iberia microplate. B) Vissers and Meijer (2012b) showed the aperture of the North Atlantic Ocean with velocity rates, and detailed the formation of the Alps and the closure of the Ligurian Tethys ocean. C) Macchiavelli et al. (2017) review the opening of the North Atlantic Ocean with new magnetic data, incorporate the Porcupine microplate and also include three different transtensive segments in the Betic-Rift to accommodate better the movement of Africa against Europe, the Gibraltar arc formation and a model of double polarity subduction in the western Mediterranean. D) van Hinsbergen et al. (2019) focused in the last tectonic evolution of the Mediterranean region since the Triassic, and included the formation of the Alboran block and its west movement the last 30 My. E) Andeweg Thesis, 2002, focused on paleoenvironments (which parts were under marine conditions) and sediment deposition for his paleo-geographic reconstruction.

1.2 Objectives

This thesis aims at improving the current understanding of the key mechanisms controlling the evolution of continental collision and the origin of the geodynamic and topographic evolution of Iberia during the Cenozoic, using numerical modelling techniques. The specific goals are:

a) To understand how deformation is transmitted from the compressive tectonic edges towards the interior of a plate, what are the key controlling parameters and how does rheology modify the tectonic deformation.

b) To identify end-member modes of deformation in the full field of posible rheological and geometrical initial conditions in continental collision scenarions and to identify actual geological scenarios that allow testing such end-members.

c) A detailed parameterization of the spatial and temporal distribution of crustal shortening along a profile from central to northern Iberia, using a two-dimensional mechanical and thermomechanical numerical models. Discussing the results in the light of the different theories proposed for the geodynamic evolution of Iberia.

d) To identify, by numerical modelling, the geological and dynamic conditions to explain the present-day geometry, Cenozoic deformation distribution and topography evolution along a transect crossing the Central System and the Cantabrian Mountains.

e) Understanding the role of the African plate in shaping the patterns of tectonic deformation related to the convergence in Northern Iberia. Evaluating the way this deformation is transmitted from the boundaries to the inner parts of Iberia along a model profile running from the Alboran Sea to the Gulf of Biscay. Finding mechanisms for simultaneous compression and extension in the context of the Iberian microplate.

1.3 Cenozoic geodynamic evolution of Iberia

In the late Cretaceous period, the Iberian microplate was separated about 200 km from the Eurasia mainland and about ~350 km from the African mainland (e.g.; Rosenbaum et al., 2002a, Capitanio & Goes, 2006; Vissers & Meijer, 2012b, and references therein). During the Mesozoic, the Iberian microplate was located at the western boundary of the Tethys Ocean and was still an independent plate (e.g., Vissers & Meijer, 2012b). By the end of Cretaceous times the position of the Iberian microplate was the controlled by the opening of the Central and North Atlantic Ocean. Due to African previous movements to the east relative to Iberia and Europe, the Ligurian-Tethys formed, defining the boundary between Morocco and Iberia, which was formed by several rift basins. These were named as Atlas and Betic-Rift by Schettino & Turco (2011). Some authors include an independent microplate located at the northwest margin of the Iberian microplate, known as Porcupine microplate (e.g: Vissers & Meijer, 2012b; Macchiavelli et al., 2017). During the Late Cretaceous also took place the opening of the Bay of Biscay along the already initiated Pyrenean rift basin, both part of the same rift system including oceanic and hyperextended domains (Tugend et al., 2014). This opening caused an anti-clockwise rotation of Iberia of approximately 37 degrees with

respect to Europe (e.g., Srivastava et al., 1990; Roest & Srivastava, 1991; Savostin et al., 1986; Sibuet et al., 2004; Gong et al., 2008; Vissers & Meijer, 2012b). Additionally, there was an eastward drift generated by the continuous opening of the North Atlantic Ocean between Newfoundland-Terranova and Iberia (e.g., Ziegler, 1988). Both motions, the opening and the drift, caused a north-south convergence between the Iberian microplate and the Eurasian plate, consuming the Tethys ocean. Coeval to this Cenozoic plate kinematics, Africa moved northwestwards relative to Europe, leading to the collision of Iberia with both the African and the Eurasian plates (e.g., Vergés & Fernàndez, 2006).

During the Cenozoic, tectonic compression dominates both at the Iberia-Europe plate boundary and at the Iberia-Africa plate boundary. Most studies agree that the Iberian plate was not deformed along its southern margin until the Oligocene (Olivet, 1996; Rosenbaum et al., 2002b; Sibuet, Srivastana, & Pakman, 2004; Macchiavelli et al., 2017). From Oligocene to present, the Iberian plate remained welded to the Eurasian plate after their continental collision.

In the Late Cretaceous and Early Cenozoic the northern boundary of the Iberian plate subducts beneath the Eurasian plate along the Pyrenees and partially beneath the newly-open Gulf of Biscay crust up to the Miocene (Sibuet et al., 2004; Le Pichon et al., 1987). This convergence between Iberia and Europe generates the inversion of the Pyrenean Mesozoic rifted basins, uplifting the Pyrenees and the Basque-Cantabrian Mountain Range (García-Mondejar, 1990; Muñoz, 1992; Puigdefàbregas et al., 1992; Teixell, 1998; Pulgar et al., 1999; Beaumont et al., 2000; Gallastegui, 2000, Gómez et al., 2002). In this northern margin, the convergence was completed along the Pyrenees during the Early Miocene and during the Middle Miocene in the and Basque-Cantabrian basin.

Roughly, we can divide the Betics formed by the tectonic inversion of the SE Iberian margin into Internal and External Units as well as the Alboran domain. Although there are many tectonic structural studies of the southern margin of the Iberian Peninsula, the complexity of the Betic-Rif System still provides a debate about its evolution. Many of such recent studies interpret the region formed as a result of the slab roll-back of the Ligurian-Tethys lithosphere subducting under the Alkapeca tectonic domain (Alboran-Kabylies-Peloritan-Calabria)(e.g., Bouillin et al.,

1986; Lonergan & White, 1997; Michard et al., 2002; Vergés & Fernàndez, 2012). The concept of Alboran as a microplate or domain was coined by Andrieux et al. (1971). During the convergence between Iberia and Africa in the Cretaceous, these domains have had different evolutionary stages. During the Thanetian (59 to 56 Ma), the convergence led to crustal shortening in both the Internal and the External Betics. This epoch is when the Pre-Betic uplifted (e.g., Kenter et al., 1990; de Jong, 1990; Balanyá et al., 1997). At the end of the Oligocene and beginning of the Miocene, an extensional tectonic movement happened in the internal Betics while the Alboran block migrates westwards.

Several models have been proposed for the evolution of the southern plate boundary of Iberia, such as, 'extensional collapse' model of Platt and Vissers (1989), or the arc migration model of the Betic-Rif orogen by Lonergan and White (1997). For the purpose of addressing the deformation of Iberia, however, we have focused in this study on the model by Schettino and Turco (2011), and more recently, by the model proposing a double polarity subduction proposed for the western Mediterranean (Vergés & Fernàndez, 2012). Nevertheless, there is a large number of models for the evolution of the Alboran Basin as has been discussed recently in an exhaustive review by Doblas et al. (2007), and more recently by Casciello et al. (2015). The Betic Rif arc appeared from a SE dipping subduction of oceanic crust beneath Africa. The compressional tectonic movement continues in the Alboran block until present times with evidence of left-lateral strike-slip displacements (Gràcia, E. et al., 2019). In the last million years, a slab break-off took place, under the westernmost Gibraltar Arc causing the uplift of the Betics and leading, together with the ongoing tectonic compression, to the current relief. According to Vergés and Fernàndez (2012), two original segments of the former Ligurian-Tethys oceanic domain initiated subduction with opposite dip; NW-dipping in the Algerian segment and SE-dipping in the Betic segment during the convergence of Africa-Iberia. Although this model directly confronts the mostly established model of the Alboran crustal block (e.g; Rosenbaum & Lister, 2004; Mauffret et al., 2007) is the only one that fits the opposite vergence of the orogenic systems of Kabylies-Tell (SE-verging) and Betic-Rif (NW-verging) as detailed in Vergés and Fernàndez (2012). Both, the Kabylies-Tell and Betic-Rif orogenic systems were formed by subduction-related processes ending with a fast event of

subduction roll-back, delamination and final slab break-off with the remains of the sinking slabs beneath the Betic and Kabylies orogenic systems (Zeck, 1996; Spakman & Wortel, 2004; Peral et al., 2020, Kumar et al., 2021).

The compression of the Iberian independent microplate caught between the Eurasian and the African not only affected the boundaries of the plate but also deformed the Iberian plate interior especially inverting previously weakened crustal regions. Several models have been proposed for this transmission of deformation from the edges of the plate inwards. Some studies based on block rotation or crustal thickening related to thrusting generated the high topography in the interior of Iberia (Vegas et al., 1990; Fernández Lozano et al., 2011, and references therein). Studies based on numerical models suggested that the tectonic compression generated folding of the entire lithosphere (e.g., Cloetingh et al., 2002). Some works suggested that several intra-crustal detachment levels may have allowed the transmission of stresses from the plate boundaries towards the interior and thus building the mountain ranges of the Iberian Ranges, the Central System, and the Catalan Coastal Ranges (Banks & Warburton, 1991; Quintana et al.,

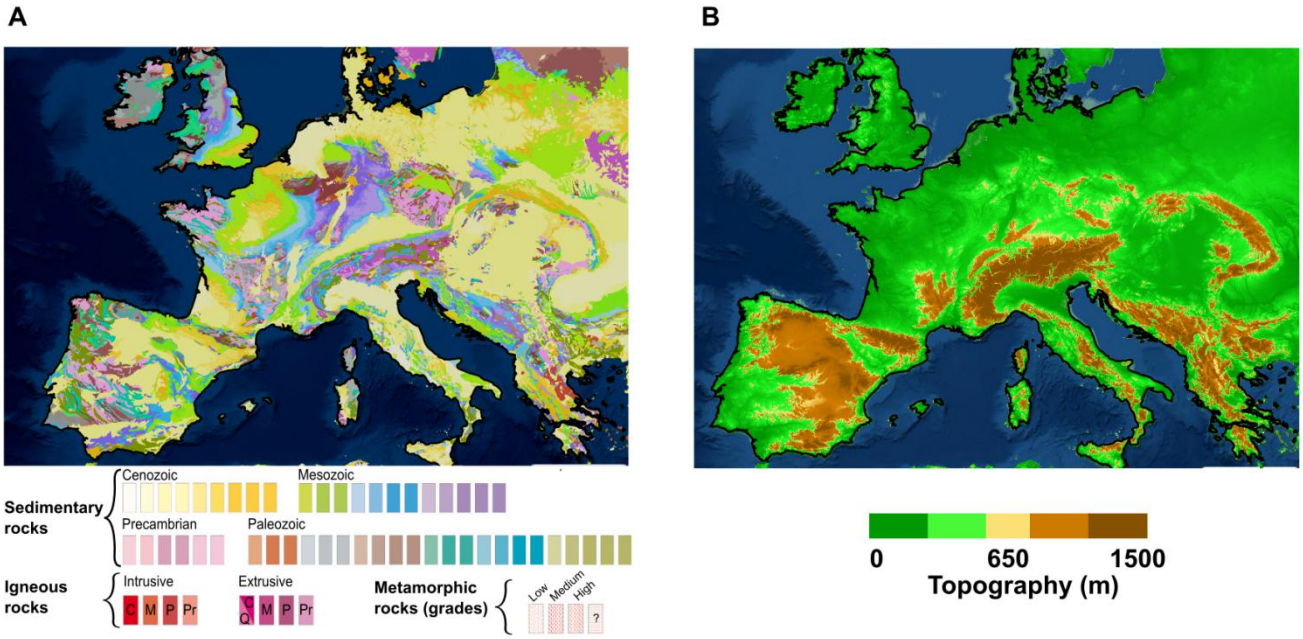

Figure 1.3. A) Simplified geological map of Europe (Asch, 2005, IGME 5000). B) Two colours map of the topography of Europe to compare the high average altitude of the Iberian Peninsula vs. The rest of Europe.

2015). Vergés and Fernàndez (2006) pointed out that not only the tectonic compression during the Cenozoic contributed to the high elevation of the Iberian microplate relative to Europe, but also the inherited structures of the Variscan orogeny and the upper mantle thinning related to the opening of the western Mediterranean during the Neogene uplifting the entire eastern coastal regions of Iberia (see also Lewis et al., 2000).

In addition to all these mechanisms for the propagation of deformation, Conway-Jones et al. (2019) based on models for the Cenozoic river incision, dating marine terrace and biostratigraphic observations such as fossils with high accuracy with the paleo-water depth, suggest that additional uplift occurs related to an abnormally warm upper mantle underneath Iberia during the last 35 My. This warmer mantle would be responsible for an average elevation in Iberia of 0.3 to 0.8 km.

This thesis is divided in six chapters, including this brief introduction of the Cenozoic evolution of the Iberian microplate and the main objectives. Chapter 2 will focus in the fundamental physics and mathematics governing the equations used in numerical modeling, among some limitations and considerations to build a suitable model, and describe the Underworld2 code used for all the models. In Chapter 3, by using a mechanical numerical modeling, I analyse the physical parameter that controls the way deformation accommodates while an orogen develops in a collisional scenario. It revises the role of inherited structures in the orogens building. Chapter 4 evaluates the mode of deformation along a transect in the Central-North Iberia, crossing the Central System and the Cantabrian Mountains. I use a thermomechanical numerical modeling to understand the accommodation of the deformation during Cenozoic and the transmission of this deformation to inner parts of the Iberian Peninsula. Finally, I discuss the effect of a southern margin on the intraplate deformation of Iberia. In Chapter 5 there is a general discussion of the geodynamic models results presented in Chapters 3 and 4. Last chapter 6 summarizes the main conclusions of this thesis.

Chapter 2

Fundamentals and Methodology

Numerical models are used in this thesis to understand better the geodynamic evolution of the Iberian microplate in the last 65 million years, but it is also necessary to introduce general concepts of tectonic movements and possible implications to the lithosphere structure and evolution. This chapter focuses in the methodological and conceptual ideas that have been applied in this research. After a brief introduction to what is the concept of **lithosphere**, special attention will be paid to:

- Lithosphere deformation: continental collision and intraplate deformation.
- Rheology of the Earth. Stress and strain/strain rate relations.
- Momentum, constitutive and thermal equations.
- Underworld II is a python friendly code. Considerations for constructing a thermo-mechanical model.

The lithosphere is the rigid outermost layer of the Earth. It is commonly divided into two parts: one thinner and shallower layer called crust, and below the lithospheric mantle. The first time the concept of a solid layer overlying a fluid was used was in 1896 by J. Dana, supported by gravimetric studies. Later in 1914, Barrel described the deformable fluid below the lithosphere as **asthenosphere**.

Gutenberg in 1954 using seismological methods revealed a low-velocity zone (LVZ) in the Earth located between 100 and 150 km depth. McKenzie, 1967, describes a mechanical lithosphere where the transmission of stresses has a geological time-scale. During decades, new definitions of this concept emerged, depending on the parameter under study and the techniques used. Nowadays, five definitions are commonly used to describe the lithosphere (Figure 2.1, modified from Artemieva, 2011): the **mechanical** or **elastic** lithosphere is a strong layer in isostatic equilibrium which holds elastic stresses. The **thermal** definition describes the layer of the Earth where the thermal energy is mostly transferred by heat conduction. Studies of Parsons & Sclater, and Chapman & Pollack in 1977 extend this definition to which the mantle rocks approach their **solidus** temperature. The solidus temperature was a laboratory measured temperature where all minerals are molten or have started to melt. The **seismic** lithosphere typically is defined as a high viscosity layer above a low viscosity zone, but this velocity contrast depends on the point of view, i.e., if it is associated with the convection mantle, the boundary of the lithosphere may be deeper than the thermal but a severe change

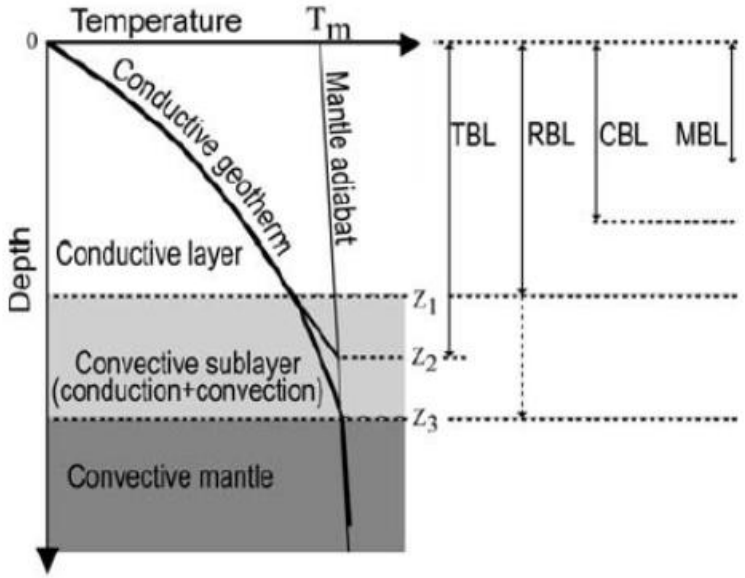

Figure 2.1. Scheme of the 4 accepted definitions of the Lithosphere-Asthenosphere Boundary (LAB). TBL, RBL, CBL, and MBL are the thermal, rheological, chemical and mechanical boundary layers. Above Z1 the layer has only conductive heat transfer. Z2 is representative of the TBL where a linear geotherm intersect the mantle adiabatic or solidus temperature. These definitions (except chemical boundary layer) are temperature-dependent where a dramatic change in mantle viscosity occurs. Modified from Artemieva (2011).

in viscosity may locate the LAB shallower than the thermal one. The **electrical** lithosphere corresponds to a high change in the mantle conductivity. The **chemical** lithosphere contains the material differentiated or extracted from the mantle, being relatively depleted in basaltic components compared to the underlying asthenosphere.

2.1 Lithosphere deformation

The lithosphere is not continuous, and it breaks in segments called plates. Plates generally move with the same speed and direction as a unit. The theory that explains how the plates move with time, known as **plate tectonics**, started with Alfred Wegener's hypothesis of **continental drift** in the 1920s. By the 1960s, scientists had amassed enough evidence to support the missing mechanism, i.e., why the plates moves, for Wegener's hypothesis of continental drift to be accepted as the theory of plate tectonics. The missing mechanism was proposed by Harry Hess in 1959. He figured out that at ocean ridges adjacent plates diverge from each other in a process known as seafloor spreading. Meanwhile they diverge; hot mantle ascends filling the gap in between. This hot mantle cools down and accretes to the plate creating new seafloor. The boundary between these plates is known as an accreting plate boundary or commonly known as diverging margin. If there is a diverging margin where a new plate is being created, there should be a convergent margin where a plate is being consumed due to the Earth's surface mass has to be constant. This happens in the ocean trenches where the plate bends and descends to the interior in a process known as **subduction**.

In a convergent margin, there can be two possibilities: subduction and **continental collision**. The subduction of oceanic lithosphere at convergent boundaries also builds mountain ranges. Subduction occurs when a dense oceanic lithosphere meets a more buoyant one and descends into the mantle. As the oceanic lithosphere descends, it pulls the ocean floor down into a trench. Within the trench, ocean floor sediments assemble between the subducting and overriding plates, creating an accretionary wedge or prism. Also, fragments of continental

material, including **microcontinents**, over the subducting lithosphere can stitch to the wedge into a large area. An example of this is the Pyrenean Chain, during the Jurassic the Iberian plate and Eurasian plate where separated by the Valais-Ocean. This ocean was consumed by the compressive tectonic movement between Iberia and Europe consumed during the Paleogene (Schmid et al., 2004).

Subduction can consume all the oceanic lithosphere between two continental margins. In those cases, subduction stops due to the equal buoyancy of the plates. The two converging continental lithospheres smash upwards to create large mountain ranges. The combined mass of the mountains forms a depression in the lithospheric plate known as a foreland basin. The Persian Gulf is a modern example, created by the weight of the Zagros Mountains. In the Iberian Peninsula, the Duero and Ebro basins are past examples of foreland basins.

2.1.1 Continental collision

Continental collision is one of the main processes in shaping the Earth's relief. This occurs when the oceanic domain between two continental lithospheres subduct entirely leading to crust accretion and exhumation when the two continental blocks collide (e.g. Dewey & Bird, 1970). Such processes, among others related to the subduction like sediment transport which can derive into magmatism, affects the posterior dynamic and evolution of the orogeny. Surface processes, like erosion or sedimentation, also play an important role in the evolution and growing of the orogens (e.g., Willet, 1999).

During the last decades, the knowledge on the development of orogens using numerical models in a continental collision scenario and their deformation pattern has experienced significant improvements highlighting the relevance of crustal rheology as the principal factor controlling the first-order deformation style in such scenarios (Beaumont et al., 2000; Brun, 2002; Faccenda et al., 2008; Gerya et al., 2011; Calignano et al., 2015; Vogt et al., 2017; Vogt et al., 2018). Strenght contrast has a relevant impact in the evolution of the orogen in continental

collision and heterogeneities in the lithosphere have significant repercussions (Carry et al., 2009; Jammes & Huismans, 2012; Jammes et al., 2013; Vogt & Gerya, 2014). Depending on convergence velocity that accretes crustal material and thermal age, we can divide orogens in three categories: i) Small and cold orogens. Small, due to the little amount of mass accumulation compared to other ranges, such as the Himalayan-Tibetan system, and cold due to the crustal heat sources are not enough high to exceed for a long time period the partial melting threshold. Usually evolve into a symmetric double vergent orogen like in the Cascadia margin–Olympic Mountains (Brandon et al., 1998) or the Pyrenees. ii) Transitional orogens such us Central Alps or Pyrenees and iii) large hot orogens that usually evolve to a big plateau like the Himalayas (Jamieson & Beaumont, 2013).

2.1.2 Intraplate Deformation

Not only deformation can accommodate in the margins during a continental collision scenario but it also can spread to distance further than 1600 km from the collision front. The capacity of the lithosphere to transfer stress over long distances has relevant implications. Intraplate deformation is the folding, breaking, or flow of the Earth's crust within plates instead of at their margins (Ziegler, 1995). Some rheological conditions, material changes and thermal perturbations promote the transmission of stresses over large distances (Cloetingh et al., 1999; Gerya et al., 2011; Ranalli, 2000; Simpson et al., 2006; Dymkova et al., 2016) generating high contrast in lateral strength as well as between crustal layers. Intraplate structures like the imbrication of the Central Alps, have been usually explained with a simple shear detachment at the base of the crust which transmits deformation (e.g., Pfiffner, 1993). Sometimes weak materials, such as past sediment like the **Keuper** material or salt deposits, are confined between two stronger layers, and due to compression, act as a **décollement**. Throughout the thesis, we use the terms décollement and detachment levels as weak zones without distinction for simplification. Despite this simplification, both terms are usually seen as synonymous, but Brun et al. (2018) remark that a detachment is

controlled by rock friction and can cut across different lithologies whereas a décollement corresponds to a displacement within a weak zone and runs parallel to the layering. Also intraplate structures have been explained with compensation by thickening of the lithospheric mantle and lower crust acting as ductile materials. Other studies demonstrate that tectonic compression can affect the entire lithosphere and intraplate deformation is by folding of the lithosphere (Davy & Cobbold, 1991; Martinod & Davy, 1994; Burg & Podladchikov, 1999; Cloetingh et al., 1999, Cloetingh & Burov, 2011). Not only the lithosphere can entirely fold but also the crust can have different wavelength folds. Examples of crustal folding can occur in front of orogenic belts, like in the Pyrenees (Bourrouilh et al., 1995) and the Zagros folded belt (Mouthereau et al., 2006) with small wavelengths, and in regions of plate collision like in Western Gobi (Burov et al., 1993) originating higher wavelengths. The inherited structures from past geological events can reactivate during the tectonic compressional evolution of the plate, varying the stress distribution and changing how deformation accommodates within the crust (e.g., Quintana et al., 2015; Calignano et al., 2015).

2.2 Rheology of the lithosphere

The concept of rheology concerns the way materials behave under deformation and how materials flow when stresses are applied to them.

The lithospheric behaviors against stresses vary on the temperature, depth and with time. Nowadays, it is well-known that a geological time scales the mantle starts to obey the rules of a pure viscous material and to flow rapidly when depth increments. This conduct establishes the difference between the lithospheric mantle and the sublithospheric mantle. The rheological limit of this part of the mantle is an isotherm which value usually is about 1300 to 1350 °C depending on the physical parameter used to define the limit between the lithospheric mantle and the sublithospheric mantle. Depending on age, an oceanic lithosphere has this limit shallower than an old one, which is related to the distance to the diverging

margin. Also, the limit in continental lithosphere ranges between 100 and 250 km depth subject to the age of the lithosphere (e.g., Chapman & Pollack, 1977; Turcotte & Schubbert, 2002). This zone it is known as the lithosphere-asthenosphere boundary (**LAB**). The mantle above this limit can be considered cool enough to not behave as a pure viscous but like a rigid material.

2.2.1 Stress and Strain

While plates are moving, the rigidity of the lithosphere allows stresses to travel within them during geologic intervals. The *stress* is a force per unit area that is placed on a rock. For a small volume of material there must be a mechanical equilibrium, and, therefore, from the balance of forces and momentums it results in a symmetric stress tensor, with 9 components defining the stress state of the deformed volume:

$$\sigma = [\sigma_{ij}] = [\sigma_{ji}] = \begin{bmatrix} \sigma_{11} & \sigma_{12} & \sigma_{13} \\ \sigma_{21} & \sigma_{22} & \sigma_{23} \\ \sigma_{31} & \sigma_{32} & \sigma_{33} \end{bmatrix} \quad [1]$$

This tensor refers a unit-vector direction vector **n** to the traction vector $\mathbf{T^{(n)}}$ through an imaginary surface perpendicular to **n.**

$$T^{(n)} = n \cdot \sigma \quad [2]$$

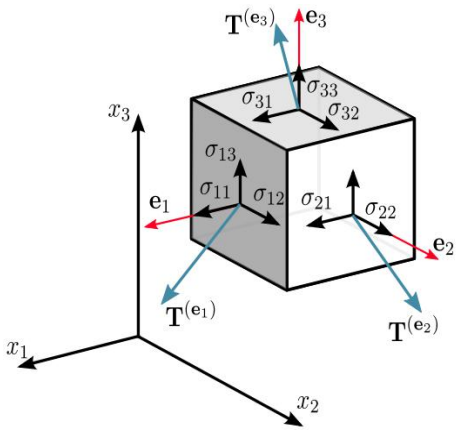

Figure 2.2. Representation of the three dimensional stress components of a small volume.

In geoscience, the stress tensor can be separated into two components: 1) the **hydrostatic stress** which is related to volume change of the material; and 2) the **deviatoric stress** related to shape change only. For an incompressible material,

$$\sigma_{hydrostatic} = \frac{1}{3}(\sigma_{11} + \sigma_{22} + \sigma_{33}) = \ -P \qquad [3]$$

This tensor is the extra part of the **isotropic stress** state from the stress tensor:

$$\sigma'_{ij} = \sigma_{ij} + P\delta_{ij} \qquad [4]$$

where i and j are the coordinate indexes, P is the total pressure and δ_{ij} is the Kronecker's delta function.

Another important component from the stress tensor is the second invariant of the deviatoric stress ($II_{\sigma_{ij}}$) or **effective shear stress** (τ or σ_e). It is a scalar value that do not depends on the orientation and the coordinate system and takes into account the local deviation of stresses:

$$II_{\sigma_{ij}} = \sigma_{II} = \left(1/2\ \sigma'^{2}_{ij}\right)^{1/2} \qquad [5]$$

When stress causes a material to change its shape and/or size, it has undergone **strain** or deformation. Assuming the same small volume of material, the amount of deformation or infinitesimal strain tensor is calculated:

$$\varepsilon_{ij} = \ \frac{1}{2}\left(\frac{\partial u_i}{\partial x_j} + \frac{\partial u_j}{\partial x_i}\right) \qquad [6]$$

where the material displacement vector is $\vec{u} = \left(u_x,u_y,u_z\right)$, and x_i and x_j are the components of the spatial coordinate system (x,y,z). To study the flow of a material, instead of the infinitesimal strain tensor, we use the strain rate tensor:

$$\dot{\varepsilon}_{ij} = \ \frac{1}{2}\left(\frac{\partial v_i}{\partial x_j} + \frac{\partial v_j}{\partial x_i}\right) \qquad [7]$$

where the velocity vector is $\vec{v} = \left(v_x,v_y,v_z\right)$. Analogous to the stress tensor, we can define the deviatoric strain rate and the second invariant as:

$$\dot{\varepsilon}'_{ij} = \dot{\varepsilon}_{ij} + \frac{1}{3}\dot{\varepsilon}_{kk}\delta_{ij} \qquad [8]$$

$$\dot{\varepsilon}_{II} = \left(1/2\, \dot{\varepsilon}_{ij}^{'2}\right)^{1/2} \quad [9]$$

where *i*, *j* and *k* are the coordinate axes directions and $\dot{\varepsilon}_{kk} = \dot{\varepsilon}_{xx} + \dot{\varepsilon}_{yy} + \dot{\varepsilon}_{zz}$ is the mean strain rate tensor.

When rocks are stressed, the resulting strain can be elastic, viscous, or plastic. **Elastic deformation** is strain that is reversible after a stress is released. Under low pressures, temperatures and short time scales, the material come back to its original shape. The straining or unstraining takes place instantaneously, i.e., whether deformation occurs in seconds or over million years; the elastic deformation is time independent and recoverable. In this thesis we not consider this deformation and its contribution due to we pretend to model a period of time of around 60 My. For the same reason, several authors do not consider this term for long time periods, and consider the lithosphere behaviour as a fluid.

Viscous deformation occurs when enough stress is applied to a material that the changes in its shape are permanent, and the material is no longer able to revert to its original shape. Viscous materials flow where a force is applied to them and it is thermally activated. When temperature overpasses the fusion temperature of the material, atoms and dislocations have enough energy to move slowly and constantly. This is called **creep** deformation. In geodynamic modelling is used the relation, where the deviatoric stress is related to the strain rate and temperature through the constitutive equation:;

$$\sigma_{ij}^{'} = 2\eta\dot{\varepsilon}_{ij} \quad [10]$$

where η is the viscosity of the material that strongly depends on temperature and pressure (Ranalli & Murphy, 1987). This linear approximation has been used to describe the lower mantle as there are high temperatures (1000-1500 °C) and very low strain rates (10^{-16} to 10^{-18} s^{-1}). The way the material flow in the lower mantle is the **diffusion** creep. When the stresses are high, the material behaves as **non-lineal** or **non-Newtonian** and it is called the **dislocation** creep. Both creeps follow mathematical rules known as power law creep or constitutive equations, which allow to study the mechanical behaviour of materials (Ranalli, 1995), and the viscosity corresponding to each power law, is expressed as,

$$\eta_{creep}(T,P,\dot{\varepsilon}_{II}) = (A_D)^{\frac{-1}{n}}(\dot{\varepsilon}_{II})^{(\frac{1-n}{n})}\exp\{\frac{E+PV}{nRT}\} \quad [11]$$

where T and P are the temperature (K) and pressure (Pa) respectively. A_D is the pre-exponential factor, E the activation energy, V the activation volume and n is the creep exponent or power-law exponent. These parameters are experimentally determined and R is the gas constant.

We have said that rocks first deform as a perfect elastic material. This behaviour can be seen in Greenland due to removal of the cover of ice where the deformed land its upwelling, recovering its shape. But, if this load continues in time there is a stress limit for each material where permanent strain begins and it is called the yield stress. If a solid does not deform until the yield stress is reached, it can be considered as an ideal **plastic** material. At the yield stress, plasticity behaviour corresponds to a permanent and irreversible deformation.

For an elastic material, when stresses reach the strength limit of the material, it breaks, creating fractures. The material loses its **cohesion**. For stresses above the yield stress, the flow law changes to a plastic behavior. The nonlinear effective viscosity corresponding to the plasticity of materials is given by,

$$\eta_{yield} = \frac{\tau_y}{\dot{\varepsilon}_{II}} \quad [12]$$

where $\tau_y = (C_0 + \mu_f \cdot Z)$ is the yield stress determined from Byerlee' frictional law. The yielding stress τ_y depends on cohesion C_0 at zero confining pressure, frictional coefficient μ_f and depth Z (Byerlee, 1978; Solomatov & Moresi, 1997; Moresi et al., 2003).

2.3 Numerical modeling

A numerical model is an artificial description of reality via mathematical expressions and laws that correlate numerous physical-chemical parameters using computational resources. If the mathematical expressions, physical and chemical laws are well chosen, the numerical model will be capable to explain a big variety of observational features.

To solve a numerical model, it is necessary to formulate a series of equations that relate the unknowns to functions that include the effect of each parameter. One of these equations is the conservation of the mass (Lomonósov-Lavoisier law), where in an isolate system the mass has to conserve. For a continuous medium can be described by the continuity equation, in a Lagrangian description (i.e. for a dynamic system):

$$\frac{D\rho}{Dt} + \rho\nabla \cdot \vec{v} = 0 \qquad [13]$$

where ρ is the density, t is time and $\vec{v}$ is the velocity vector. In geodynamic numerical models is commonly used the incompressibility approximation where density remains constant (e.g., Beaumont et al., 1992; Gerya, 2009; Schellart & Moresi, 2013; Capitanio et al., 2014). The mass conservation under this assumption can be expressed as,

$$\nabla\vec{v} = 0 \qquad [14]$$

According to Newton's second law $\left(\sum \vec{F} = \sum m{\cdot}\vec{a}\right)$, the variation in time of the momentum of a fluid and under the influence of a gravity field, is uttered as:

$$\frac{\partial(\rho v_i)}{\partial t} + \frac{\partial(\rho v_i v_j)}{\partial x_j} - \frac{\partial \sigma_{ij}}{\partial x_j} - \rho g_i = 0, \qquad [15]$$

taking into account equation [14], we finally arrive to:

$$\rho\frac{Dv_i}{Dt} = \frac{\partial \sigma_{ij}}{\partial x_j} + \rho g_i \qquad [16]$$

where g_i is the i component of the gravity vector $(\vec{g})$ and Dv_i/Dt is the material derivative of the velocity vector of the component *i.*

If we include the equation of the stress tensor [2] in the conservation of momentum for a continuous medium in a gravity field, we have the **Navier-Stokes** equation of motion for fluids:

$$\rho \frac{Dv_i}{Dt} = \frac{\partial \sigma'_{ij}}{\partial x_j} - \frac{\partial P}{\partial x_j} + \rho g_i \quad [17]$$

It is commonly in geodynamic numerical models to ignore the inertial forces for high viscosity fluids due to are insignificant respect to the other forces, and the Navier-Stokes equation for a slow flow simplifies to,

$$\frac{\partial \sigma'_{ij}}{\partial x_j} - \frac{\partial P}{\partial x_j} + \rho g_i = 0 \quad [18]$$

In addition to the set of equations described in this section, the temperature variations is calculated solving the energy equation,

$$\frac{\partial T}{\partial t} + v_i \frac{\partial T}{\partial x_i} = \kappa \frac{\partial^2 T}{\partial^2 x_j} + H \quad [19]$$

$$\kappa = k/\rho C_p \quad [20]$$

where $x_{i,j}$ are the coordinates, v_i is the velocity, T the absolute temperature (K), κ is the thermal diffusivity ($m^2\ s^{-1}$), k or K is the thermal conductivity ($W\ m^{-1}\ K^{-1}$), ρ is the density ($kg\ m^{-3}$) and C_p is the specific heat ($J\ kg^{-1}\ K^{-1}$). H stands for the different heats production of the Earth. They are the radioactive, the shear, the adiabatic and latent heat productions.

The density is calculated as a function of the temperature and pressure (for more details we refer to Afonso et al., 2003; Boonma et al., 2019):

$$\rho_{crust} = \rho_0(1 - \alpha(T_z - T_{surf}) + \beta P_{li}) \quad [21]$$

$$\rho_{mantle} = \rho_0(1 + \alpha(T_a - T_z) + \beta P_{li}) \quad [22]$$

Where T_{surf} = 15 °C is temperature on the surface, ρ_0 reference densities for the different materials and for the asthenosphere, α and β are thermal expansion and compressibility of rocks. $P_{li} = \rho_0 g z$ is the lithostatic pressure.

2.3.1. Numerical code

In this thesis, the ***Underworld*** code was applied in to perform the geodynamic models of the Cenozoic evolution of Iberia. It was developed in the School of Earth Science from Melbourne University (Melbourne, Australia). In this thesis, we used the 2.5 and 2.6 versions of the code that is a python friendly open source coupled with C language. It is a Lagrangian integration point finite element method. This method combines an Eulerian mesh and Lagrangian particles among with the Paticle-in-Cell approach (PIC, Harlow, 1955). Physical properties are transported by Lagrangian particles that move according to the velocity field interpolated from the mesh. The mesh is used to solve diffusion-dominated parts. The nodes of the mesh are fixed in space and material can move through them. The Stokes flow problem is solved with the Uzawa method that is an algorithm for solving saddle point problems. With these approaches and using multigrid technique for inner iterations the separation of the computational mesh from the swarm of points which track the history, it's much easier and computationally faster. So, complex geodynamic problems can be solved in a local machine. The Underworld code allows the user to define the mathematical relations between different variables and to build the geometry of the domain. For a more detailed description of Underworld code, we refer to Moresi et al. (2001 & 2003, https://www.underworldcode.org/). Moreover, this second version is available through Dockers, a tool design to run applications by using containers that allow the application to use the personal computational resources without installing any additional needs such as libraries or other dependencies. Through the last decade the code have been developed to solve more and more complicated scenarios and recently new improvements in the method permit to scale the problem to 3D (Moresi et al., 2007). In the cases considering big domains or including a huge

number of particles or high resolution, parallel computation is needed. Even with high resolution (HR) and complicated 2D settings, high computational resources are necessary to solve the inner solvers, i.e., a big number of cores (~64 for our HR-2D models and <256 for 3D models), enough storage space for output data (~30 gigabyte (GB) each 2D model and <200 GB for a single 3D model), and high random-access memory (RAM). During this thesis a large 2D high resolution model (~$6.65 \cdot 10^5$ nodes with 10 to 15 particles per cell) for the Iberian Peninsula needed approximately three weeks for calculation time in a supercomputer. This was the typical numerical model done during the thesis. Up to two months of time calculation has been needed for the model with the highest resolution, nodes and particles (~15 million particles). The workstation employed first was a supercomputer with 64 cores called MITE property of the Geo3bcn institute. Increasing resolution of the models took longer than one month to run in this workstation. To solve this problem, MARENOSTRUM computer from the Barcelona Supercomputing Center (BSC), one of the biggest supercomputer in Europe was needed during several different 3 month periods decreasing the calculation time from more than one month to 2-3 weeks. For each period, a reported was needed, explaining the main objectives of the study, the previous results and the storage and number of cores for the next 3 month period.

Underworld comes with the ***LaVavu*** library for visualization of the preliminary results. In this thesis, we have used ***matplotlib*** from python for graphics, such as, **thermal gradients** or **density-viscosity profiles**, and material evolution through markers, such as, topography or the base of the crust. I used the ***Paraview*** [Kitware Inc] software to acquire the 2D-3D view of the model evolution. This visualization tool offers a better quality of the results due to their interpolation method. Paraview has also been used to analyze the stress distribution, the crustal accretion or the velocity field of the mantle.

2.3.2. Modeling strategy and supercomputing resources

A model should be carefully planned taking into consideration the previous studies done by other modelers, the limitations in technology and iterative methods to solve the Navier-Stoke equations and the simplifications made by the researches in their models. A good strategy in modeling is to start with the simplest set up to study the response of different physical parameters and isolate its importance during the geodynamic evolution of the model. This initial model can be an initial benchmark to compare posterior models. It is important for the set up to determine a good domain size, to consider the boundary conditions, to choose wisely the material properties and the dependencies between physical parameters, for example, how the density changes with pressure, temperature and depth. Also, a modeler has to take into account the limitations of the code to solve efficiently the inner solvers. For example, incrementing the resolution's model implies smaller cells where the stokes problem needs to be solved. Also, between two adjacent cells, the model can have a contrast of more than five orders in magnitude for specific physical parameters and not converge to a solution through the iterative procedure implemented. Also, more resolution requires more computational resources, or more calculation-time. For example, increasing the domain in our models, implies a major number of cells and particles, and a model that usually takes three weeks to reach the final time step, it can increase up to 2 months. The same if we increase our resolution. Sometimes, when increasing the accuracy of the model, a supercomputer has not enough RAM to solve the inner iterative methods for the velocity and the pressure and more powerful machines are needed.

Models try to represent reality in a virtual environment. With the development in technology, more and more modelers try to simulate nature efficiently. Nowadays, in geodynamics is common that a numerical model incorporates a visco-elasto-plastic rheology for materials. Some geodynamic models in convergent geological processes integrate temperature dependence (e.g., Beaumont et al., 2000; Cloetingh et al., 2013; Zlotnik et al., 2014; Ruh et al., 2015;

Vogt et al., 2017). In this thesis, I study a long term geodynamic processes and therefore, the rheology used is the visco-plastic behavior (Willet, 1999; Capitanio et al., 2013; Jammes et al., 2013; Andríc et al., 2018).

Another restriction in modeling of relevance is the boundary conditions. A model can be consider as an open box where new particles can be introduced to compress the inside particles of the model. This can be done from one side or multiples sides of the model domain (e.g., Ruh et al., 2013). Or a model can be considered as a "closed" box where although new particles do not enter through the domain's boundaries, but repopulate the domain every time the inner solver calculates. This procedure fills in the cells to not run out of enough particles to converge to a solution. The repopulation technique was employed in all the models for the thesis. So final number of particles are always more than the initial number of particles. Accounting to the walls three kind of conditions have been considered through all the models in the thesis; non-slip walls where particles are not allow to move and break through them; free-slip boundary walls, where particles are allow to move in the same axis than the wall but can't cross it and periodic boundary conditions where particles that cross the wall appear in the opposite one allowing a continuous flow. In this sense, some authors consider the top wall as a free surface where normal stress is zero to simulate vertical movement as topography growth. Another stream of authors use the sticky air method where a very low viscous layer acts as air letting the layer below to have vertical movements without applying stresses on it. Crameri et al. (2012) evaluate both methods using different codes and concluding that for Eulerian mesh sticky air is a good approximation for a free surface and is the approximation used for the numerical models in this thesis.

A common strategy consist of fixing the Temperature values at the top and bottom boundaries. An initial thermal distribution is figured as linear functions between the top and bottom walls and a fixed temperature in the LAB. Then, the advection diffusion solver from Underworld solves the energy equation every time step. An average thermal gradient for the mantle of ~0.5 °C km^{-1} is imposed in our models which is widely spread value used in geodynamic modeling. Using the initial thermal gradients imposed for the lithosphere we have a function of the temperature with depth. This function is called **geotherm**.

Chapter 3

Continental collision: Crustal folding vs. double vergence. Insights for numerical modeling

In this chapter, I quantitatively study through the use of mechanical numerical models the relevance of several structural and rheological parameters which may control the deformation style of orogens, and the transmission of deformation beyond the collision zone. To this purpose, we design a collisional structural set up in which we change 1) the crustal density, 2) the angle of a weak suture zone on the collision contact in the lithospheric mantle, and 3) the viscosity contrast in crustal layers, changing the maximum values and the plasticity criteria. In a second section, I investigate the effect of décollements on the distribution of strain rate at lithosphere scales and the evolution of the orogeny. I will consider the Pyrenees Mountain and the Zagros Simply Folded Zone to discuss the modeling results (Figure 3.1).

The Pyrenean orogen formed as a consequence of the convergence between the African and Eurasian plates that started around 83.5 Ma in the Santonian. This orogen is located at the northeast part of Iberian Peninsula, at the collisional boundary between the Iberian and Eurasian plates (Choukruone et al., 1989), with 420 km of extension and 125 km wide. Initial reconstructions in the central Pyrenees indicated a minimum of 100 km of crustal shortening (Roure et al., 1989).

The differences in crustal shortening between the west, (125 km; Muñoz, 1992) and the central Pyrenees (ECORS profile; 165 km), is still a debate nowadays.

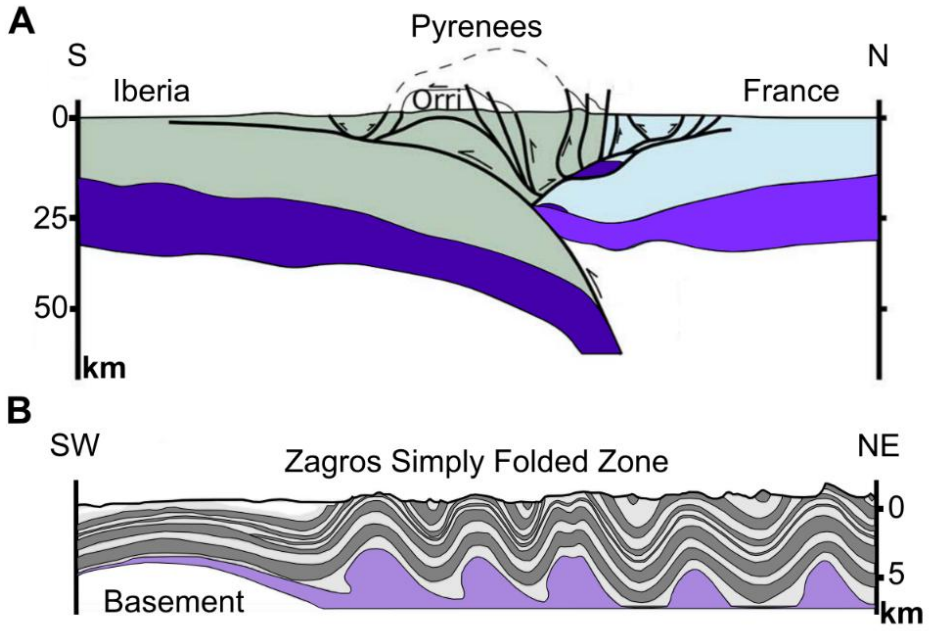

Figure 3.1. A) Crustal cross-section across the Pyrenean chain (modified from Muñoz, 1992. B) Southwestern simply folded zone in Zagros, near the Persian gulf, SW Iran (modified from Hessami et al., 2001).

Beaumont et al. (2000) explained the geodynamic evolution of the eastern Pyrenees using the concept of the split point *S* developed in previous numerical models and introducing weak layers in the crust to reproduce the basic trends of the present structure of the orogen along the ECORS section. Their model generated double vergent orogens by deforming only the crust and adding the result as an isostatic load. Recent studies suggest the importance of inherited structures from previous tectonic events between Eurasian plate and the Iberian micro-continent in Cretaceous times, e.g. opening of the bay of Biscay, lateral strike-slip movement related to opening of the Atlantic ocean or different shortenings in the entire north Iberian boundary (Rosenbaum et al., 2002b; Galindo-Zaldívar et al., 2015; Pedreira et al., 2015; Macchiavelli et al., 2017; Pedrera et al., 2017). Those inherited structures include two detachment levels at different depths: the Triassic Keuper salt at upper crust levels and a middle-lower crust weakness layer related to previous extension during the Mesozoic which

favored decoupling of the crust (Beaumont et al., 2000). Jammes et al. (2013) also included an exhumed mantle area in the Cretaceous basin between Eurasian and Iberian plates that explains lateral variation in the present Pyrenees.

Zagros Mountain Belt is a 200 to 280 km wide folded belt from a collision between the Arabian plate and the Iranian continental blocks (Mouthereau et al., 2007). The northeaster boundary is marked by a ~80 km wide imbricated zone. The folding mechanism is governed by multiple detachment levels above the Hormuz salt level located at 10-12 km depth. The upper mobile level is the Gachsaran evaporites and represents the main detachment decoupling between the above (Passive) and below (Competent) groups. This detachment migrates from anticlines to synclines, which produce disharmonic folding in combination with thrusts. The Zagros fold belt has maximum shortening values of 15% for the central to northwest part of the belt (Vergés et al., 2011).

3.1 Model setup

All numerical models presented here correspond to a continental collision scenario, ignoring the pre-collisional stage of oceanic subduction and are composed of layers with different densities, from top to bottom: sticky air, upper-middle crust and lower crust, lithospheric mantle and sublithospheric mantle (Figure 3.2). Each layer has a homogeneous material property. The model domain has 1200 km horizontal length and 500 km depth. I have defined a discretisation mesh with a vertical resolution of 1.2 km in the crust, increasing with depth up to 2.5 km at the bottom of the domain, and horizontal resolution of 1.8 km. I defined 10 particles per cell to track the material, within a total of 204800 cells in the whole domain. Sublithospheric sidewalls have periodic boundary conditions, and the lithosphere sidewalls are fixed. The top and bottom walls are free slip guaranteeing a lateral material flow. We impose a velocity zone into the lithosphere 20 km wide (grey square with arrows, Figure 3.2C) with constant horizontal velocity of 2.5 mm yr^{-1} where particles going inside this zone will move accordingly to the imposed initial velocity. The resulting subduction velocities in

the models are much faster than the timescale for thermal diffusion, and therefore the energy equation is not included [eq. 19]. Surface processes such as sedimentation or erosion are not incorporated. Models are mechanical and the effective viscosity is modified by plastic strain adopting a linear plastic constitutive law disregarding the dependence on temperature, similar to earlier studies (e.g., Capitanio et al., 2006; Schellart et al., 2013). The effects of the thermal regime will be seen in chapter 4 later in this volume.

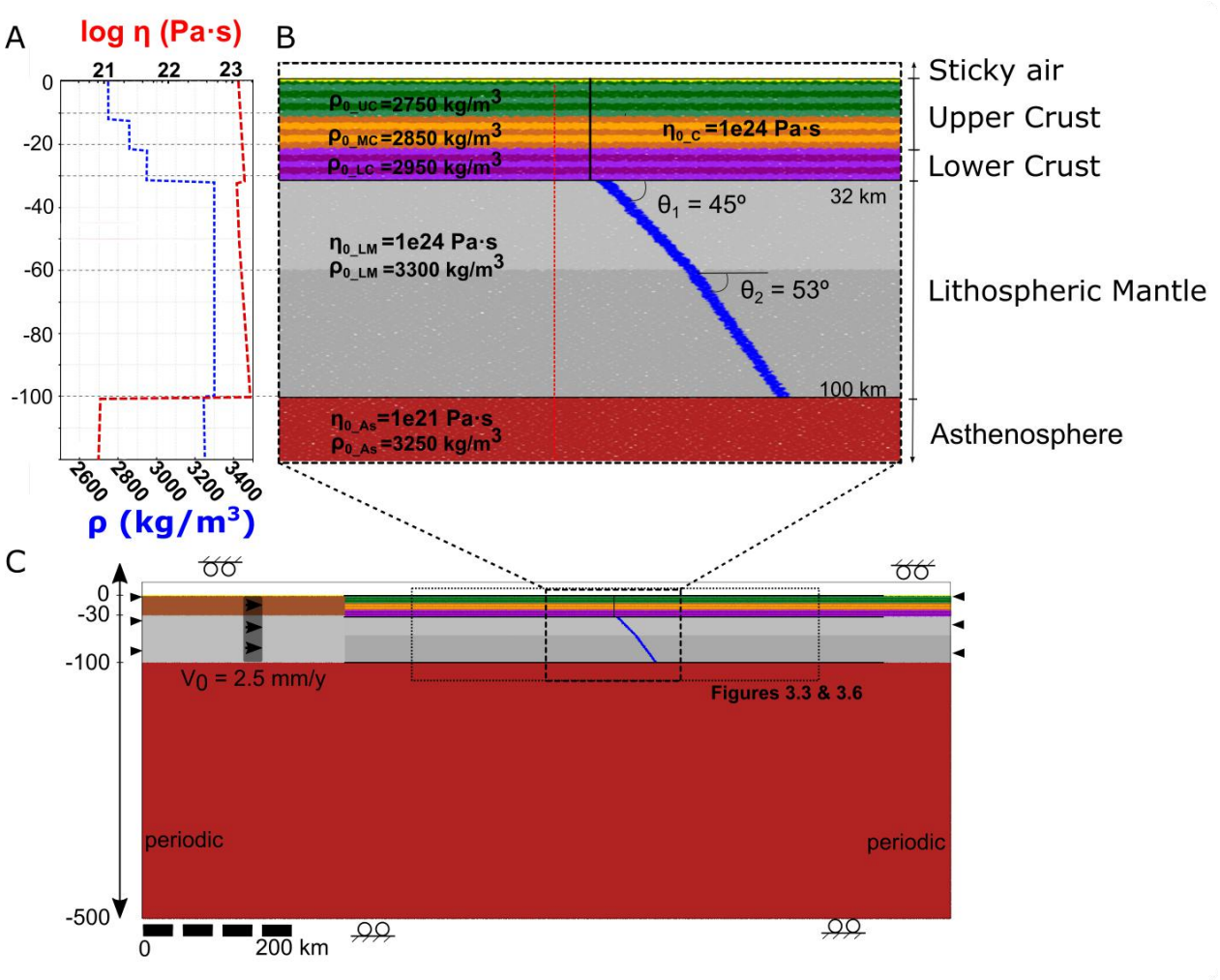

Figure 3.2. Cross-section of the model set-up for the mechanical reference model (M1.0). See Table 3.1 for more material properties. UC, MC and LC stand for upper, middle and lower crust densities. C stands for crust viscosity. LM and As stand for the lithospheric mantle and the asthenosphere respectively. In panel C the rectangular dashed box is the region showed in Figures 3.3 and 3.6.

The crust is set to an initial thickness of 32 km and is divided in two visco-plastic regions: the upper crust (which includes the middle crust) and the lower

crust. The Byerlee failure criteria is used, which allows high stresses to relax by replacing the viscosity into an effective viscosity which is decreased through an iterative procedure [eq. 12]. Therefore, the viscosity has an initial value of 10^{24} Pa.s for all layers, except for the lower crust which is defined in Table 3.1 (first row), and this viscosity can be decreased accordingly with the plastic criteria. Plastic criteria is defined through the cohesion value C_0 at zero pressure (free surface) for each layer, and they are listed in Table 3.1 (rows 2 to 4). The effective viscosity is reduced by the internal friction angle as well, which value is 0.15 MPa km^{-1} (μ_f) [eq. 12]. This value is commonly used for different authors for lithospheric rock failure criteria (e.g., Tan et al., 2002; Gerya & Meilick; 2011; Zlotnik et al., 2014). Red dashed profile of Figure 3.2A shows how this plastic criterion works with $\dot{\varepsilon}_{II} = 10^{-15} s^{-1}$ for the reference model (M1.0). Initial viscosity and densities are printed in Figure 3.2B overprinted on each layer. The lithosphere-asthenosphere boundary is set at 100 km depth, which is suitable for a young continental lithosphere.

Model		M1.0(ref.)	M2	M3	M4	M5	M6
Viscosity log (Pa·s)	**LC**	24	22	21		24	
Cohesion (MPa)	**UC**	30	30	30	30	30	48
	LC	30	30	30	5	5	5
	LM	16	16	16	16	30	16

Table 3.1. List of modified parameters between the models. The viscosity is the cut-off for the upper-middle crust (UC), the lower crust (LC), and the lithospheric mantle (LM). The UC and LM cut off viscosities are 10^{24} Pa.s.

Models include a layer on top of the crust with low viscosity, sticky air (10^{19} Pa·s), acting as a free surface for the crust (details are in Chapter 2). The topography is defined as the contact between the upper crust and the sticky air and it can be followed the topography evolution with this contact changes. To simulate the suture zone between the two continental lithospheres colliding a 6 km wide weak contact is included, enough to induce subduction. This weak zone just imposed in the lithospheric mantle has a lower cut off viscosity (10^{20} Pa·s),

and an angle of 45° from the Moho depth down to 30 km and 53° from there to LAB depth. This methodology incrementing the angle in depth is chosen to simulate the curvature of the slab while subducting. Observations indicate that the pre- collision stage of oceanic lithosphere tends to bend becoming the dip angle more vertical within depth.

3.2 Results

The imposed viscous parameters of the reference model (M1.0) are the same for the whole crust (Table 3.1), i.e., the viscosities cut offs and the plasticity behaviour. It means that there is no decoupling between the upper crust and the mantle. Later, the crustal density and the dip subduction angle parameters are modified from the M1.0 (ref.) model to discard these parameters as the main factors controlling the orogeny type. Then, a series of models (M2 - M6) modifying the parameters of the viscosity are analyzed.

Figure 3.3 shows the model evolution after 5 to 40 My of convergence velocity. From the strain rate second invariant (Figure 3.3e-h) we can see that the weak suture accommodates most of the deformation, favoring the underthrusting of the lithospheric mantle and evolving in subduction (Figure 3.3 a & d). The crust deforms as a whole, and it is slightly pulled down but without being involved in the subduction. During the first 20 My, we can observe that only one anticlinal/synclinal shape develops in the crust just above the suture weak zone (Figure 3.3b). At 30 Ma (Figure 3.3c), a second synclinal structure appears in the incoming plate, while the main structure that remains active is the one above the pre- defined weak zone. The lower crust does not subduct, the crust is thickening in the surroundings of the weak zone generating a mountain root (Figure 3.3d). The incoming lithospheric plate (the left plate) is just deformed in the subduction zone. The overriding plate (the right plate) deforms mostly at crustal levels near the subduction zone, but also the mantle lithosphere is bent (with a wavelength of ~300 km).

This model set up generates, at first stages, two main crustal shear bands of high strain rate just above where the lithospheric mantle subduction initiates

(Figure 3.3e). The pro- shear band (left) has higher strain rates than the retro - shear band (right), and is only located in the crust whereas the retro- shear band reach to half of the mantle lithosphere. These two shear bands are maintained over time due to the transmission of high stress generated by the convergent lithosphere, and the pro- shear band joins the retro- shear band at Moho level after the first 20 My (Figure 3.3f). Most of the deformation is accommodated near the subduction zone, by thickening the crust and increasing the topography. Although initially, the deformation is concentrated on the subduction zone, after several

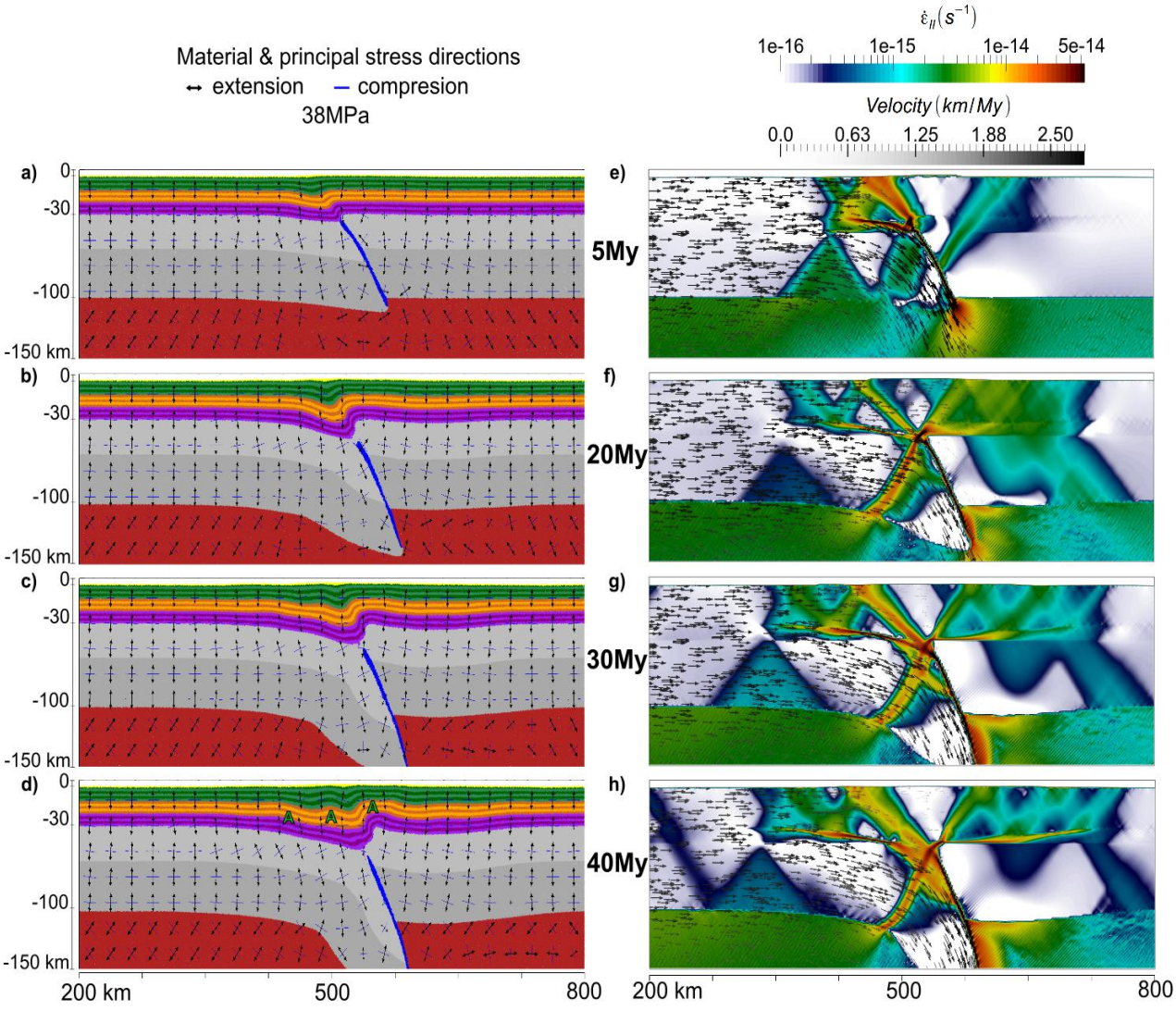

Figure 3.3. Geodynamic evolution of the mechanical reference model (M1.0). Left panels exhibit material deformation (colours) and the principal stress directions (bars for compression and arrows for extension). Right panels show strain rate second invariant (colours) and velocity field (arrows). Capital letter A from d) panel stands for the anticlinal geological term.

million years of convergence the deformation is transmitted away from the collision zone in the direction of the incoming plate.

After 20 My of convergence, the stress is transferred into the overriding plate and with the crust thickening generate a curvature of the whole lithosphere (Figure 3.3d). From 20 My onwards, a secondary shear band forms in the subducting plate about ~75 km further from the main suture (Figure 3.3f). The main stress field is compressional on the horizontal direction, with a few rotations on the subduction zone. The velocities (>3 mm/yr) are in the subducting lithospheric mantle at this scale, and they are the result of the convergence plus the slab pull. (Figure 3.3e-h).

3.2.1. Influence of crustal density variations and dip angle

Crustal density

The crustal density distribution adopted for the reference model (M1.0) is modified in the upper and lower crust to test the effect on the orogenic deformation and the transmission of the strain rate into the plate. Lithologies like granites, cuarcites or sediments can modified the average density in a continental upper crust. Also, the middle and the lower crust can vary their average density depending on the lithologies. For example, previous studies for the Iberian Peninsula suggested values for the lower crust between 2850 to 3100 kg/m^3 from a felsic to a mafic one (e.g., Torné et al., 1996; Teixell, 1998; Tejero & Ruiz, 2002; Gómez-Ortiz et al., 2005; Martín-Velázquez, et al., Carballo et al., 2015; Pedreira et al., 2015). Increasing the density of the upper crust by 30 kg/m^3 (red line, M1.1 model, Figure 3.4), after 100 km of upper crust shortening, topography is similar to the reference model (M1.0, blue line, Figure 3.4), with a maximum above the subducting suture zone and two topographic minimum (basins) at both sides. The resulting base of the crust is also similar to the reference model (blue). Discrepancies relative to the reference model occur in the amount of subduction of the incoming plate. A denser upper crust results with the subducting lithosphere

down to 173 km, meanwhile, the reference model reached 196 km. The resistance to subduct is reflected on the average depth of the entire LAB, which is 5 km deeper than the reference model (red dash line), showing that the deformation of

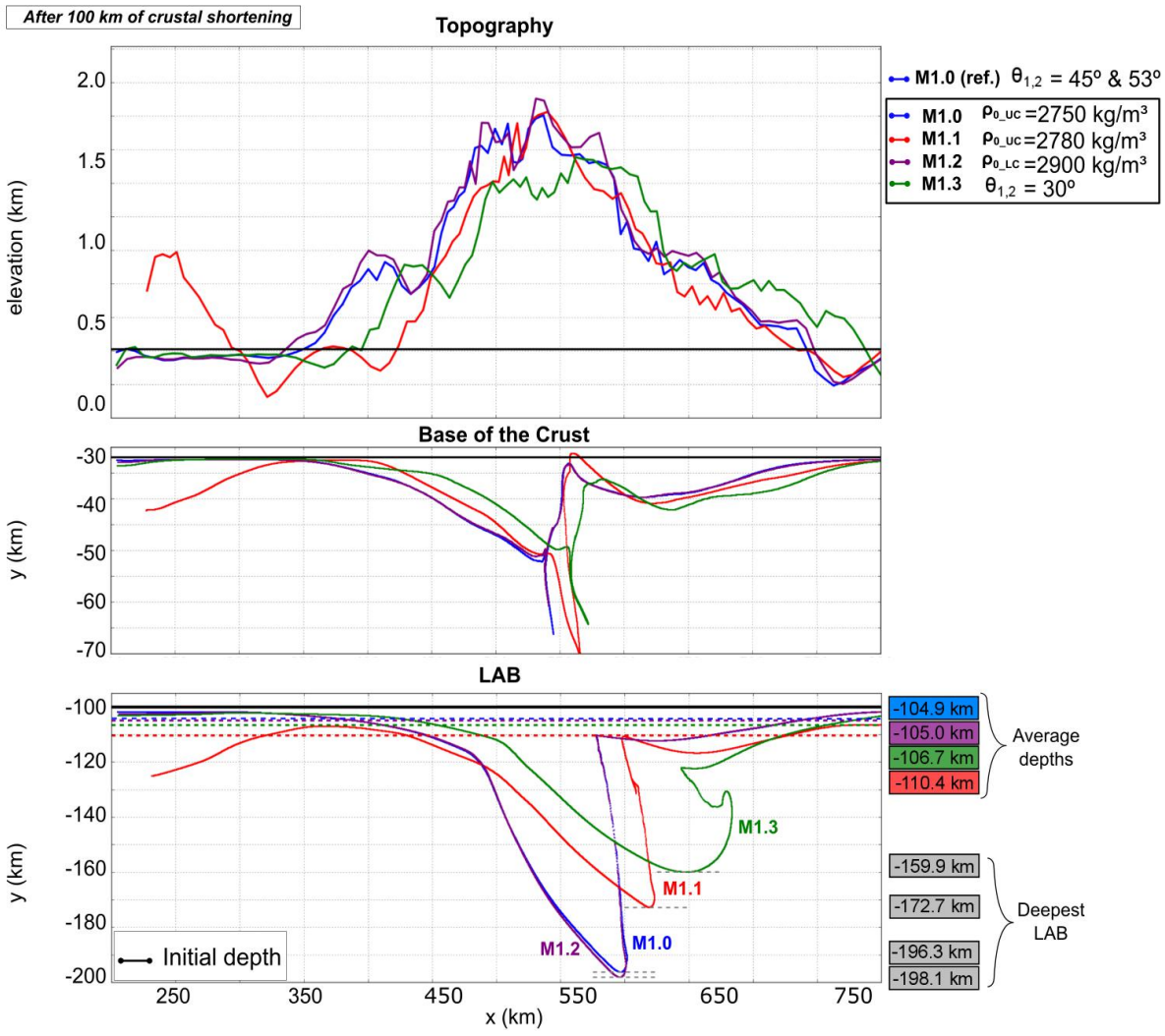

Figure 3.4. Profiles for the topography, the base of the crust depth and LAB depth of the reference model: Blue colour corresponds to values from Table 3.1, M1.0 model. Red colour is for a denser upper crust model M1.1. Purple colour stands for a lower crust less dense model M1.2. For green colour M1.3 model the initial dip angle was changed to 30°. colour boxes indicate the average depth of the different LAB. Grey boxes indicate maximum depth of the subducting LAB (slab).

the lithospheric mantle is spread along the profile and no localized on the subduction zone like in model M1.0. The incoming plate also bends due to subduction resistance, generating a secondary maximum elevation in the incoming plate and lithosphere thickening is accommodating part of the deformation.

M1.2 model with a lower crustal density (from 2950 to 2900 kg/m^3) results with the same slab subduction pattern, the base of the crust thickens likewise M1.0 model, and then, no significant changes on the topography (purple profile, Figure 3.4). Although the densities tested in our study reach the limits of those typically attributed to the crust, the style of deformation remains that of a double-vergent orogen. Therefore, it can be concluded that cortical densities do not play a main role in the deformation style of the orogens.

Subduction angle

Subduction angles in nature vary from 10 to 70° and there could be a correlation between that angle and how the deformation of the lithosphere accommodates (e.g., Lallemand et al., 2005; Schellart, 2008). Figure 3.4 also shows the results of model M1.3 considering a lower angle (30°) of the subduction zone for the entire lithospheric mantle are shown (green lines). Incrementing the angle between the two colliding lithosphere implies a larger contact subduction channel, and could favour the coupling between the lower and upper plates. Based on the results, a low angle favors the underthrusting rather than subduction, resulting with higher displacement of the lower plate to the right below the upper plate, but remaining shallower. However, the style of the formation is still a double vergence orogen. After 100 km of crustal shortening the deepest LAB (at 160 km deep) is shallower than in the reference model and it is displaced 50 km more to the right. As a consequence, the maximum topography is also displaced a few kilometers to the right and it is about 300 m lower.

3.2.2. Influence of viscosity contrast between crustal layers

The lower crust couples the lithospheric mantle with the upper-middle crust and it plays a significant role in the mode of lithosphere evolution. To analyse this coupling and the resulting mode of deformation we test several models changing

the viscosity contrast between upper-middle crust, lower crust and lithospheric mantle.

The lower crust viscosity cut off is reduced in models M2 and M3, compared to the reference model (M1.0) (Table 3.1). A weak lower crust should act as a décollement, favoring the mantle-upper crust decoupling and the not transmission of stresses between the lithospheric mantle and the upper crust.

The lower crustal viscosity of model M2 is two orders of magnitude lower than the cut off viscosities of the upper crust and lithospheric mantle. This model shows that these viscosity contrasts are not enough to effectively decouple the mantle from the crust. Consequently, the subduction of the lithosphere barely changes the deformation pattern; it is similar to the reference model and still has the double-vergent style of deformation, with a maximum topography and two basins besides (red colour, Figure 3.5A).

In model M3, the lower crust viscosity cut off is three orders of magnitude lower than those from the upper-middle crust and the lithospheric mantle. In this case, the lower crust acts as a décollement and some crustal folding appears. After 40 My of tectonic compression, the maximum topography forms above the subduction zone but it also develops away from the collision zone several crustal folds with an average wavelength of 54 km (Figures 3.5 and 3.6). Models M1.0 and M2 have two basins at about 250 km at both sides of the orogen, at sea level altitude. M3 model instead of two basins, presents some folds in both sides of the main orogen, about 500 m above sea level at the pro-side (incoming plate) and 300 m above sea level in the retro-side (overriding plate). Although all these changes, the depth of the crust is still similar to M2 (Figure 3.5B). Some differences are observed on the subduction zone, the subducting lithospheric mantle is dragging part of lower crust, pulling the base of the crust in this area (Figure 3.6b).

Differences between M1.0 to M3 are on the cut off viscosities, in the next three models (M4 to M6) I will analyse the effect of changing the plastic cohesion that decrease the effective viscosity (see Table 3.1). In these models, M4-M6, the plasticity cohesion for the lower crust is reduced by a factor of 6. It means that the lower crust can sustain lower stresses and it will reduce its viscosity in the areas

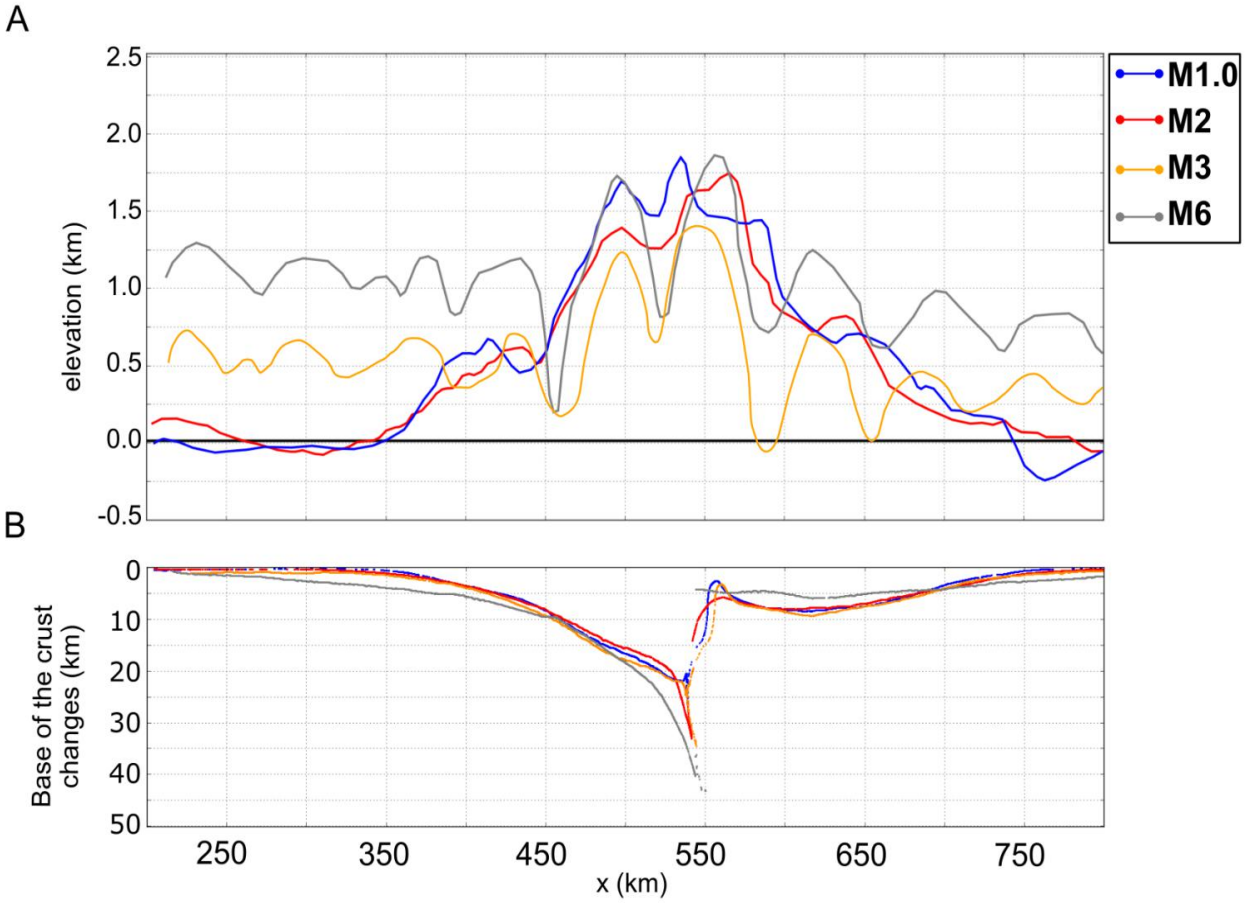

Figure 3.5. After 100 km of upper crust shortening A) Topography and B) base of the crust changes for models M1.0(blue), M2 with a 10^{23}Pa·s as maximum viscosity cut-off (red), M3 with 10^{22} Pa·s as maximum viscosity cut-off (orange) and M6 with a softer lower crust reduced by the plasticity cohesion (grey) (see Table 3.1).

under high stresses. It will result in an uncoupled mantle-upper crust near the subduction suture and, therefore, deformation is better transmitted through the lower crust to further distances.

The resulting topography of M4-M6 models is similar, Figure 3.5 shows M6 model as an end-member crustal folding style of deformation. M6 has the highest contrast cohesion between upper-middle and lower crust (and between upper-middle crust and upper mantle), where the lower crust is softer and the upper-middle crust is stronger compared with M1.0 (ref.). In model M6, the upper-middle crust mode of deformation is principally by folding, and the topography shows folds of around 50-60 km wavelength (Figure 3.5).

Average topography is higher in the incoming plate than in the overriding, M6 has the highest average altitude among all the models. Also, the base of the crust is deeper in the incoming plate than in the overriding one. The subducting lithospheric mantle of this model is dragging the weak lower crust down to ~70 km depth (Figure 3.6). The maximum slab depth reached by M6 is 210 km, in contrast to the 196 km from M1.0. overriding lithospheric mantle of M6 remains flat without the sinusoidal deformation observed on M1.0 (Figure 3.6). Double vergent models have thicker crust and lithosphere of the overriding plate and crustal folding models have thicker crust and lithosphere in the incoming plate.

Figure 3.6 shows the lithosphere structure and strain rates from models M1.0,

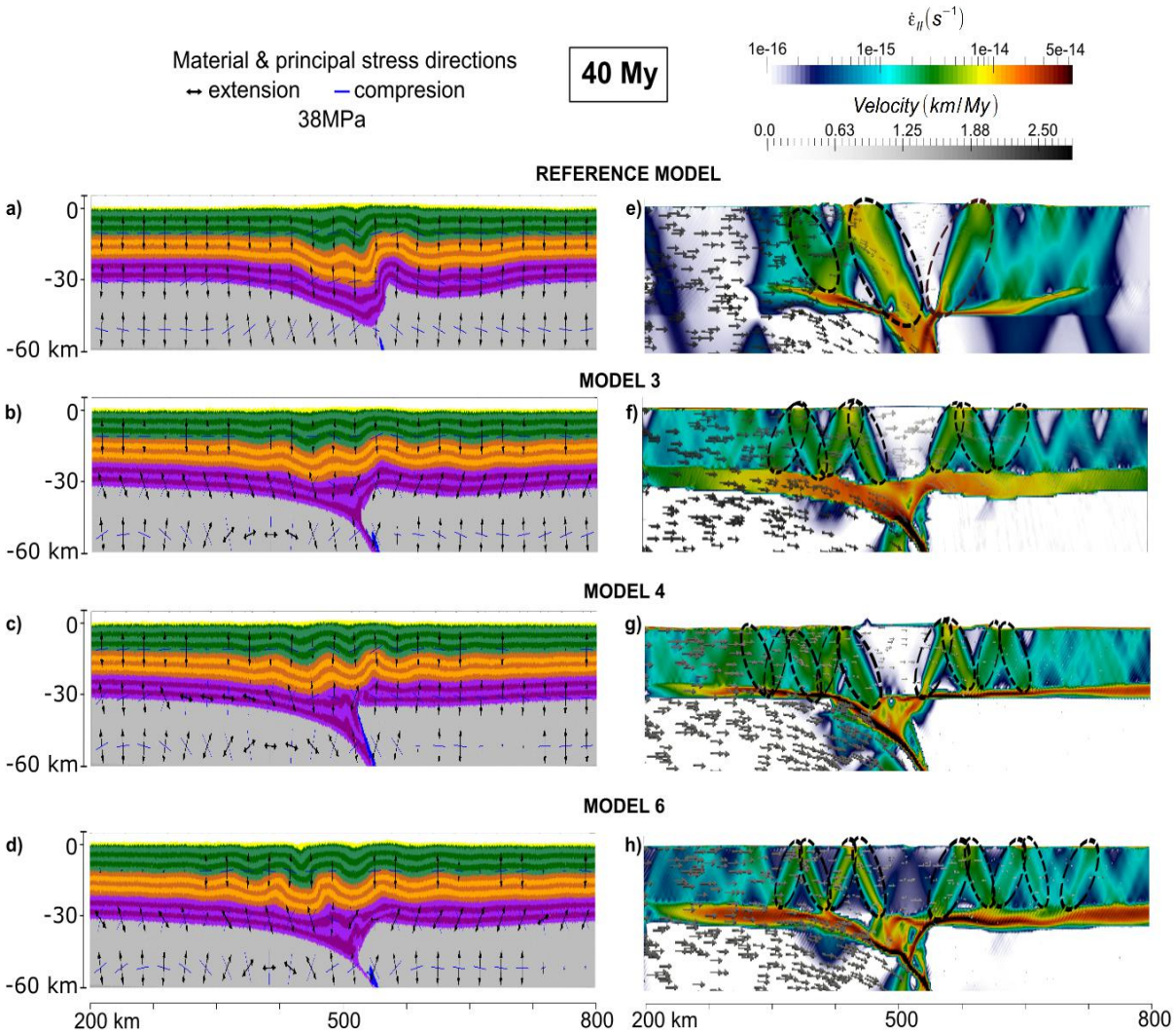

Figure 3.6. Left panels show the different layers with the principal stress direction. Right panels are the strain rate second invariant distribution with velocity field. For a double vergent model (M1.0), and three crustal folding models M3, M4 & M6. Dashed lines locate the main shear bands. Vertical exaggeration x3.

M3, M4 and M6 after 40 My of convergence. The strain rate observed in the lithospheric mantle of the overriding plate from M3, M4 and M6 models is practically zero ($<10^{-16}$ s^{-1}), and on these models the main mode of deformation is by crustal folding. Strain rate is reducing the effective viscosity in the surroundings of the subduction zone, where the lower crust is being transported and subducted, showing a higher viscosity reduction in models with upper crust folding. In these cases, the lower crust acts as a décollement, the lithospheric mantle and the upper-middle crust get decoupled, and the crust is deforming independently, generating pro shear bands and retro shear bands.

A main difference between M3 and M4-M6 is the thickness of the weak layer at crustal base levels. In M3 this layer is thicker and encompasses lower crust and lithospheric mantle, while in M4 and M6 all the strain is localized at the base of the lower crust (Figure 3.6f-h). Shear bands appear first in the upper crust in the surroundings of the subduction zone and more retro shear bands appear in the overriding plate over time. In general, when the lower crust is weaker enough to act as a detachment level, the decoupling of the mantle and upper crust favors the dragging of the lower crust into the mantle through the subduction channel (reaching 60 km depth) and principal stress directions in the lower crust of the incoming plate shows extension rather than compression.

This uncoupled deformation is observed also in Figure 3.7. Figure 3.7 shows the position of an initial vertical line after 100 km of shortening. Models favoring the folding deformation are those that have the highest decoupling between crust and mantle (M3 to M6), resulting in a difference displacement of ~20 km between the upper and lower crust (above and below the star, Figure 3.7). Double vergent models are those with the coupled crust and therefore the initial vertical markers move by nearly the same distance. The lower-crust markers of the reference model travel even further forward, dragged by the lithospheric mantle. From the uncoupled models, we can see the different displacement on the lower crust between the material attached to the upper crust and the one dragged by the mantle.

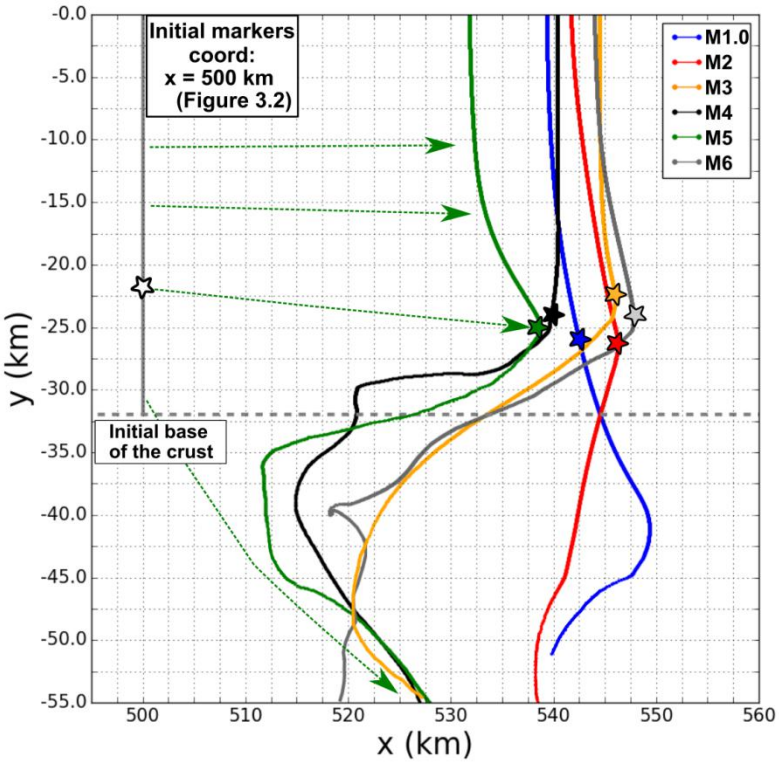

Figure 3.7. Crust markers after 100 km of upper crust shortening. Initially the line is vertical at the coordinate x of 500 km (black vertical line in the crust in Figure 3.2 B). Each line colour shows the position of the vertical black line after 100 km of shortening for the different models. Stars indicate the upper-lower crust boundary.

Summary of modeling results

The results allow us to identify two end member models for orogeny deformation: the **double-vergent orogenic wedge** (Figure 3.8A) and **the crustal folding** response (Figure 3.8B). The double-vergent deformation style is best represented by model M1.0 and is characterized by two main shear bands verging with opposite dip from the lower crust to the surface. Both shear bands form in early stages, rooting where the lower crust subducts and developing upwards to the surface with similar angle. In this orogeny deformation model, maximum topography occurs just above the subducted lithosphere, and the mountain range rises up with one principal pop-up structure and additional little pop-up structures, generating a foreland basin and the corresponding retro-land basin

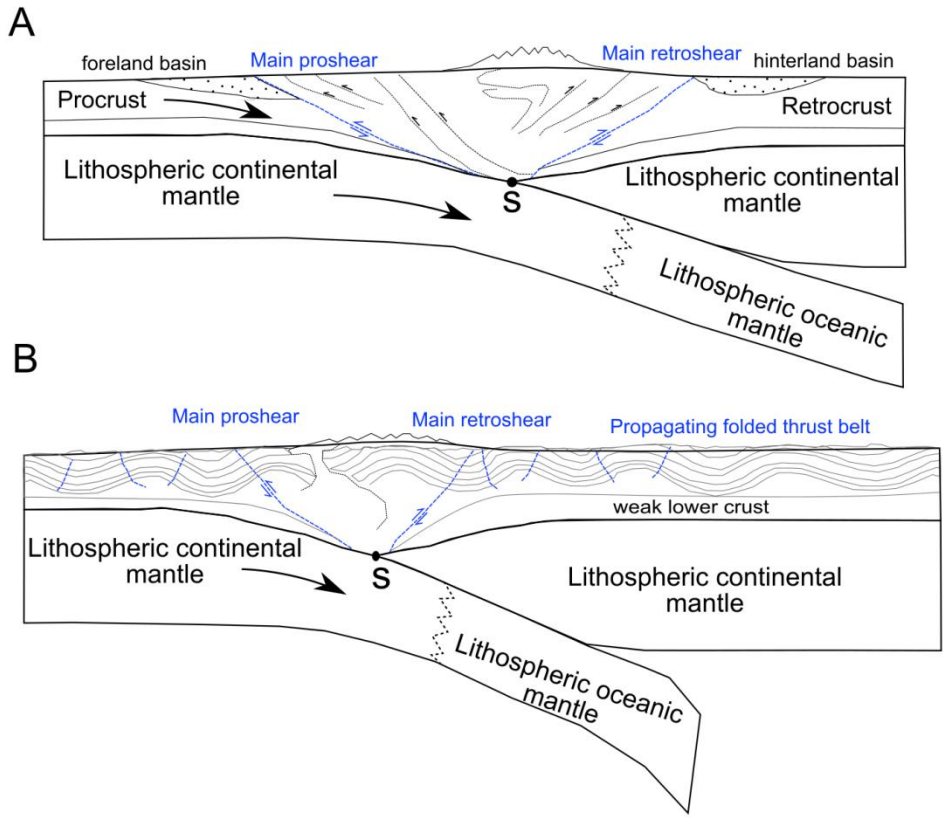

Figure 3.8. A) Scheme of a double-vergent orogen (modified from Willet et al., 1993). B) Upper-middle crustal folding scheme (this work).

In nature, structures are more complex, such as in the Eurasian Alps or Pyrenees where during compression, lower crustal material is transported into the upper plate along the retro-shears, which are crustal-scale vergent back thrusts. In the case of the Pyrenees, there is a limited subduction of the Iberian lithosphere beneath the Eurasian plate where initial pop-up structures evolve to an antiformal-stack (e.g., Muñoz, 1992; Grool et al., 2019). Figure 3.8B shows a distribution of shear bands more complex than Figure 3.8A and further from the colliding area. In this case, we do not obtain a double-vergent orogen, but we can classify this type of deformation as crustal folding at initial steps of the collision. It has an initial growth with a pop-up structure or double-vergent model with two main shear bands but lately deformation starts to accommodate in the pro- and retro-crust. I have presented in this section several models in which modifying a specific initial mechanical parameter leads to a change from a double-vergent orogen to crustal folding.

Now that the role that has the density of the crust, the deep subduction angle, and the viscosities in the distribution of the deformation have been observed, in the next section I study the effect of weak structures inherited in the cortical layers in the way orogens evolve. For this purpose, we are inspired by the geological scenario of the Pyrenees.

3.2.3. Influence of a décollement in orogen deformation

Previous studies investigated how décollements or detachment levels influence the way orogens evolve (e.g., Beaumont et al., 2000; Bonini, 2003; Ruh et al., 2012). Bonini (2003) noted the differences in crustal fold-thrust-belts evolution with two end-members of models, the outward fold propagation (OFP) with high viscosity décollement ($\sim 10^{19}$ Pa·s) and passive roof thrust (PRF) with low viscosity décollement ($\sim 10^{16}$Pa·s). I focused on the effect on the style of deformation of localized décollements within the crust and how affect the propagation of deformation in the direction of the incoming plate. The set up was inspired by the style of deformation in the Pyrenees in a similar way to the series of numerical models done by Beaumont et al. (2000). M2 model's viscosity cut-off provides a lower crust coupled with the upper mantle, allowing the crust to subduct as observations suggest (e.g., Muñoz, 1992; Teixell, 1998). Therefore, the plastic criteria for model M2 is adopted (Table 3.1) and two décollements are introduced (Figure 3.9). One detachment is shallower (4 km depth), equivalent to the very low viscous Triassic salt layer accounted for in Beaumont et al. (2000). For the other mid-detachment level (20 km depth) we adopt a cohesion value of 1 MPa. This cohesion value ensures the plastic deformation of the imposed detachment level and the preferential localization there of strain. Beaumont et al. (2000) used a coupled lower crust with the mantle to subduct the lower crust, as the interpretation of the ECORS seismic profile suggested for the Pyrenees. Their models also introduced low viscosity layers to decouple lower crust with upper

crust, and one shallower sub-horizontal layer simulating Keuper material (Triassic salt). Their configuration serves as a starting point to understand how the detachment levels control the deformation pattern. One drawback in Beaumont's model was that they did not explicitly incorporate the deformation of the mantle, but had to include a load to simulate the isostatic compensation, via a thin-plate flexural lithospheric model. In contrast, our model domain for Underworld reaches to 500 km depth and the lithospheric mantle deforms and subducts in a way consistent with the deformation of the crustal domain. We also increased the model resolution (0.8 x 1.2 km) to have more accuracy and see the influence of these detachment levels as inherited weak zones. We run two models: (1) The first model (M2.1) inferred from Figure 3.9A, where the mid-detachment level overpass the subduction suture 50 km into the hinterland plate (light blue polygon with black and blue dashed lines named as "Extended detachment"). Final configuration after ~150 km of upper crust shortening for the M2.1 model is in Figure 3.9B. (2) The second model (M2.2), the right boundary of the detachment level is 50 km

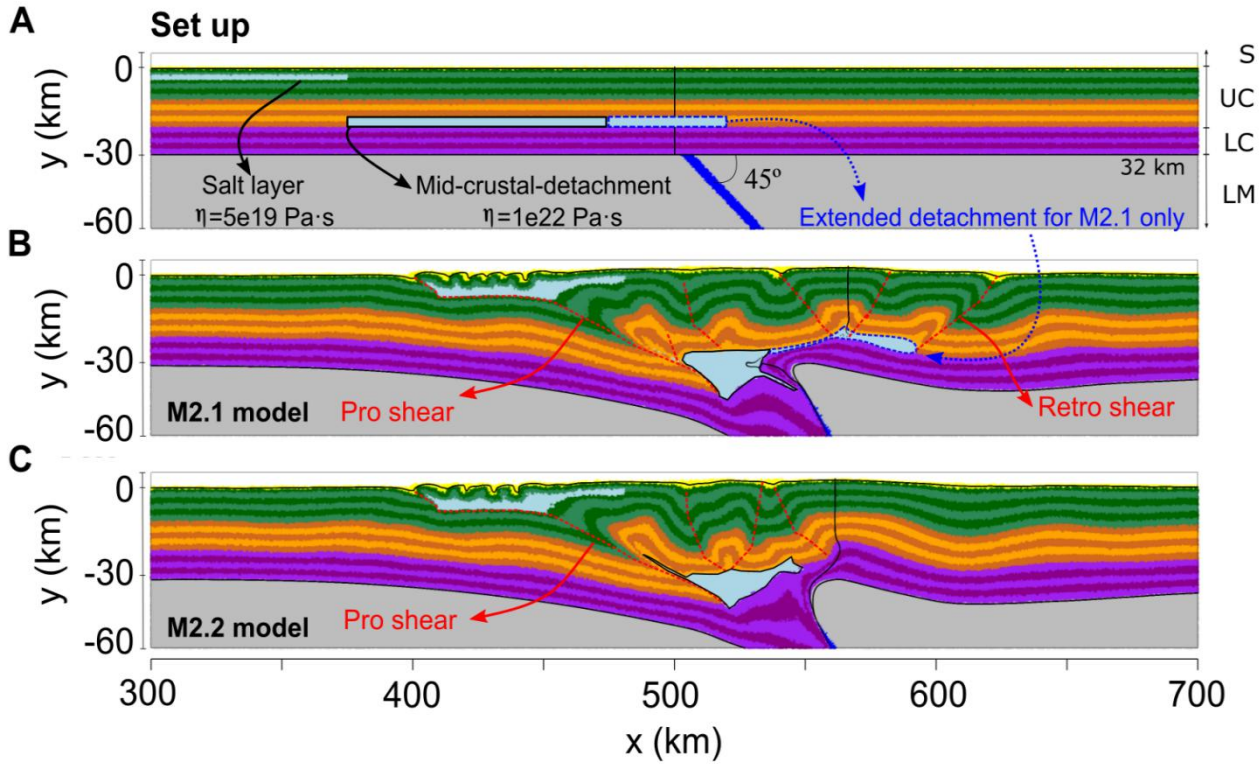

Figure 3.9. A) Set up with two detachment levels for models M2.1 and M2.2. The weak layer in the upper crust (representing the Mesozoic salt) is identical for both models, whereas the the mid-crustal detachment level is 50 km longer in M2.1. In M2.2 the mid detachment level does not overpass the center of the collision (dash blue line). B) Final stage for the M2.1 model. C) Final stage for the M2.2 model. Both reach ~150 km of upper crust shortening.

before the subduction suture (without the "Extended detachment", light blue polygon with blue dashed lines, Figure 3.9A). Figure 3.9C is the final configuration of the M2.2 model. The purpose is to see how affects the size of these levels and position in the later evolution of the orogen what is a matter of factor in the Pyrenean Chain which its evolution is affected by the hyperextension of the crust between the Iberian microplate and the Eurasian plate before the Cenozoic compression (Jammes et al., 2013; Grool et al., 2019).

After ~150 km of crustal shortening, the amount of shortening estimated for the separation between Iberian and Eurasian plate (Olivet 1996; Beaumont et al., 2000; Rosenbaum et al., 2002b; Vissers & Meijer, 2012b), the results obtained for both set ups are distinct. In both, the shallower detachment level generates a small upper crustal folding just above the layer. This folding does not happen in the entire longitude of the detachment and it is characterised by a small wavelength of ~15 kilometers. Both develop a main pro- shear thrust (see Figure 3.9 B and C), that connects both detachment levels, and both develop similar thrust units in the pro-direction. Discrepancies appear in the hinterland of the overriding plate. In M2.1 model (Figure 3.9B) a main retro-shear develops, and a pop-up structure is generated just before the subduction zone. In contrast, in M2.2 model the retro-shear does not develop, just a slight crustal folding. Both models present folding in the overriding crust in the right side, ~100 km in wavelength in the base of the crust (limit purple-grey colour), and lower values of ~65 km for the upper-middle crust (green and brown colours).

In this chapter we have seen two end-members models and the relevance of the viscosity in the way orogens evolve in a continental collision scenario, as well as the how weak zones or décollements modify orogens evolution and transmit the deformation far from the collision zone, and compared to the Pyrenean Chain. I will apply this knowledge to a N-S transect in the Cantabrian Chain, which is the orogeny situated westwards of the Pyrenees and influenced by the same tectonic movements.

Chapter 4

2D Numerical models along a lithospheric transect of North Iberia from the Central System to the Bay of Biscay

The present-day topography and structure of the Iberian Peninsula is a consequence of the last tectonic events since Cretaceous times. During the Cenozoic, tectonic compression uplifted the mountain ranges in the north and south boundaries of the Iberian Peninsula and the intraplate chains, sometimes with a high difference in elevation between the top of the chains and the endorheic basins. For example, Cenozoic sedimentary thickness in the Duero basin is ~3 km or 2.5 km in the Madrid Basin (central sector of Tagus Basin, Figure 4.1) and the Central System has a vertical throw over the Madrid Cenozoic basin of 5 km (e.g., Gomez-Ortiz, et al., 2005; de Vicente, et al., 2007; de Vicente & Muñoz, 2012; Fernández-Lozano, et al., 2015; de Vicente et al., 2018). The Central System is a linear chain extending from the central part of Iberia to its western margin with a NE-SW orientation. It is considered to be a crustal pop-up with uplifted Variscan basement (Vegas et al., 1990). This chain has two adjacent basins, the Tagus basin southwards and Duero basin northwards. The uplift of the Central System was controlled mainly by two reverse faults inherited from the

Variscan orogeny (Arthaud & Matte, 1975). Some authors propose high-angles faults implicating the entire crust (e.g., de Vicente & Martín-Muñoz, 1993).

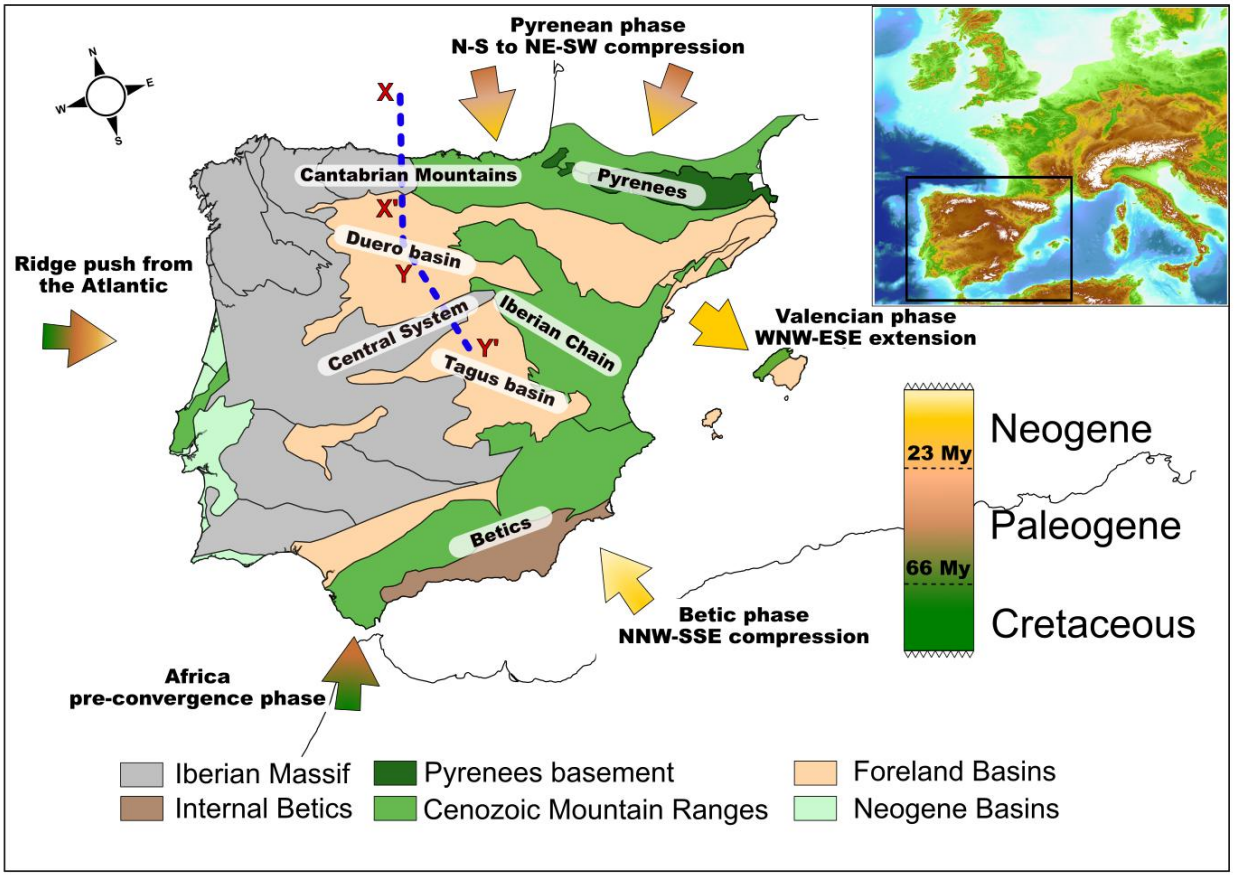

Figure 4.1. Present simplified geological domains in the Iberian Peninsula. Present topography in the upper right corner from Etopo data base. Arrows indicate the most important tectonic movements and their colors correspond to the timing of the events. Dash blue line corresponds to the transect modeled in this study.

Specifically for this area, de Vicente et al. (2007), suggested that recent uplift in the Central System area can be related to isostatic rebound generated by crustal thickening. In addition, other previous studies connect the NW-SE Betic compression in Neogene times to the onset of the regional flexure in the area (Andeweg, et al., 1999a; De Bruijne & Andriessen, 2002).

Likewise, there is an open debate on the causes of the high average elevation of the Iberian Peninsula. Some studies have suggested a mechanism consisting on the buckling of the Iberian plate as responsible for the high topography of Iberia (e.g., Fernàndez-Lozano et al., 2012) or a uniform uplift of the Iberia micro continent

after the complete erosion and formation of the Iberian peneplain at the end of the Tertiary (Vázquez Hoehne, 1992). Other studies suggest that the tectonic compression generated a folding of the entire lithosphere (e.g., de Vicente et al., 2007; Cloetingh et al., 2002). Nevertheless, the different shortening generated in the lower crust (derived from a north dipping subduction under the Cantabrian Mountains) relative to the upper crust (based on structural tectonic restorations) cannot be explained by these theories. Therefore, it has been suggested several detachment levels that transmit the stress from the edges towards the interior, raising intraplate mountain chains (Banks & Warburton, 1991; Quintana et al., 2015). At the same time, the inherited heterogeneities have a strong influence on the intraplate deformation, heterogeneities like rheological variations acquired during different tectonothermal events (Cloetingh et al., 2002; Vergés & Fernàndez, 2006) that results in lateral stresses variations. All these theories have to explain the different timing of the uplift of the chains. Many several studies suggested that the uplift started in the north boundary and then migrated to the south with the accommodation of deformation generated by the tectonic compression (Figure 4.1).

Several mechanisms have been proposed to describe the transmission of intraplate stresses towards the interior of the Iberian Peninsula (see Chapter 1). Large-scale lithospheric folding can be one of the main mechanisms responsible for the propagation of tectonic deformation away from active plate boundaries in Variscan structural lithospheres (Cloetingh et al., 2002). A mid-crustal detachment level could shift the location of the deformation from the edges of the plate towards the interior and may explain the discrepancies in shortening quantifications for the upper and lower crust in the Cantabrian Mountains (Banks & Warburton, 1991).

Using 2D numerical geodynamic models in this chapter, I aim to understand the accommodation of the deformation due to the tectonic compression during the last 65 My and the transmission of this deformation to inner parts of the northern Iberian Peninsula. I will also try to adjust the overall structure of this passive margin, where the lower crust was hyperextended during the Cenozoic,

southwards underthrust during the Alpine compression, forcing the northward subduction of the Iberian middle-lower crust. This brings us to a subsequent question currently under debate and to which we can bring a new light: how can we explain the higher average elevation of the Iberian Peninsula relative to the continental Europe? I will analyze the mechanisms involved in the generation of the relief of the Iberian Peninsula as well as the configuration of the Moho discontinuity and the lithosphere-asthenosphere boundary in a transect crossing the northern part of Iberia, from the Cantabrian Zone to the Tagus Basin (Figure 4.2). I analyse the conditions necessary to obtain the estimated shortening from previous works for the different areas and the geodynamic timing of the two mountain chains.

The section goes from the Bay of Biscay to the Tagus basin, crossing the Cantabrian Mountains, through the Duero basin and the Central System. The model configuration has been constructed using the geological restoration done by Pedreira et al. (2015) in the Cantabrian Zone and by de Vicente et al. (2009), in the Central System (Figure 4.2). Martín-Velázquez et al. (2012) modeled the deformation patterns during the Cenozoic in the Central System introducing thermo-mechanical heterogeneities that generate variations in strength of the lithosphere which favors the irregular thickening and folding. Pedreira (PhD Thesis, 2004) performs a series of geodynamical numerical models for the Cantabrian margin, where inherited Mesozoic structures from the Cretaceous hyperextension exert considerable control in the Alpine deformation with thin Iberian margin geometry and a limited extension of a detachment level located in the roof of the lower crust.

In this chapter, I will attempt a series of 2D mechanical (section 4.1) and thermo-mechanical (section 4.2) models, to relate the way of deformation between both mountain ranges, and correlate the transmission of stresses from the boundary to the interior. I will also discuss the different shortenings at crustal levels below Cantabrian Mountains and the Central System adjusting the overall lithosphere structure.

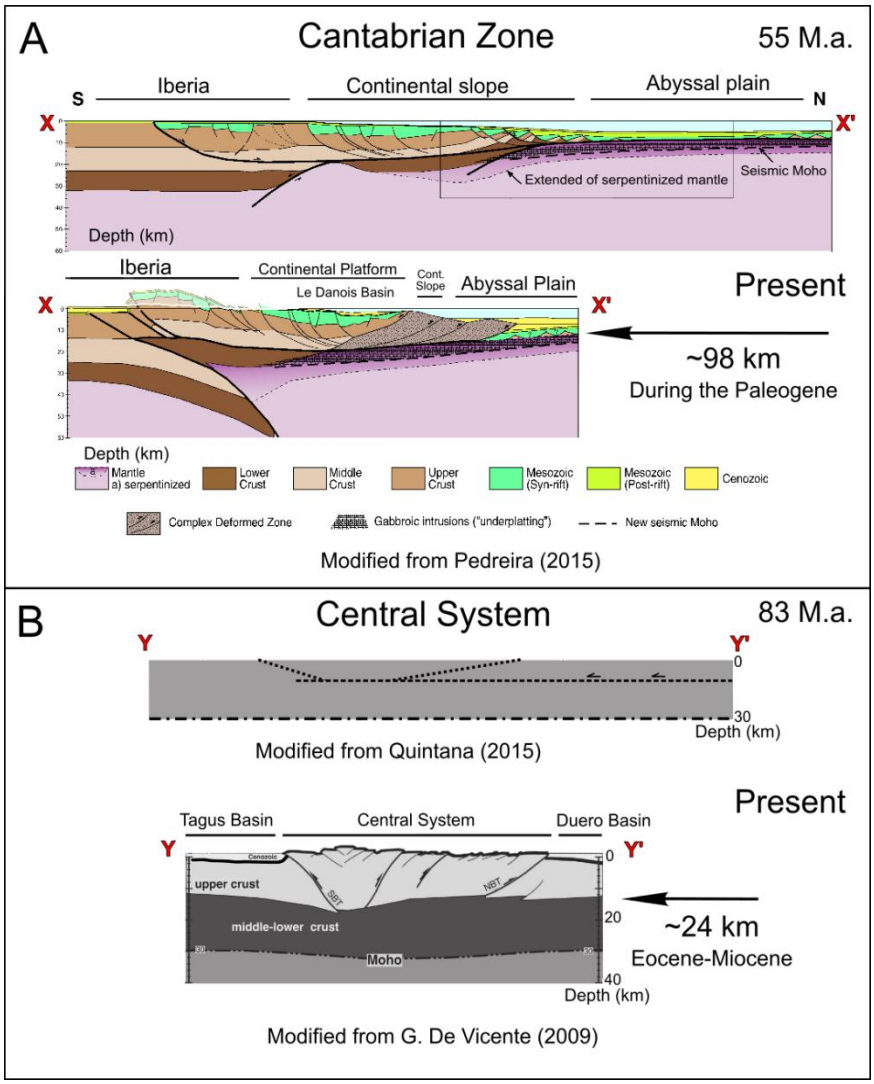

Figure 4.2. A) Restoration of north transect (XX' in Figure 4.1), the Cantabrian Zone modified from Pedreira et al. (2015). B) Restoration of the Central System Zone (YY' in Figure 4.1) with a mid-detachment level with low-angle faults and present structural configuration of the Central System modified from Quintana et al. (2015) and de Vicente et al. (2009).

4.1 Mechanical models

The initial set up for all models in this chapter are inspired by the geological restoration done by Pedreira et al. (2015) in the Cantabrian Mountains, and by Quintana et al. (2015) in the Central System (Figure 4.2). The transect goes

through the Bay of Biscay to the Tagus basin crossing the Cantabrian Mountains, the Duero Basin and the Central System (Figure 4.1 blue dashed line). We define three lithospheric domains: The Iberian domain is subdivided into 1) Central System and 2) Duero basin; and the Cantabrian zone as a 3) hyperextended continental margin.

In this section, the rheological behavior of different layers are not temperature dependent, the models are discuss according their mechanic parameters. Using the Underworld code described in chapter 2, the main parameters that control the way the deformation accommodates during the tectonic compression are analyzed: i) **décollements**; ii) the plasticity in the lithosphere; iii) the crustal density and iv) inherited weaknesses from the Variscan orogeny.

The 2D numerical model configuration is shown in Figure 4.3. The model section is 1400 km long by 680 km deep and is discretized in 576 (horizontally) by 320 (vertically) uniformly distributed cells, being the resolution of the model 2.4 x 2.1 km. The numerical set up thus discretizes the model domain in a total of 184320 cells with 15 particles per cell, which gives an total initialparticle number of 2764800. In all the models there is an upper thin layer of 20 km of very low

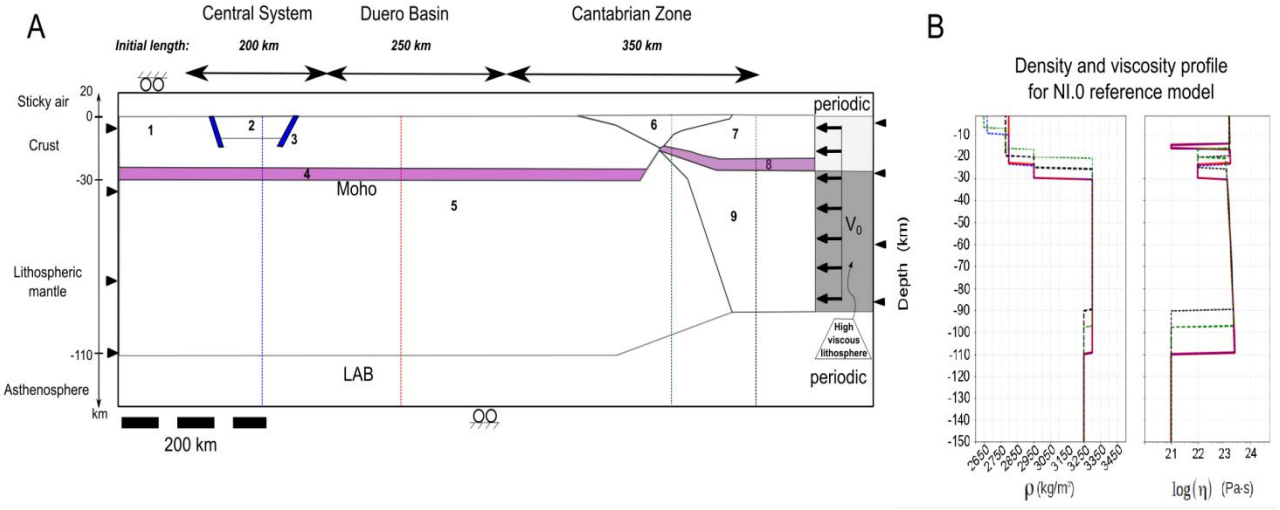

Figure 4.3. A) Reference model (NI.0) geometry showing the layering thickness of the different bodies which densities and viscosities are listed in Table 4.1. Constant velocity of 2.5 mm/y, it is an indentation of a high viscous mantle of 10^{24} Pa·s without plasticity criterion to prevent high deformation. B) Density and viscosity profiles of four different sections of the reference model (dashed lines Figure 4.3A). Note that the viscosity profile corresponds to values in the model and is computed based on a constant strain rate ($10^{-15}s^{-1}$). Vertical axis is exaggerated.

viscosity (10^{18} Pa·s) material or sticky air. Between the crust and the sticky air there is a 500 m thick sediment layer with low viscosity of $5 \cdot 10^{22}$ Pa·s and density of 2550 kg/m^{3,} where we embedded horizontal markers to follow the evolution of elevation. Although, the sticky air is a proven method in order to consider the crust as a free surface (e.g., Crameri et al., 2012), I introduce the sediment layer because the particles to prevent the sticky air dragging crustal particles which spring out. All models include two types of lithospheres, the Iberian and the Eurasian lithosphere. On the left side (south), the Iberian lithosphere is composed by an upper-middle crust layer (IC, 22 km thick, see Figure 4.3 and Table 4.1), a lower crust (ILC, 8 km thick), and a lithospheric mantle (IM, 80 km thick). In the Central System domain, there is a low-density upper crust of 10 km thick acting as a granitoid block (GB-body 2, Figure 4.3A). The lithosphere on the right side (north) simulates a thinner Eurasian lithosphere with an upper-middle crust (EC, 20 km thick), a lower crust (ELC, 5 km thick), and a 65 km thick lithospheric mantle (EM). Below the LAB, the asthenosphere has constant low viscosity of 10^{21} Pa·s and a constant density of 3250 kg/m^3. Between the two lithospheres in the Cantabrian Zone (CC-body 6, Figure 4.3A), there is a less dense crust simulating the high concentration of Mesozoic sediments. This model is the first attempt to understand how the deformation is accommodated assuming a simple model geometry inspired by the reconstructions of north Iberia from previous studies.

The boundary conditions on top and bottom walls are free slip, and on sidewalls periodic ensuring a horizontal flux of particles. Convergence is simulated with a constant velocity zone (of 2.5 mm/y) prescribed in a high viscous lithosphere at north of the Cantabrian Zone domain. The modified parameters for each model are in Table 4.1. The reference model corresponds to geometry shown in Figure 4.3.

Since the different model runs deform at different rates of deformation in various domains, we need some strategy to decide when to stop the model in order to compare results between models. The comparison between models will be done at the time when the accumulated shortening in the Cantabrian zone is ~98 km, it is between X and X´ from Figure 4.2. Previous studies evaluated the total

shortening in the Cantabrian-Basque zone with values vary between 85 and 98 km (see chapter 1). Total upper crust shortening of ~98 km was estimated from geological restoration by Gallastegui (2000) and more recently supported by seismic and geophysical modeling by Pedreira et al. (2015). Most of the shortening of the Cantabrian Mountains occurred between 60 to 20 Ma, and the shortening of the Central System between 50 to 10 Ma. To reach in the model 98 km of shortening in approximately 40 My, the imposed initial velocity in the northern part it's an average velocity of the area for the total shortening, implying a much more manageable to control the Cantabrian shortening in the correct timing. Final consideration is that all the models start at t=0 My.

	Bodies	Lithospheric Unit	ρ_0 (kg·m^{-3})	C_0 (MPa)			μ (MPa·km^{-1})		
				NI.0	NI.2	NI.3	NI.0	NI.2	NI.3
Reference Model- NI.0	1	Iberian Crust (IC)	2800	30	30	30	0.15	None	0.3
	2	Granitoid Block (GB)	2670						
	3	Faults (F)	2670	-	-	-	-		-
	4	Iberian Lower Crust (ILC)	2950	30	30	30	0.15		0.3
	5	Iberian Mantle (IM)	3300	16	10	30	0.3		0.15
	6	Cantabrian Crust (CC)	2650	30	30	30	0.15		0.3
	7	Eurasian Crust (EC)	2780			40			
	8	Eurasian Lower Crust (ELC)	2950			40			
	9	Eurasian Mantle (EM)	3300	16	10	30	0.3		0.15
NI.1	10	Décollement	2800	-	-	-	-	-	-
NI.3	11	North Weak zone (WK)	3300	-	-	1	-	-	-

Table 4.1. Density and plastic parameters adopted for each body defined for the models in this setion. The plastic parameters are the cohesion (C_0) and the frictional coefficient (μ) from equation 12 (Chapter 2). NI.1 and NI.3 models incorporate new bodies. Green shade corresponds to changes in the plastic parameter column for each body. Note that NI.2 model does frictional coefficient is equal to 0 and the Byerlee's law becomes only dependent on cohesion term

To facilitate comparison between model results, we choose a reference model that has reached these 98 km of total shortening in the Cantabrian Domain in 68

My. This reference model corresponds to the parameter values listed in Table 4.1. The shortening in the Duero basin is 19 km and 38.5 km in the Central System (Figure 4.4A). These values are higher than those suggested before by other authors. Banks and Warburton (1991) and later, Quintana et al. (2015), suggested a Central System shortening up to 50 km which would imply a mid-crustal shear level within the Iberian basement. The northern convergence thickens the Eurasian and Iberian lithospheres and two lithospheric roots develop below the

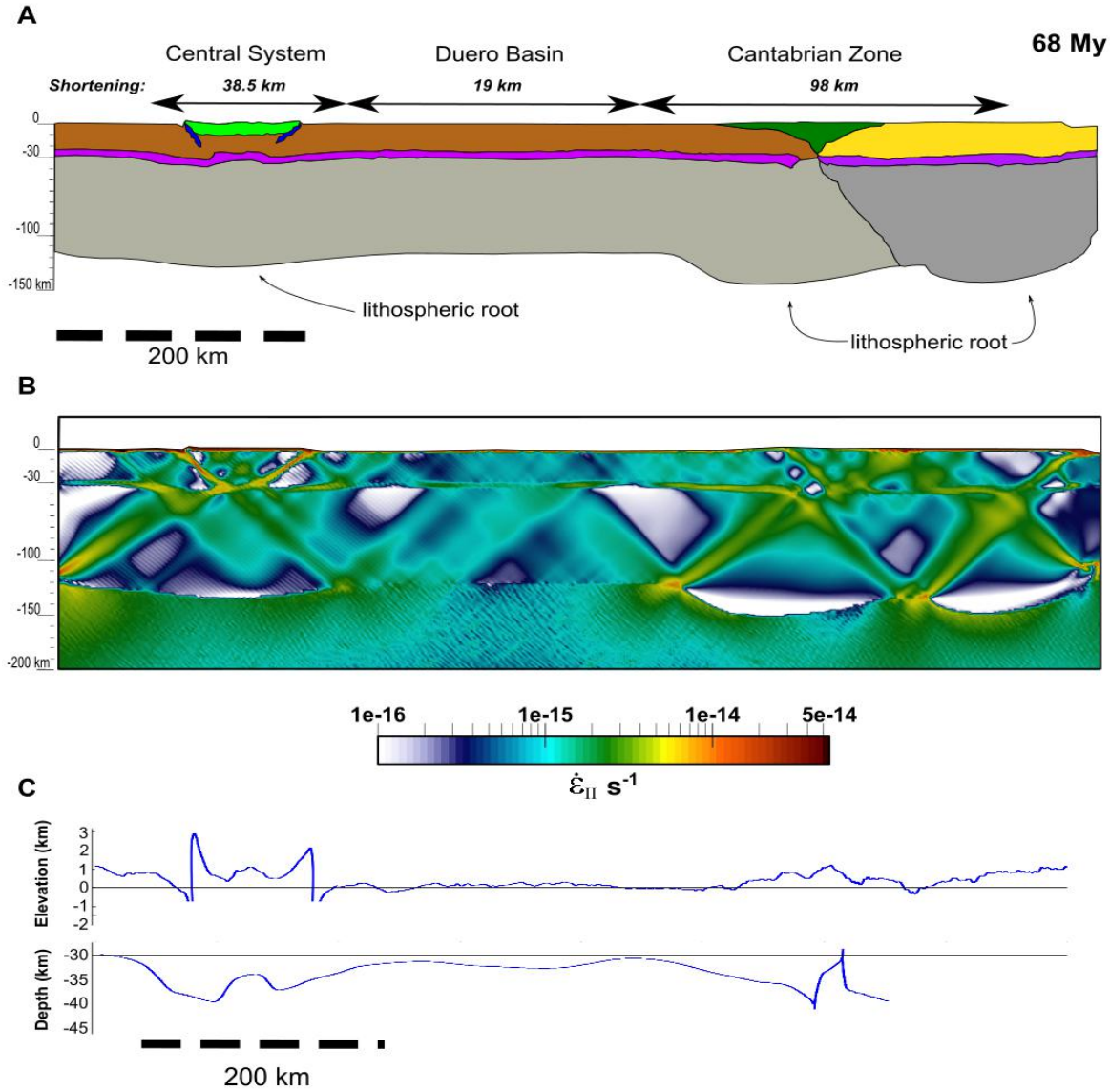

Figure 4.4. A) Reference model's final stage of the layering material after 98 km of Cantabrian zone shortening. Central System has ~38 km and Duero basin ~19 km of upper crust shortening in 68 My of numerical evolution. B) Strain rate second invariant for the final stage. C) Final elevation and depth of the base of the crust (note that it is only plotted the Iberian base of the crust).

Cantabrian domain. Below the Central System another lithospheric root appears. At the final stage, the average depth for the Iberian and Eurasian Moho discontinuities are similar, meaning a major thickening in the Eurasian Crust domain (EC). In the Iberian part the maximum thickening of the crust locates below the faults of the Central System (Figure 4.4B & 4.4C). These faults are active and reach to the base of the crust as we can observe from the strain rate second invariant (Figure 4.4B). At the Cantabrian domain the deformation is being accommodated mostly in the Cantabrian crust (body 6 in Table 4.1) and in the Eurasian crust. This means that most of the shortening is accommodated in the Eurasian crust by thickening the crust. Within the lithospheric mantles, higher strain rates second invariant are located where the lithospheric roots have developed. The topography and the base of the crust profiles reveal where the maximum thickening of the crust occurs (Figure 4.4C). This maximum is related to the uplift of the Central System as a pop-up structure using the imposed faults that have been active the entire model evolution. Duero basin domain has a flat and sea level topography but its base thickens in the middle. Cantabrian Mountain range topography is lower than the Central System's. The Cantabrian Mountain range presents ~50 km wavelength folds and a considerable crustal thickening(Figure 4.4C). In this reference model, the topography of the Eurasian crust is far above sea level due to the tectonic compression and that the initial thickness is overestimated.

Model NI.1 consider a mid-crustal detachment (Figure 4.5A) to analyse its influence on the transmission of deformation, its accommodation and to explore the hypothesis for 50 km of total shortening in the Central System domain from Banks and Warburton (1991). The detachment does not change the way the deformation accommodates (Figure 4.5B). We can observe that the time lapse of the total shortening in the Cantabrian domain as well as the shortening in the Duero Basin is slightly inferior than in the reference model. Nevertheless, the strain rate second invariant is visibly distinct. In the Central System faults do not root to Moho's depth and the detachment is active in the southern part of the Cantabrian domain (Figure 4.5C). In the center of the Cantabrian domain, clear

shear bands can be observed in the strain rate distribution, suggesting one principal pop up structure than uplifted the range and secondary structures modifying the first one. Figure 4.5D reveals one maximum of topography in the Cantabrian Mountains followed by a second northern promontory. The Eurasian crust is above sea level and Iberian thickening is very close to that predicted by the reference model.

Model NI.2 considers three important changes respect to the previous model; 1)

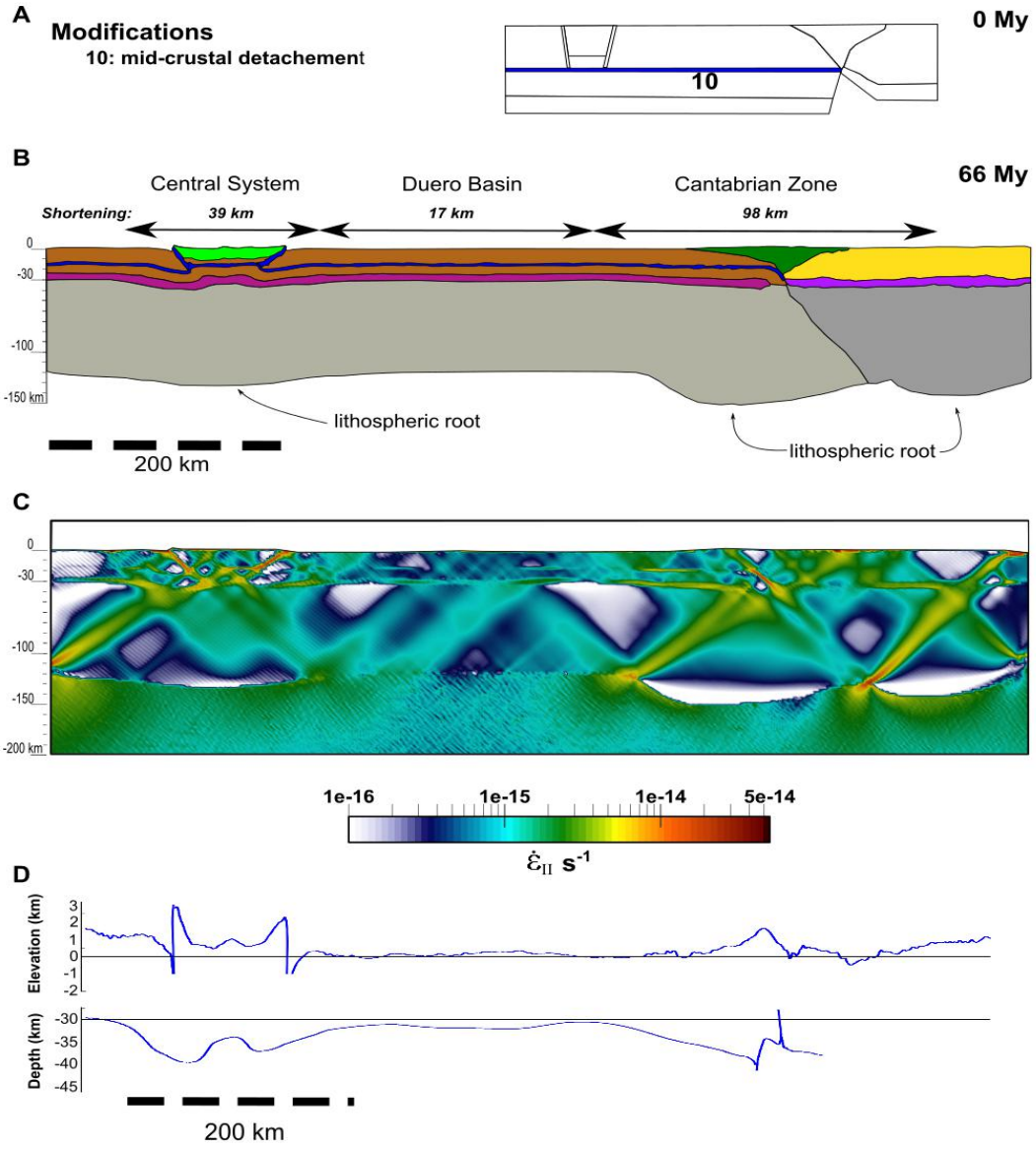

Figure 4.5. A) Modifications to the NI.0 model. Here we add the tenth body acting as a detachment. B) Final stage of the layering material for NI.1 model after 98 km of Cantabrian zone shortening. Central System has ~39 km and Duero basin ~17 km of upper crust shortening in 66 My of numerical evolution. C) Strain rate second invariant for the final stage. D) Final elevation and depth of the base of the crust.

A weaker Iberian lithospheric mantle, 2) a denser Eurasian crust and 3) the Byerlee's law only depend on the cohesion therm (Table 4.1).

Substantial dissimilarities occur when changing the plastic criteria in model NI.2 (Figure 4.6), where the plasticity is modified and the Byerlee's law only depend on the cohesion term [eq. 12]. Moreover, the Eurasian crust density has been changed from 2780 to 2860 kg/m^3 to avoid that the Eurasian topography surpasses the sea level, like in the NI.0 (ref.) and NI.1 models. In the NI.2 model, not only the time-lapse has been reduced by several million years to reach 98 km of shortening in the Cantabrian Zone (from 66 to 56 My), but also the shortening in the Central System mountain chain (64 %) and the Duero basin (66 %). By lowering the cohesion value in the mantle from 16 to 10 MPa only one asymmetrical lithospheric root appears below the Cantabrian domain (Figure 4.6A). Model NI.2 strain rate second invariant distribution [9] concentrates essentially in the Cantabrian domain. The distribution pattern of the strain rate second invariant in the Central System and Duero basin domains accumulates in their weakest parts, such as the faults in the Central System, the lower crust, and the mid-crustal detachment (Figure 4.6B). Virtually all the stress is concentrated in the crustal part of the lithosphere meanwhile the lithospheric mantle remains undeformed in the Iberian plate. During the evolution of this numerical model the weak parts from the crust have transmitted stresses from the junction of the plates to inner parts of the Iberian plate. The asymmetric geometry of the lithospheric root in NI.2 under the Cantabrian Mountains and the localization of strain along the weak zone results in a configuration that resembles a south-dipping subduction (subduction towards the left in Figure 4.6A) that is incompatible with the observations discussed above (Figure 4.2A). This is a consequence of making denser the Eurasian crust and weaker the lithospheric Eurasian mantle. Not transmitting enough strain rate to inner parts of the Iberian plate modify the topography profile noticeably. In NI.2 model, the highest topography is located in the Cantabrian Mountains (Figure 4.6C) and also the maximum crustal thickness. The Cantabrian orogen evolves as a double vergence orogen without crustal folding. It has a triangular shape with two adjacent basins. In the Duero Basin, the

topography and the base of the crust practically are not changing during the evolution. There exists a depocenter in the northern part of the Duero basin topography profile (see topography profile in Figure 4.6C). To the north of the depocenter, there is a thickening of the crust and there are high concentrations of the second invariant of strain rate, suggesting that all the shortening takes place there. This concentration of strain rates is a flexural response of the Iberian lithosphere caused by the beginning of Eurasian subduction.

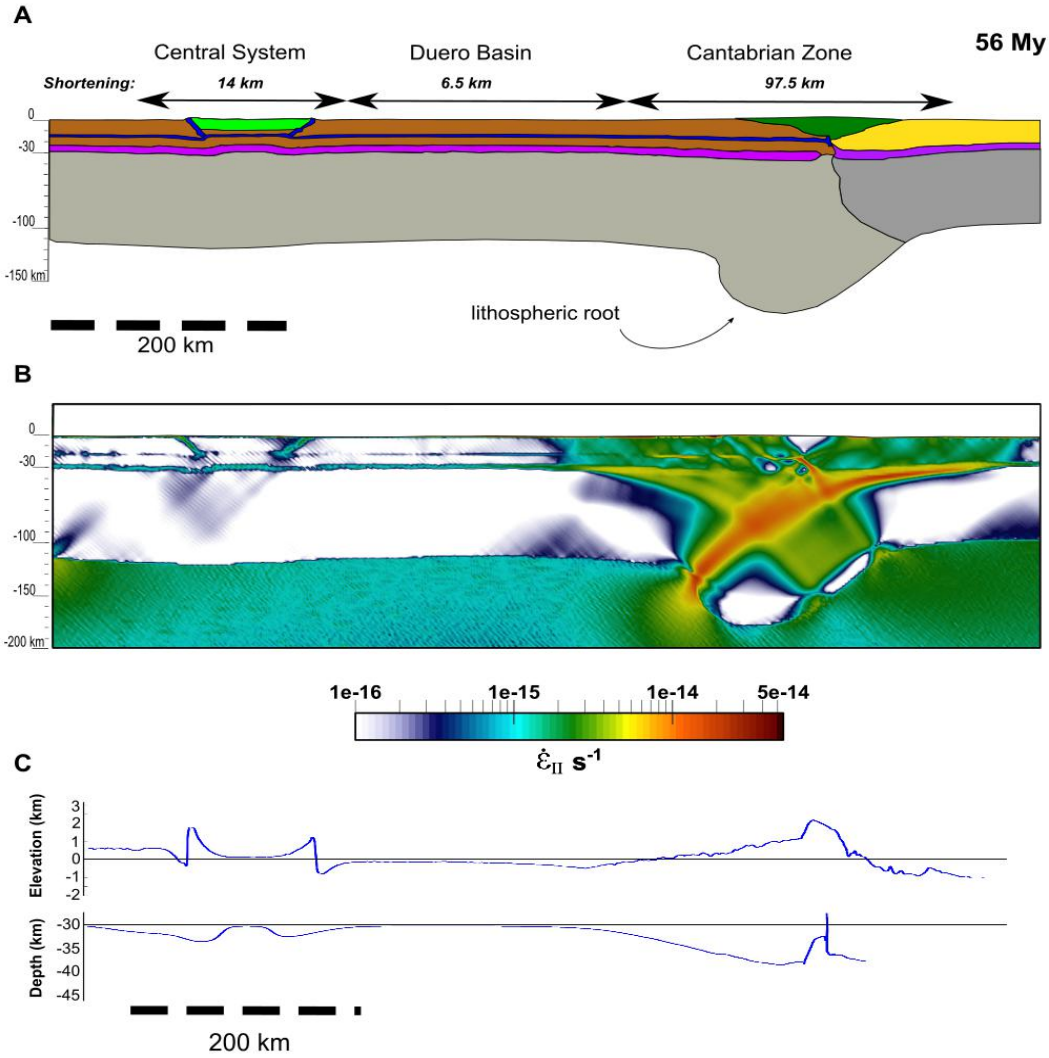

Figure 4.6. A) Final stage of the layering material for NI.2 model after ~97.5 km of Cantabrian zone shortening. Central System has ~14 km and Duero basin ~6.5 km of upper crust shortening in 56 My of numerical evolution. B) Strain rate second invariant for the final stage. Note that this model does not have any new body but plasticity criterion has been changed for all the lithosphere's bodies from the Byerlee's law depending on the frictional coefficient and depth to a non-dependency these terms and only depending on the Cohesion. C) Final elevation and depth of base of the crust.

Instead of modifying the plasticity criterion and the density of the Eurasian crust like the previous model, model NI.3 exchanges between the mantle and the crust the values of the frictional coefficient from the Byerlee's law; thereby it is increasing the strength of the crust while decreasing it in the lithospheric mantle. This model incorporates a weak zone between plates in the lithospheric mantle to focalize the deformation during the tectonic compression (WZ, body 11 Table 4.1 and Figure 4.7A). This artificial way to force subduction is widely used in geophysical modeling. The geophysical observations indicate that the Iberian

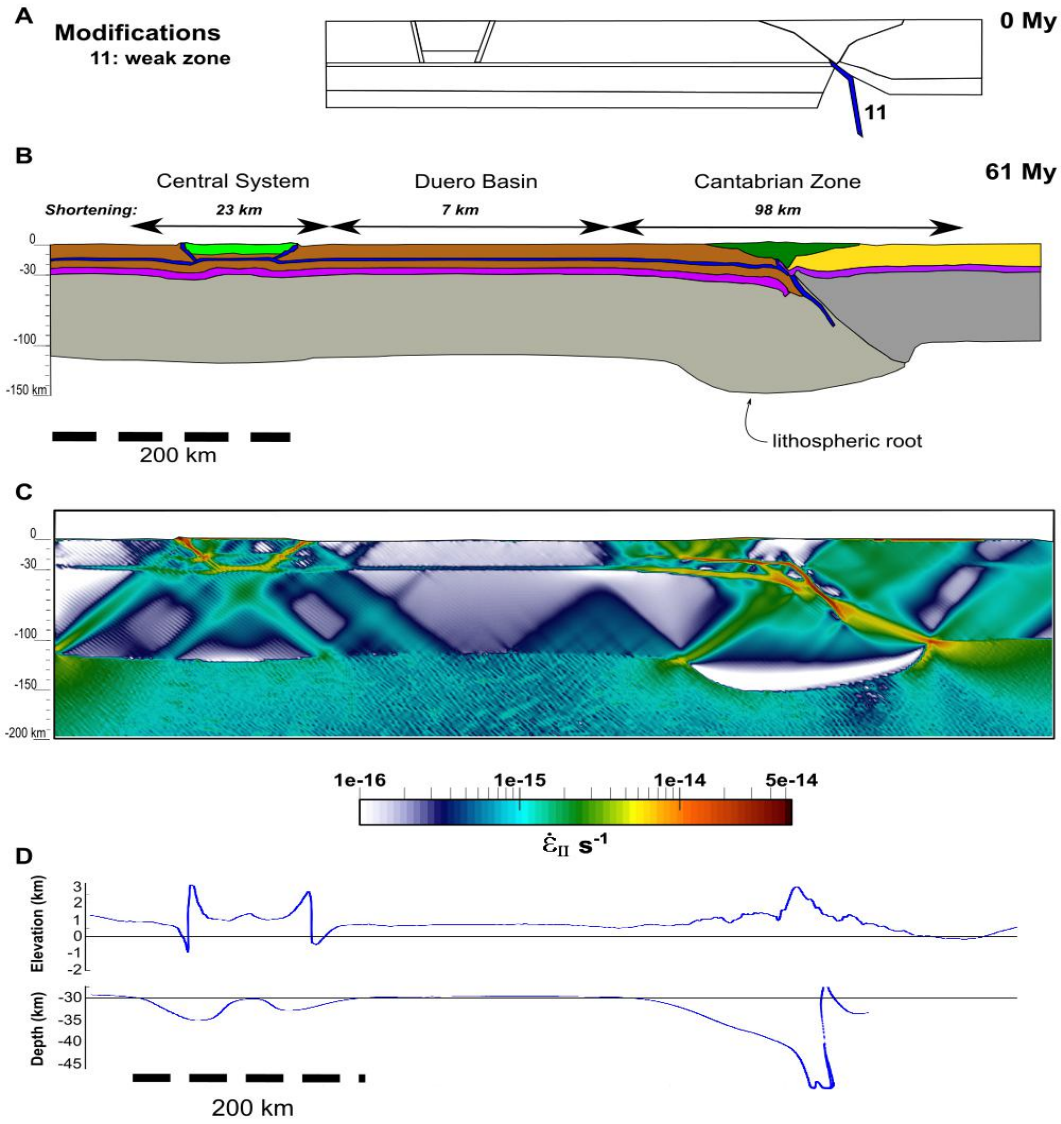

Figure 4.7. A) Modifications to the model. In this NI.3 model we add the eleventh body acting as a weak zone or detachment. B) Final stage of the layering material for model 3 after 98 km of Cantabrian zone shortening. Central System has ~23 km and Duero basin ~7 km of upper crust shortening in 66 My of numerical evolution. C) Strain rate second invariant for the final stage. D) Final elevation and depth of the base of the crust.

lower crust subducts northwards in the northern margin following the continental collision in the Pyrenean chain where all the lithosphere subducts. Despite there is no evidence of lithosphere subduction in the Basque-Cantabrian and Cantabrian Mountains, a westward propagation of an Iberian crustal root has been proven by several authors (Gallastegui, 2000; Pedreira et al., 2015; Pedrera et al., 2017).

With these modifications this model not only has the Cantabrian zone shortening in the correct timing but also there is little shortening in the Duero Basin and a suitable shortening for the Central System. We now have a symmetrical lithospheric root below the Cantabrian Zone. The mid-lower crust of Iberia has a northward subduction while the Eurasian lithospheric mantle underthrust southwards between the Eurasian lower crust and the Iberian crust. How the weak zone accommodates the deformation in the Cantabrian Zone can be observed in Figure 4.7C. High strain rates focalize the subduction and connects with the mid-crustal detachment level until the Duero basin domain. The weak zones of the Central System also localize high concentrations of strain rates, and both faults root to the base of the crust. A high topography is located just above the crustal root on the Cantabrian Mountains (Figure 4.7D), where the crust has its maximum thickening. A remarkable feature of this model is that all the Duero Basin is elevated to 500 m on average and little shortening (~7 km). Enough shortening in the Central System allows a high topography and also internal deformation.

Thus far, we have compared results from different model setups that reach an upper crustal shortening of the Cantabrian domain of ~98 km. As seen, not all model runs reach that value in the same amount of geological time, for example model NI.2 needs 56 My in contrast with the reference model that finish at 68 My. An efficient way to compare our models is to show the timing of the shortenings from each domain as in Figure 4.8. Models that reach in less time 98 km of shortening in the Cantabrian domain also have less shortening in the Central System and Duero basin (models NI.2, red line, and NI.3, green line). The reference model (NI.0) and NI.1 model have two shortening rates for the Central System domain: a low shortening rate before t=25 My, changing to a faster shortening rate.

This change is also related to the exponential increment of shortening in the Duero basin for these two models. Opposite tendency has model NI.2 which shortening rate in the Central System domain vary from ~0.32 mm/y to almost zero for the last 15 My (Figure 4.8). Most of the deformation is concentrated in the weak lithospheric mantle in the north margin of the Iberian part, which seems starting a subduction process south dipping.

The result obtained by Banks and Warburton (1991) of 50 km shortening in the Central System requires a south compression of the Iberian Peninsula that transmits stresses from the Betics to the Central System via the mid-crustal detachment. Recent studies (e.g., de Vicente & Muñoz, 2013) suggest a maximum total shortening in the Central System of ~24 km. Quintana et al. (2015) also explore the possibility of both shortening estimations but with a nuance: the 25 km of maximum shortening in the inner part of the Iberian Peninsula is due to a mid-crustal detachment that only exists from the north boundary to the Central System latitude even if there is south Iberian compression. Considering the aforementioned study, our models should not exceed the 25 km value of total shortening for the Central System. Model NI.3, the one developing a north-dipping mid-lower Iberian crust subduction (Figure 4.7B) satisfactorily fits the shortening values inferred for the Cantabrian and Central System domains based on structural tectonic studies. Even so, the timing of the Central System shortening does not adjust to previous geological publications, which suggest that area should have occurred between ~50 Ma and ~10 Ma (de Vicente et al., 1996, 2007; de Vicente & Muñoz-Martín, 2013; de Vicente & Vegas, 2009). The mechanical behavior imposed for the models implies an uninterrupted Iberian plate compression and shortening of all domains from t=0 until last time step (Figure 4.8). Moreover, the non-existence of lateral heterogeneities under the Central System provides a crustal deformation with two minimum for the base of the crust. Martín-Velázquez and de Vicente (2012) demonstrate the role of lithosphere heterogeneities for the location of intraplate deformation. In order to have a crustal root or concave thickening in the lower crust reaching 36 km depth, it is needed thermomechanical heterogeneities generating variations in the strength of the crust.

In next section, using thermomechanical models, I will better explain the geological and structural observations, the shortening of the different domains and their timings.

Figure 4.8. Upper crustal shortening for the different domains of the models presented in this section until 60 My time step. Blue line corresponds to the reference model. Purple dashed line stands for model NI.1 with a mid-crustal detachment level introduced in the Iberian crust. NI.2 model, red line, has its plasticity criteria changed not considering the frictional coefficient and only the cohesion term in the Byerlee's law. Green line corresponds to the last model, the one with an inherited weak zone introduced in the junction of the two lithospheric mantles. (Note that y-axis scale is different for each graphic)

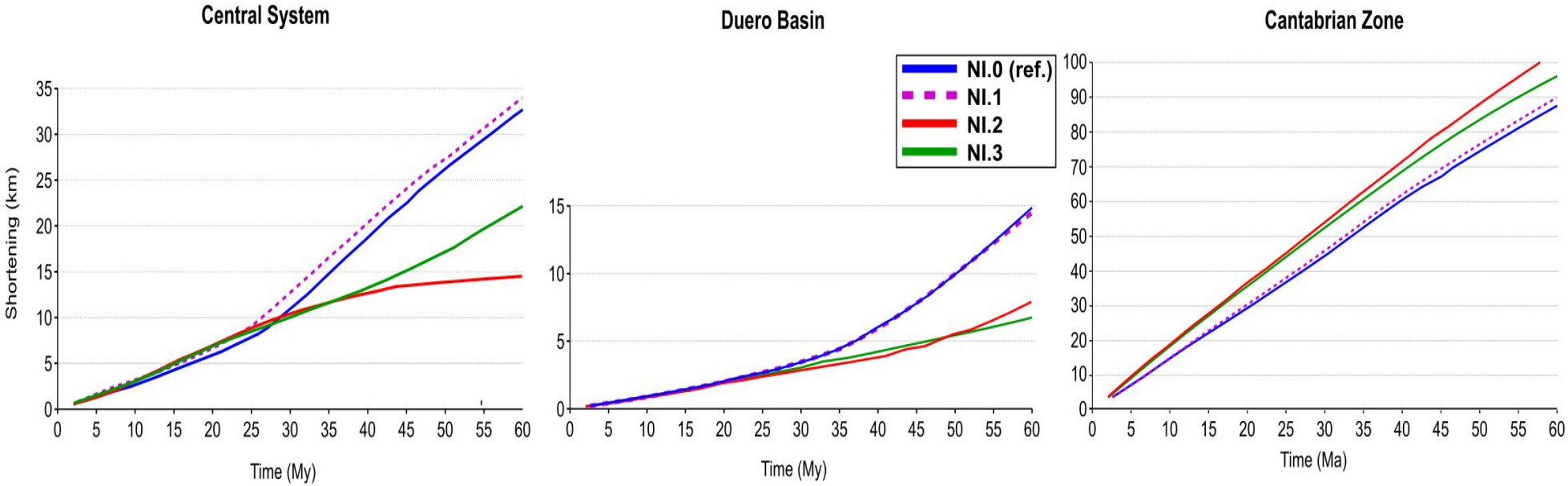

4.2 Thermomechanical models

The previous section shows the influence of different parameters in mechanical models inspired in the Alpine compression of the north Iberian Peninsula since upper Cretaceous times. In this section, we aim at better understanding the transmission of the deformation from the boundary to the inner parts of the Iberian lithosphere, performing a series of thermomechanical models varying rheology and including weak parts inherited from the Variscan orogeny in the same N-S oriented transect crossing the Central System, Duero Basin and Cantabrian Zone domains. In order to see the influence of rheology, we incorporate the temperature and temperature dependence for density and viscosity using the formulas and relations described in Chapter 2.

Initially, temperature is set to increase linearly with depth, from 15°C at the top of the crust (surface) to 650°C at the base of the crust, and from there to 1330°C to the lithosphere-asthernosphere boundary. The temperature for the whole sticky air layer is set to 15°C. The values of 650°C and 1330°C for the base of the crust and the LAB, respectively, were chosen considering previous studies based on surface heat flow on the Iberian lithosphere (Fernández & Marzán, 1998; Tejero & Ruiz, 2002; Martín-Velázquez & de Vicente, 2012). These studies calculate the temperature range for the Moho in central Iberia ~600°C with 32 km of crustal thickness and a surface heat flow of ~65 $mW \cdot m^{-2}$. These studies also consider an isotherm of 1350 °C for the LAB with a lithospheric thickness of ~110 $\pm$ 5km. The vertical sub-lithospheric gradient is approximately 0.5 °/ km, according to the adiabatic gradient.

The transect is 1200 km long, and it incorporates the hyperextended crust in the Bay of Biscay and a weak zone down into the upper mantle below the continental slope (Figure 4.9). The influence of this weak zone has been noticed in the mechanical models (section 4.1), where not only allows the northward subduction but also favoured the transmission of deformation to connect to the mid-crustal detachment of the Iberian crust. This transect is inspired by the

detailed geological map studied by Pedreira et al. (2015, Figure 4.2) where concave weak zones rooted to the mantle connecting the mid-crustal detachment after the hyperextension.

The two faults included in the Central System are structures inherited from the Variscan orogeny, with a different angle at each sides of the Central System which can be considered as a granitoid block. De Vicente et al. (2007 & 2009) suggested that these faults were reactivated during the first stage of the N-S Cenozoic compression of the Iberian crust and lasted until the Pliocene. The southern thrust is active practically all the Cenozoic while the northern thrust border appears to be more dispersed with a sequence of thrust towards the Duero basin. Both thrust root to lower crust depth.

Although many studies (e.g., de Vicente et al., 2009) suggest the reactivation of faults in the Central System during the Mesozoic compression, we start with a reference model (TM0) without such inherited weak zones (Figure 4.9A). The goal is to verify if those weak zones are needed in order to adjust the timing of the deformation and shortening in the Central System or if, alternatively, rheological contrast between the different domains/blocks can explain the present structure and its timing by itself.

The adopted rheology is viscoplastic for all the lithologies considered and consists of a power law creep (see Chapter 2) which parameters are listed in Table 4.2. The mantle rheology [eq. 11] is the combination of diffusion and dislocation power laws, using the activation volume for each one:

$$\frac{1}{\eta_{mantle}} = \frac{1}{\eta_{diff}} + \frac{1}{\eta_{disl}} \quad \begin{cases} V_{diff} = 7\ J\ MPa^{-1}mol^{-1} \\ V_{disl} = 11\ J\ MPa^{-1}mol^{-1} \end{cases} \qquad [22]$$

These values are taken in agreement with laboratory experiments (Hirth & Kohlstedt, 2003). Plasticity, as in previous section, decreases viscosity values where high strain rates accumulate, incrementing stresses that surpass the yield strength of materials, and the flow law shifts to the Byerlee yield criterion. We use

a value of 0.3 MPa km^{-1} for the frictional angle coefficient for diffusion and 0.15 MPa km^{-1} for the frictional angle coefficient for dislocation.

	Bodies	Lithospheric Unit	ρ_0 ($kg \cdot m^{-3}$)	Creep Parameters				Plastic Criteria	
				Lithology	n	A ($MPa^{-n} \cdot s^{-1}$)	E ($kJ \cdot mol^{-1}$)	C_0 (MPa)	Diffusion/Dislocation
	1	Central System	2670	dry granite	3,2	$1{,}8\ 10^{-9}$	123	48	Dislocation
	2	Upper Crust	2780	Wet quarcite	4	$1{,}1\ 10^{-4}$	223	30	Dislocation
	3	Middle Crust	2860	Quartzdiorite	2,4	$1{,}3\ 10^{-3}$	219	30	Dislocation
	4	Lower Crust	2950	Felsic Granulite	3,1	$8\ 10^{-3}$	243	5	Dislocation
	5	Fault	2780		-	-	-	5	Byerlee's law
	6	Cantabria Weak Zone	3400	-	-	-	-	1	Byerlee's law
TM0	7	Mantle	3300	Wet olivine	1 & 3,5	10^6 & 90	335 & 480	30	Diff & Disl
	8	Duero Crust	2780	Hydrated Quartz	2,3	$3{,}2\ 10^{-4}$	154	30	Dislocation
	9	Mesozoic Sediments	2650	Wet quarcite	4	$1{,}1\ 10^{-4}$	223	5	Dislocation
	10	European Crust	2860	2*Dry quarcite	2,4	$6{,}7\ 10^{-6}$	156	30	Dislocation
TM1	11	European Lower Crust	3120	Wet quarcite	4	$1{,}1\ 10^{-4}$	223	30	Dislocation
	12	Faults	2780	Dry granite	-	-	-	5	Byerlee's law
	13	Mid-Crustal Detachment	2860	-	-	-	-	5	Byerlee's law
TM2	14	Cantabrian Lower Crust	2900	Wet quarcite	4	$1{,}1\ 10^{-4}$	223	30	Dislocation
TM3	1	Central System	2670	Wet granite	1,9	2 10-4	137	48	Dislocation

Table 4.2. Materials properties listed for the models. The reference model has 7 different rheologies. TM1 has 4 new rheologies. TM2 has 3 new rheologies. TM3 Central S. rheology change to a more ductile one. Creep Parameters are chosen from Gleason & Tullis, (1995); Fernàndez & Ranalli, (1997); Martín-Velazquez et al. (2012); and Pedreira et al. (2015). Densities reference values are from Álvarez-Marron et al. (1996); Gómez-Ortiz et al., (2005); and Carballo et al. (2015).

Mantle density also changes with pressure and temperature using equation 22 from chapter 2. To calculate the density the values for the T_a (reference temperature at the LAB), the thermal expansion α and and compressibility of rocks β, which have been taken from Boonma et al. (2019) using the methodology described in Kumar et al. (2020), considering a continental lithosphere of 120 km thickness and an oceanic young lithosphere of 90 km (Table 4.3). In our models, we also considered the influence of pressure and thermal variations for the creep parameters but assuming a compressibility coefficient of 10^{-5} MPa^{-1} and a thermal expansivity of $3 \cdot 10^{-5}$ K^{-1}.

To control the shortening throughout the numerical model evolution we, as in previous mechanical models, introduce at upper crust levels markers which follow the Lagrangian particles dividing the domain in Central System, Duero basin and Cantabrian Zone (black triangles in Figure 4.9).

	$\alpha = \frac{\partial \rho}{\partial T}$ *[kg m^{-3} K^{-1}]*	T_{ref} [°C]	$\beta = \frac{\partial \rho}{\partial P}$ *[kg m^{-3} MPa^{-1}]*
Tecton-Ancient lithosphere	-0.1255	1241.7	0.044
Young Oceanic lithosphere	-0.1236	1085.1	0.046
sublithospheric mantle	-0.1165	1608.7	0.044

Table 4.3. These values are those used in Boonma et al. (2019) calculated using the methodology described in Kumar et al. (2020).

The reference model (TM0) presents an upper crust with a wet quartzite rheology. The Iberian middle crust lithology is quartz-diorite, which is extended to the passive margin in the Cantabrian Zone between the Iberian plate and the Eurasian. The lower crust has felsic granulite lithology along all the transect (Figure 4.9A). The Central System domain is a granitoid block with low density like in the mechanical models from previous subsection, but without the weak zones. There viscosity cut-off limit of the lithosphere is 10^{24} Pa·s and all the models include 20 km thick layer (sticky air) on top of the lithosphere to simulate air with very low viscosity (10^{19} Pa·s).

The model domain is 1200 km long and has a total depth of 500 km. The mesh resolution is 1.04 x 0.87 km. We define 10 particles per cell to track the material, within a total of ca. 6.63 million initial particles in the domain.

The boundary conditions are free slip on the top and bottom walls, the sub-lithospheric sidewalls have periodic boundary conditions guaranteeing a lateral material flow. The convergence is achieved with a constant velocity prescribed in a high viscous lithospheric mantle on the right side of the Cantabrian Zone domain. The convergence velocity imposed is 2.5 mm/year, as deduced from the

restorations carried out by previous studies (e.g., Gallastegui, 2000; Pedreira et al., 2015) where the shortening started in the Paleocene and last ~40 My (the shortening stage in this area finished about 15 Ma). I also consider other rates from different studies suggesting less convergence or different timing. For example, Machiavelli et al. (2017) kinematic model has less shortening (~85 km) in this area with an average convergence velocity of 1.6 cm/year from Paleocene to middle Miocene.

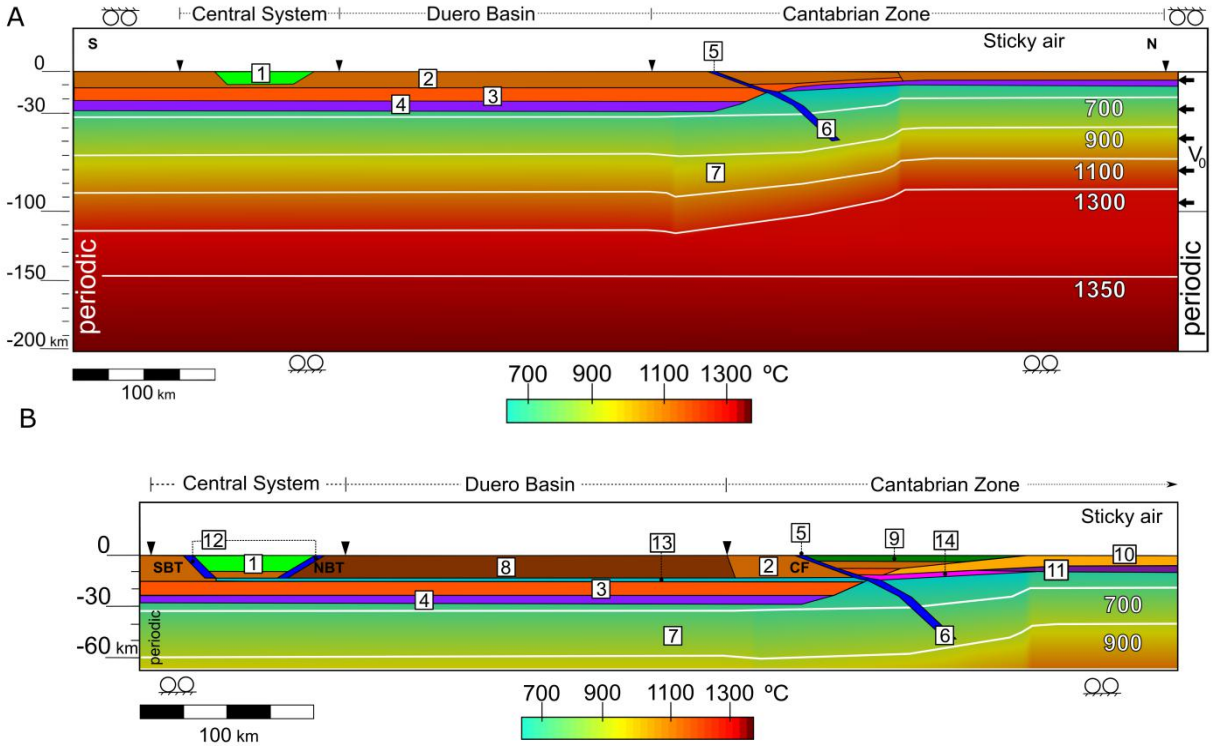

Figure 4.9. A) Set-up for the reference model (TM0). B) Set-up for the last model (TM4). Material numbers correspond to materials listed in Table 4.3. V_0 is the initial velocity of 2.5mm/y. White lines are temperature contour for the lithospheric mantle in Celsius. Black triangles of the surface correspond to the location of the upper crust markers in order to calculate shortenings for the 3 different sectors; Central System, Duero Basin and Cantabrian Zone. NBT: North Boundary Thrust and SBT:South Boundary Thrust

The final stage of the reference model (TM0, Figure 4.10A, B, C) reveals that there is an indentation of the lower crust and upper mantle from the hyperthinned domain southwards into the Iberian crust (Figure 4.10B). The Iberian middle-lower crust subducts northwards. This subduction only occurs for the crust, not for

the entire lithosphere, but generates a lithospheric root under the Cantabrian Mountains which maximum depth is 150 km. Above the lower-crustal subduction, the model has the maximum topography (Figure 4.10A). The oceanic lithosphere also thickens bringing the LAB to 112 km depth. Southwards the Cantabrian Fault (CF), the crust deforms with an anticlinal shape of 50 km width. The Duero basin crust thickens 3 km on average, the Moho descend 2 km, and the topography uplifts 1km (Figure 4.10 A & B). The Central System uplifts reaching ~1.7 km of maximum topography (Figure 4.10A), and the middle crust folds with a ~50 km wavelength. The base of the crust presents a different wavelength of ~100 km, with two maximum crustal thicknesses below the NBT and the SBT, and a minimum of thickness located below the maximum topography of the Central System, without developing a mountain root. During this 70 My of evolution, the LAB has been deepened by 20 km, having an average depth of 140 km.

The strain rate second invariant shows that deformation accommodates from the start in the Cantabrian Mountain's crust. Initially the strain rate accommodates through the whole crust and later it concentrates between the lower crust and the upper mantle. A detachment level between the middle crust and lower crust develops in the northern part of the Cantabrian Mountains. A second detachment level generates between upper and middle crust below the Cantabrian Mountains (Figure 4.10C). The strain rate spreads all over the Iberian crust, but it is more concentrated in the lower crust and in the lower-crustal subduction area. Two main shear bands appear naturally in the Central System, and join together in the middle-lower crust.

The reference model (TM0) achieves 97 km of shortening in the Cantabrian Zone in ~70 My (Fig 4.10 B). We stop the numerical model when this amount of shortening in this region is achieved to study how much time take to the model to reach this value, to investigate how much shortening the other regions have and the timing of these shortenings. The Central System gets 21 km of upper-crustal shortening and the Duero basin 36 km, resulting in a total shortening of 154 km between the three regions.

Although the Central System shortening is close to the estimations from previous studies (at least 22 km from de Vicente & Muñoz-Martín, 2003), still there are several mismatches between the model and observations and data. There is no crustal root below the Central System and the elevation of the Duero basin exceeds the present topography. Our models should have less elevation in the basin than the real topography due to our models not have the sedimentation surface process to infill the basin and increment the elevation. Although there are no studies of the amount of shortening for the Duero basin, probably the result from the model is an overestimation. The southwards indentation of the lower crust and upper mantle of the hyperextended domain, and the Iberian lower crustal subduction

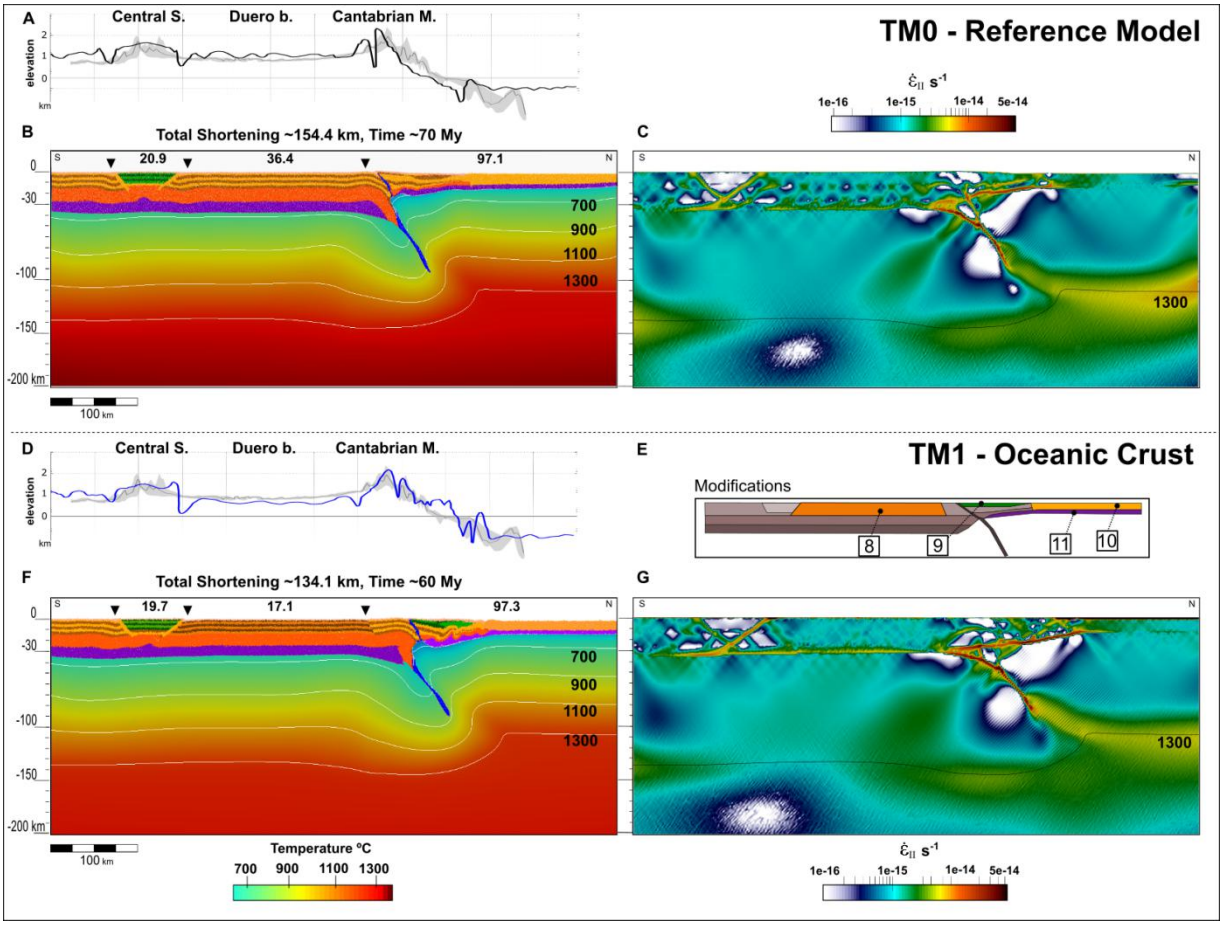

Figure 4.10. Final stage of the reference model TM0 (total shortening in the Cantabrian Range is ~97 km) showing the topography (thick grey band for data; the blue line is the model result), crustal layering structure the mantle temperature distribution and strain rate second invariant for the reference model (A, B & C) and TM1 the oceanic crust model (D, F & G). E) Shows the added bodies in TM1 relative to the reference model, the new bodies 8 to 10 are listed in Table 4.3. Topography profiles are compared with elevation data projected from a strip band of 50 km.

northwards do not match with the observations. The subduction angle should be lower to match with previous studies.

In a second model (TM1), the hyperextended crust is considered as an oceanic lithosphere, modifying the crust density and rheology (Table 4.2, body 10 & 11). This assumption comes from different studies that consider the hyperextended crust as an oceanic basement (e.g., Álvarez-Marrón et al., 1997; Muñoz, 2002). In the late Cretaceous the opening of the Bay of Biscay finished; hence, there was new oceanic crust created northwards to the nowadays coastal line, which converges to the passive margin during the Alpine compression (e.g., Rosenbaum et al., 2002b; Sibuet, Srivastava, & Spakman, 2004). I introduced a 4 km layer of Mesozoic sediments in the Cantabrian upper crust (Figure 4.10 E, body 9) as suggested by the restoration done by Pedreira et al. (2015). We hardened the rheology of the Duero basin crust, from a wet quartzite to hydrated quartz one, trying to avoid a high shortening in this section of the model (Figure 4.10 E, body 8).

Introducing these changes, we notice that the Eurasian lower crust is dipping with low angle to the south and the upper mantle accretes upwards (Figure 4.10F). Some folding is developing in the middle-lower crust of the Cantabrian Mountains, where we observed high deformation with several shear bands, considering them like well-developed thrusting faults (Figure 4.10G). The maximum topography of the model is localized in the Cantabrian Mountains, matching the observed topography. Instead of a continuous slope from the mountains to the shoreline, there is platform at 500 m over the sea level. Northward the coastline, the Eurasian crust folds and makes the topography to locally over the sea level (Figure 4.10E). The Cantabrian middle-lower crust thrusts with a steeper angle compared with to the reference model. In the upper crust, there is a topographic depression of ~500 meters depth denotes the limit between the Duero Basin and The Cantabrian Mountains (Figure 4.10D). In this model, contrary to TM0 model, the topography of the Duero basin is below the observed topography. The Central System elevates up to ~1300 m over the sea level with its maximum located in the northern part of the chain. Instead of lower crustal folding, this model has a crustal root under the Central System region but it localizes southwards the chain (Figure 4.10F).

Similar to the TM0 model, the strain localizes in the Cantabrian Mountains crust (Figure 4.10G). The oceanic lower crust and the Iberian lower crust connect through a detachment level. The strain rate transmission is mostly through the lower crust. The NBT and SBT in the Central System develop spontaneously and they join at Moho's depth. At this final stage, the strain rate is higher in the NBT, uplifting the northern boundary of the Central System (Figure 4.10 G & D).

TM1 model after 60 My of convergence the shortening in the Cantabrian Mountains is 97 km, this is 10 My faster than the reference model. The shortening along the whole profile is 134 km (Fig 4.10C), with a similar shortening in the Central System (~20 km) like the TM0 model, but less than half in the Duero basin (17 km).

There is no geological or geophysical evidence for significant tectonic shortening in the Duero basin; therefore, I design a third model (TM2) to attempt to reduce the shortening in this area. The initial angle of the Cantabrian southern thrust has been changed from 30° to 10° (Figure 4.11A). A lower angle would imply the transmission of the stress far from that area until the angle changes due to tectonic compression, concentrating the deformation in less time. I also introduce a lower crust less dense below the Cantabrian Mountains (Table 4.2, body 14), between the oceanic and the continental crust, in concordance with several authors (e.g., Álvarez-Marron et al., 1997; Pedreira et al., 2015; Carballo et al., 2015) which suggested a lighter (2900 $kg \cdot m^{-3}$) lower crust below the Cantabrian Mountains. This less dense body 14 will disrupt the local isostasy; to compensate it we removed the Iberian middle crust between the Mesozoic sediments and the body 14. So the crust rheology under the Mesozoic sediments is assumed more ductile facilitating the accommodation of deformation.

The mechanical models from section 4.1 showed that some transmission of strain rate was through a mid-crustal detachment if it is implemented in the model. The reference thermomechanical model TMO and the TM1 model even including the power law creep rheology, the strain rates second invariant do not reveal any mid-crustal detachment or weak décollement in the Duero basin crust. TM2 incorporates a mid-crustal detachment to reduce the Duero basin shortening and

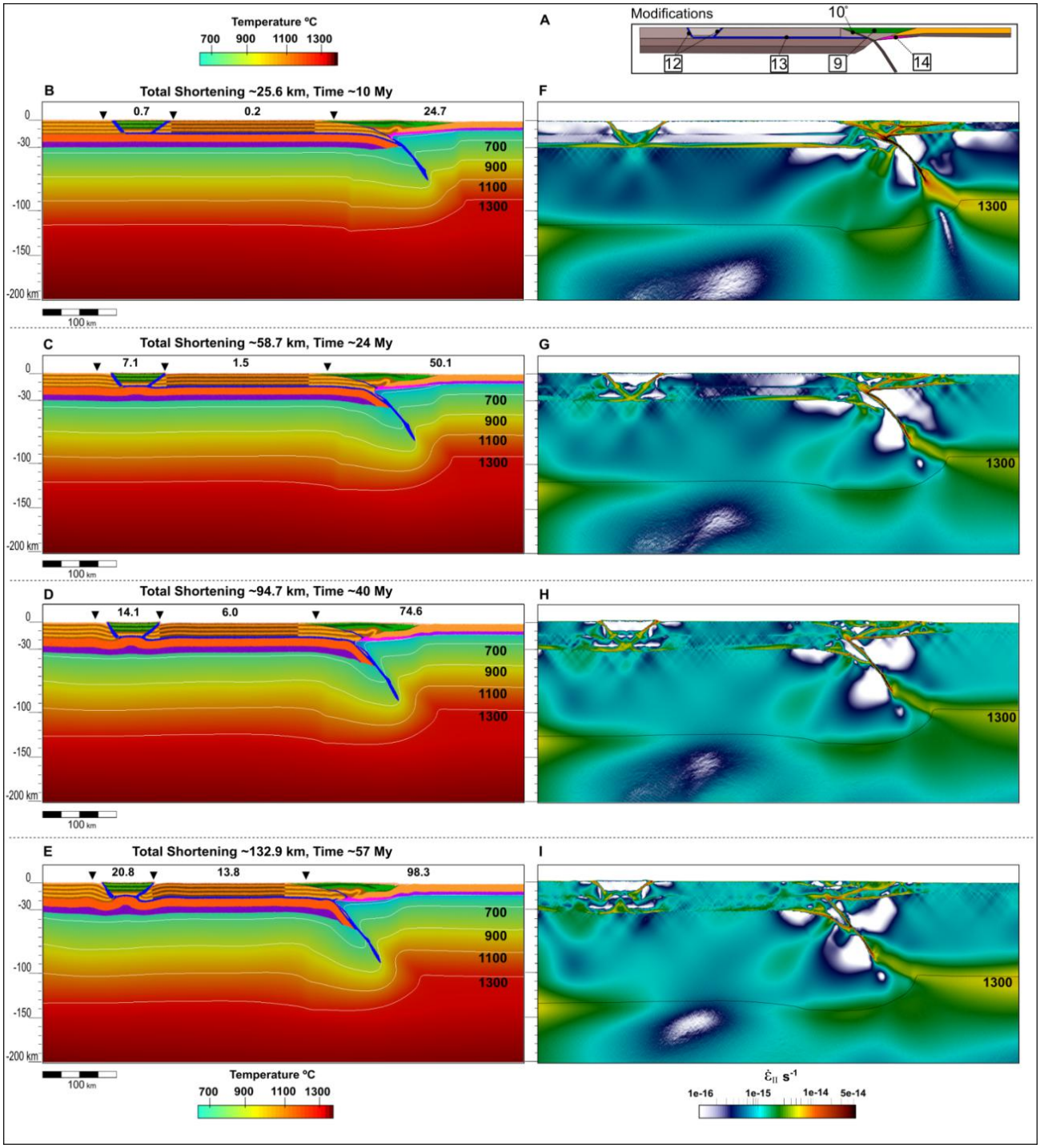

Figure 4.11. Four stages of the crustal layering structure and mantle temperature distribution of model 2 (TM2) every 25 km of Cantabrian Zone upper crust shortening. This model includes a lower angle for the southern fault in the Cantabrian Mountains, two weak zones in the Central System and a mid-crustal detachment level. A panel displays the modifications from TM1 model. Left panels (B-E) show the crustal bodies and the temperature evolution and right panels (G-I) show the strain rate second invariant evolution.

increment it in the Central System domain. The detachment goes from the north Iberian margin to the southern boundary thrust (SBT) of the Central System as

suggested by Quintana et al. (2015) (body 13, Table 4.2). Despite we have seen both TM0 and TM1 models that the NBT and SBT in the Central System appeared spontaneously, we considered to introduce two weak zones allowing the model to accommodate the deformation there from the beginning, to increment the uplift of the Central System (Figure 4.11A). This assumption is in concordance with previous studies suggesting that these two faults are inherited from Variscan times and reactivated during the Alpine compression (e.g., Casas Sainz & Faccena, 2001; de Vicente & Muñoz-Martín, 2012). Figure 4.11 shows the crustal layering structure and mantle temperature distribution (B-E), and the second invariant of the strain rate (F-I) at four different stages, between them ~25 km of Cantabrian Zone upper crust shortening.

After 57 My of convergence, model TM2 results with higher shortening in the Central System and less in the Duero basin than the TM0 and TM1 models. The north dipping angle of the Iberian middle-lower crust below the Cantabrian Mountain is less vertical. The middle crust below the Central System presents a clear folding, but not the lower crust(Figure 4.11E).

During the first 10 million years, there is barely shortening in the Duero and Central System crust, most of the strain is localized in the Cantabrian zone. Some strain rate is concentrated in the Iberian lower crust, and in the predefined weak zones on the Central System (Figure 4.11 B & F). After 24 My, the strain rate is transmitted to the Duero crust and along the whole profile (Fig 4.10 G-I). In the Central System, the predefined weak zones are active from the beginning of tectonic compression, with high strain rates second invariant values, but during the last million years, instead of both joining at Moho depth like in the reference model TMO, both are active just from surface to the middle's crust (Fig 4.11 I).

However, in the TM2 model the Central System shortening does not achieve the 22 km proposed by different authors (de Vicente & Vegas, 2009; de Vicente & Muñoz-Martin, 2013). For that purpose, in the next model (TM3), we introduced lateral variations in the middle crust below the Central System, removing the middle crust (body 3, Table 4.2) from the Central System and Tagus Basin and changing the lithology of the Central System crust from dry granite to wet granite

($A=2\cdot10^{-4}$ $MPa^{-n}\cdot s^{-1}$, E=137, n=1.9), making it more ductile. Therefore, the middle crust southwards the NBT, is softer than northwards in the Duero basin (Figure 4.12A). This procedure is inspired by the study done by Martín-Velazquez et al. (2012), who demonstrated the influence of lateral strength in the geodynamic evolution of the Central System. Moreover, the mid-crustal detachment level is in the entire Iberian crust from the Cantabrian Fault to the Tagus Basin, crossing the Central System. In the Cantabrian region, we used the Eurasian lower crust from previous models and removed the less dense body 14 (Table 4.2) to figure out the influence of it in this region.

After 60 My of convergence, model TM3 shows ~98 km of shortening in the Cantabrian region, ~13 km on the Duero basin and the main difference with previous models is that the Central System shortening increased to 31 km (Figure 4.12D). In the Cantabrian zone, the southwards indentation into the Iberian middle crust of the lower crust and lithospheric upper mantle, and crustal structure below the Cantabrian mountains, is comparable to model TM2, as well as the partial subduction dipping to the north of the Iberian lower-middle crust below the Cantabrian Mountains. The middle crust of the Duero basin region underthrust the Central System (Figure 4.12 C-E). The Central System presents a crustal root.

The mid-crustal detachment of TM3 model is active from the start, transmitting strain rate from the Cantabrian region to the Central System and Tagus basin. The middle crust and upper crust in the Duero basin do not accumulate strain rate during the first 28 My. The lack of strain rate produces the continuous deformation of the inner region of the Central System. The weak zones inclinations of the Central System increase, more in the southern fault than the northern one. From 12 to 28 My, the shortening in the Central System has its highest rate (from 4.7 to 17.3 km). After 44 My, some shear bands appear in the middle-crust of the Duero basin increasing the shortening rate (Figure 4.12 H & D). The strain rate second invariant shows the activation of the mid-crustal detachment of the Iberian crust which connects to the lower crust of the Eurasian lithosphere. Two main shear bands are in The Cantabrian Mountains during the first 28 My (Figure 4.12 F & G). Both shear bands join in the subduction zone and

rise to the surface in a V-shape. Only the northern one is active during all the evolution.

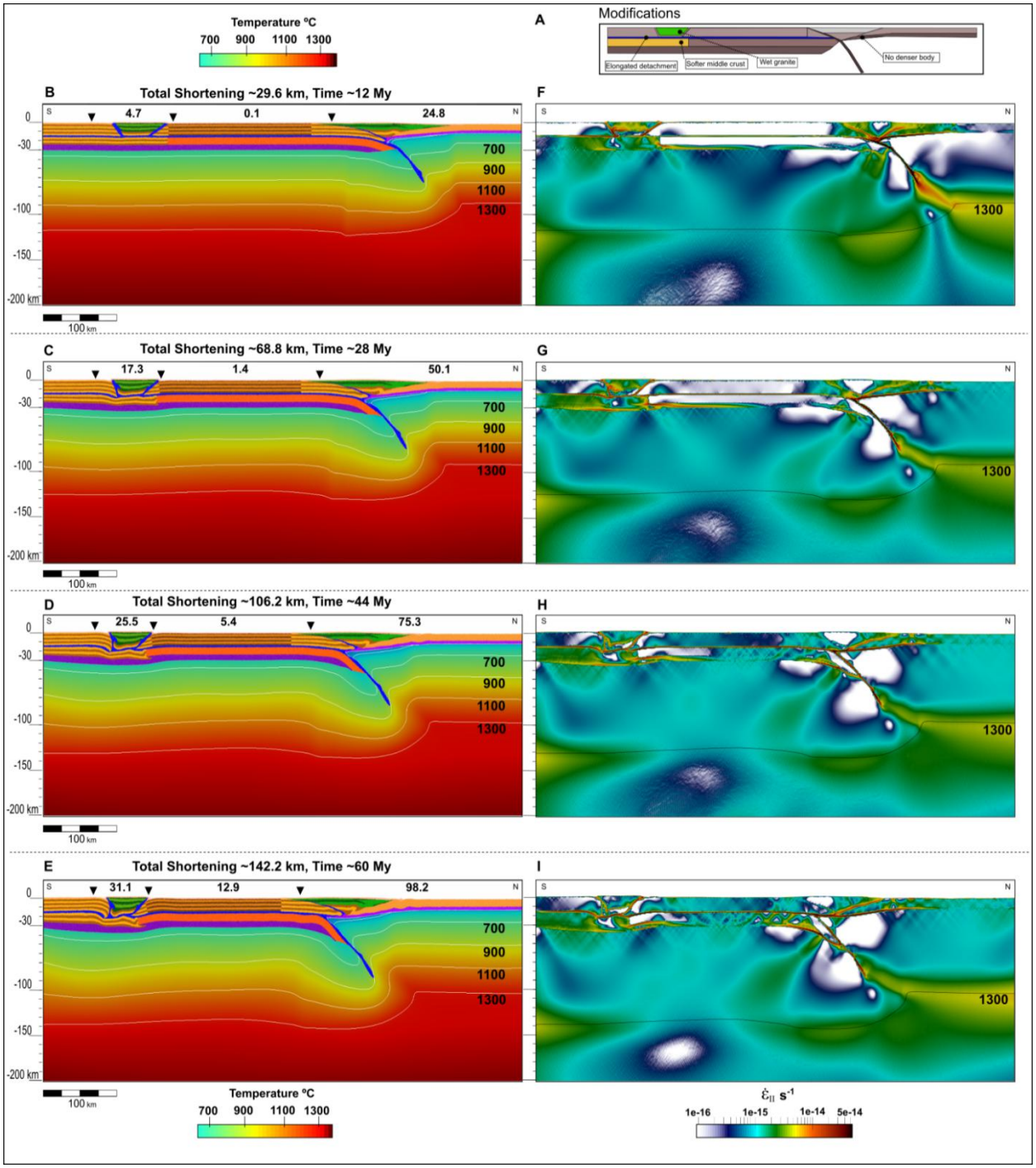

Figure 4.12. Four stages of the crustal layering structure and mantle temperature distribution of model 3 (TM3) every 25 km of Cantabrian Zone upper crust shortening with an elongated mid-crustal detachment level and softer Central System's rheology. A panel displays the modifications from M2 model. Left panels (B-E) show the crustal bodies and the temperature evolution and right panels (F-I) show the strain rate second invariant evolution.

The resulting deformation in the Central System of the TM3 model is too high (31 km of shortening). To reduce it, TM4 model get back from model TM2 the harder rheology in the Central System and the 30° angle for the Cantabrian Fault. It also gets back the less denser lower crust under the Cantabrian zone (body 14, Table 4.4). In this TM4 model, there exist middle crust under the Mesozoic sediments like in the restoration done by Pedreira et al. (2015) (Figure 4.2A). From TM2, I modify the length of the middle crust in the Iberian plate, which goes from the NTB to the Cantabrian Fault.

The ~98 km of shortening in the Cantabrian Zone are achieved in 62 My of convergence (Figure 4.13). Within this time, the Central System shortening is ~28 km and ~13 km for the Duero basin. The first 25 km of shortening in the Cantabrian zone shows two levels of decoupling in the Cantabrian upper crust which are maintained throughout the geodynamic evolution. The mid-crustal detachment in the Iberian crust transmits strain rate to the Central System during the first 29 My (Figure 4.13 F & G), after that the strain rate is distributed homogeneously in the whole Duero basin crust (Figure 4.13 H & I).

In the previous TM3 model, the mid-crustal detachment is active and connected to the oceanic's base of the crust from the Cantabrian zone, transmitting strain rate from this zone to inland (Fig 4.12 G-I). In the TM4 the mid-crustal detachment level is not active, there is no transmission of strain rate from the Eurasian lower crust to the Iberian crust through this weak layer, therefore is not playing an important role in the geodynamic evolution of the Iberian crust (Fig 4.13 G-I).

Figure 4.14 shows the elevation and the base of the crust along the profile for all the models. The reference model TM0 (black thick line, Figure 4.14), is the only model with more than 1 km of average elevation in the Duero basin. The Central System average elevation is ~1500 m. The Cantabrian Mountain maximum topography elevates to ~2400 m (which is the highest among the models) with a second peak southwards at ~1800 m. The Eurasian plate is only ~500 m below the sea level.

There is a decrease on the elevation in the Central System in model TM1 (blue line, Figure 4.14), which has ~1350 m of average altitude, with two peaks, one in

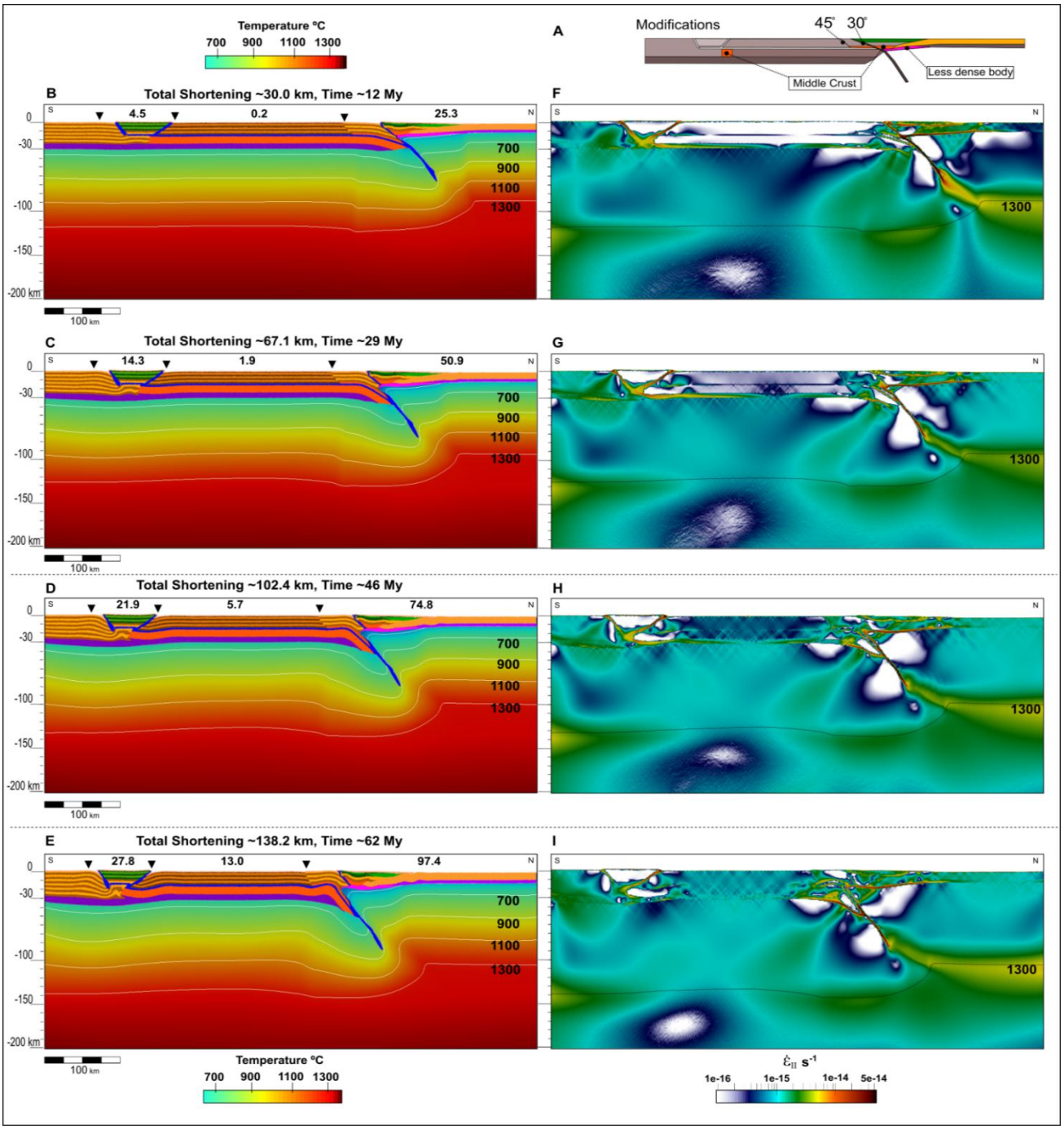

Figure 4.13. Four stages of the crustal layering structure and mantle temperature distribution of model 4 (TM4) every 25 km of Cantabrian Zone upper crust shortening with again harder Central System's rheology, bigger angle for the southern fault of the Cantabrian Mountains, 45° between the two rheologies of the Duero basin upper crust, and has middle crust in the transition part between the Iberian and the Eurasian plates. A panel displays the modifications from TM3 model Left panels (B-E) show the crustal bodies and the temperature evolution and right panels (F-I) show the strain rate second invariant evolution.

the middle and the second (the highest) in the NBT. The average elevation in the Duero Basin is ~650 m. The topography in the Cantabrian Mountains shows two peaks, the highest of ~2200 m and a northern one of ~1700 m. The Cantabrian Mountains finish with a slope that reaches 800 m depth, and then the oceanic part has a peak above the sea level. Northwards, the oceanic topography has little folding with an average depth of 1 km. All the models present this oceanic promontory which can be related to the Le Danois Bank, a submarine mountain offshore the Cantabrian Margin.

Model TM2 which includes a mid-crustal detachment, has two maximums in the Central System (2200-2400 m) and a mini basin between them with an average elevation of ~1500 m. This model shows a basin southwards the Central System in the Tagus basin region. The maximum elevation is now located in the Central System, with ~2400 m, while the maximum peak in the Cantabrian Mountains is ~1700 m. The TM2 model also presents the lowest topography in the Eurasian crust (1200 m depth). TM3 model, the one with softer rheology in the Central System, shows mainly a flat topography around ~2300 m. As in the TM2 model, the maximum peak in the Cantabrian Mountains is lower than in the Central System. TM4 model has the highest altitude among all the models of Central System exceeding 2500 m of elevation. Also, it shows two peaks in the Cantabrian Mountains with the highest located further to the north.

Regarding to the base of the crust, in the TM0 reference model the average depth below the Duero basin is 34 km, and it shows two minimums beneath the Central System. For TM1 model (blue profile), the average depth of the crustal base in the Duero basin is 32 km, it shows a bulge under the Tagus basin reaching near 34 km depth, and the Eurasian crustal base is at~12 km depth. Also, the Moho in the transition zone between the Iberia and Eurasian plates has a bulge reaching 20 km depth. TM2 model (orange profile) also shows two minimum below the Central System. The lower crust subduction below the Cantabrian Mountains has the smallest angle among all the models. TM3 model (green profile) results in a crustal root just below the Central System which reaches ~37 km depth. TM4 model (purple profile) has the deepest crustal root under the Central System. All models

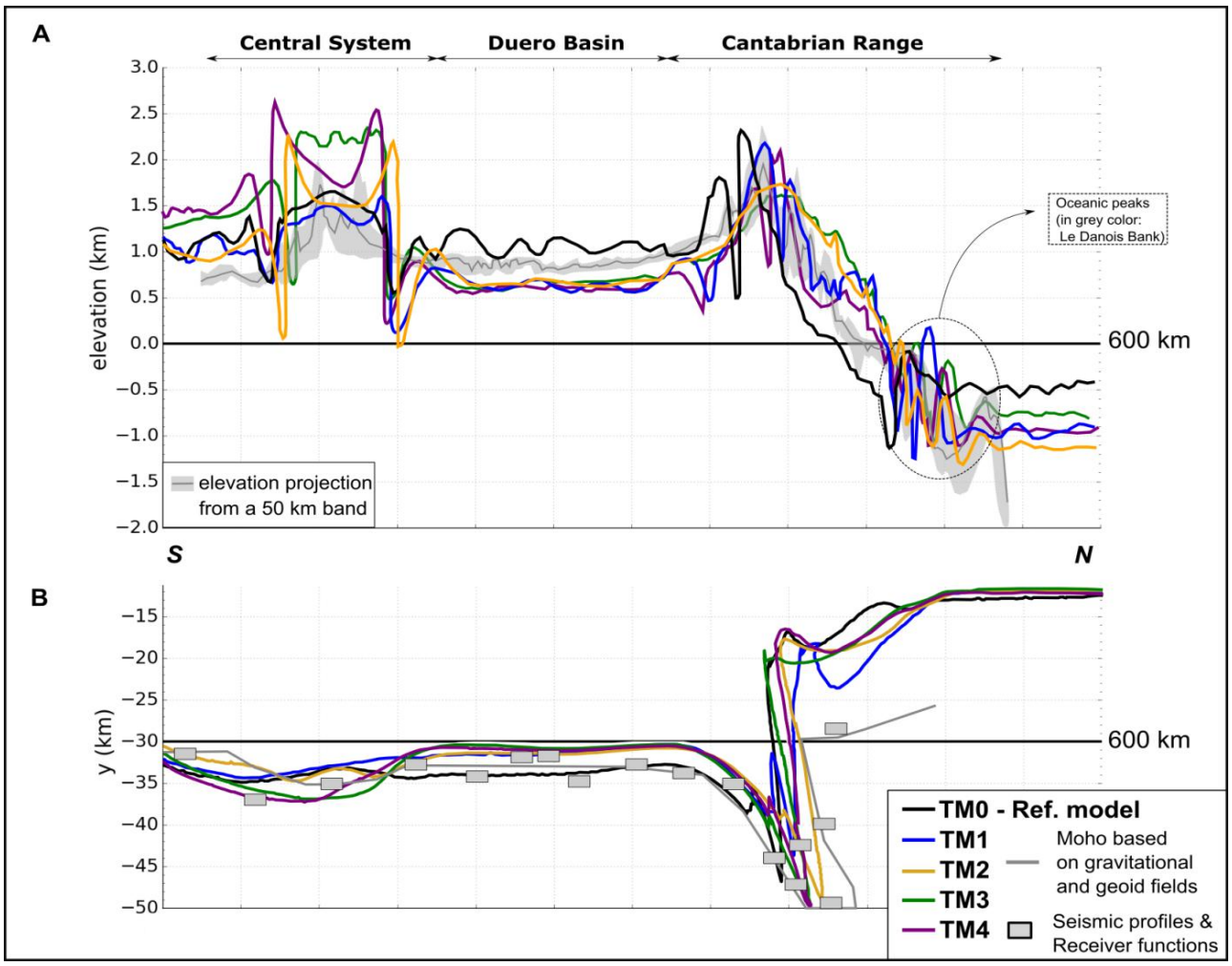

Figure 4.14. A) Modeled and observed elevation along the transect (dashed blue line from Figure 4.1). B) Depth of the base of the crust resulting from the models compared with the inferred by Carballo et al. (2015).

show how the Iberian lower crust subducts with a gentle angle below the Cantabrian Mountains. Values vary between 42 to 50 km depth being the shallowest the TM1 model and TM4 the deepest.

Figure 4.15 (at the end of this section) shows the shortening accumulation for the three regions, Central System, Duero basin and Cantabrian zone. During the first 10-15 My of convergence, practically all the shortening is concentrated in the Cantabrian zone, where all models have the highest shortening rate (Figure 4.15C). After 55 My, the TM0 model results with the lowest shortening in the Cantabrian zone, meanwhile the greatest amount of shortening corresponds to the TM2 model. More discrepancies in shortenings can be seen in the Central System (Figure

4.15A). All of the models present no shortening during the first 5 My. TM3 and TM4 models are the first ones to start accumulating shortening in the Central System and the reference model and TM1 are the latest where this accumulation occurs. The shortening rates are practically constant during the last 40 My of convergence on the TM0, TM1 and TM2 models. The shortening rates on TM3 and TM4 models are higher during the first 20 My than the last 40 My. In the Duero basin, practically there is no shortening the first 15 My. The shortening starts earlier in reference model (~10 My) and it increase faster. TM3 and TM4 are the models that accommodate less shortening in the Duero basin.

Figure 4.15. A) Central System shortening for all the models. Crosses are values of shortening from previous studies: [1] 50 km of shortening from Banks & Warbuton (1991); [2] 24 km from de Vicente & Vegas (2009), and [3] 22 km of shortening from de Vicente & Muñoz-Martin (2013). B) Duero Basin shortening. C) Cantabrian Mountains shortening, and crosses represent different shortening values from previous works: [4] 96 km of shortening from Gallastegui (2000); [5] 97 km of shortening from Pedreira et al. (2015); [6] 96 km from Fernández-Viejo & Gallastegui (2005); [7] 85 km from Machiavelli et al. (2017), and [8] 80 km from Teixell et al. (1998)

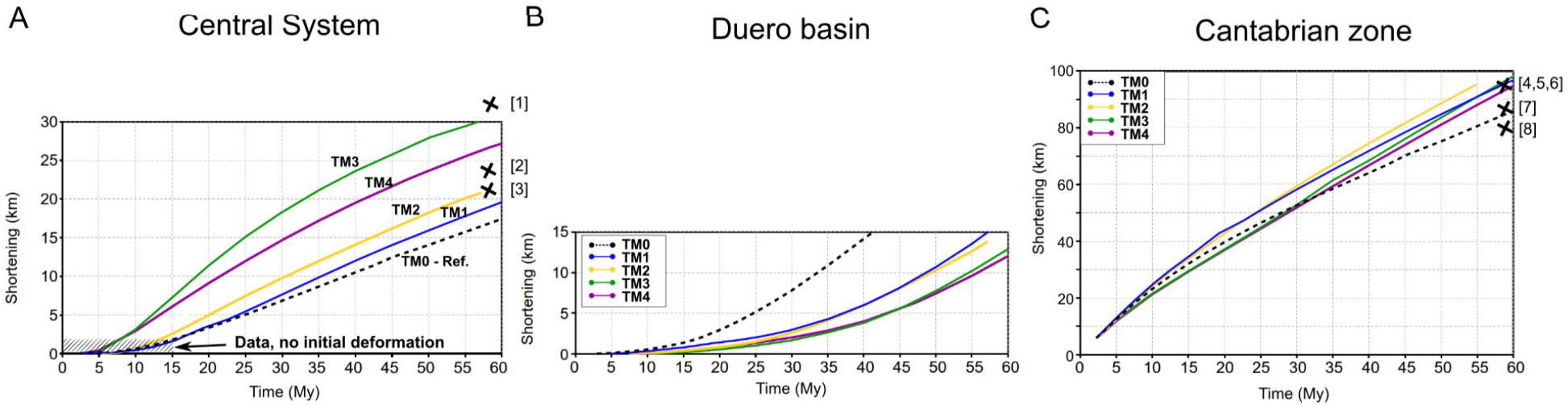

4.3 Thermomechanical 2D model of the Iberian microplate.

In order to link the deformation in Northern Iberia with the relative plate motions between Africa and Iberia, in this section the previous lithospheric section is prolonged south-eastwards (Figure 4.16). The main objective is to test if the southern compression of Africa against the Iberian microplate may have modified the distribution of shortening in the Central System by transmitting stresses from the south boundary to the interior as suggested by previous studies for this area (e.g., Banks and Warburton, 1991; Quintana et al. 2015).

The new part of the section crosses southern Iberia from the Central System domain to the Rif Mountains in Morocco. For this part, we were mostly inspired by the kinematic model done by Vergés and Fernández (2012), (Figure 4.16B). These

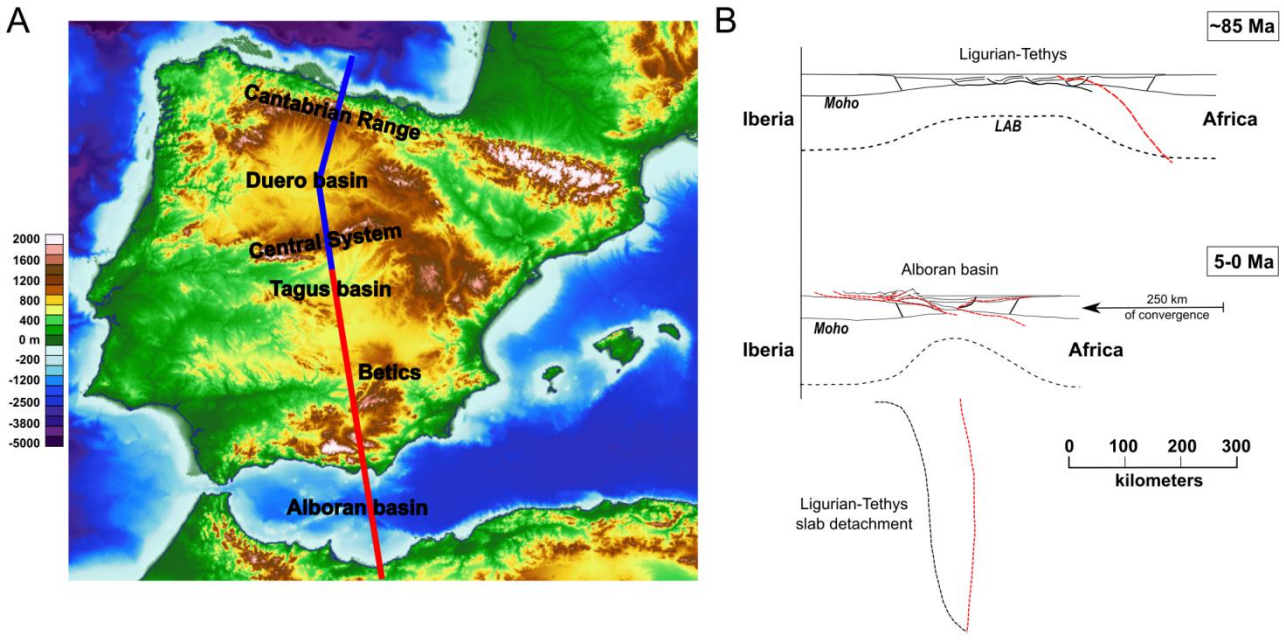

Figure 4.16. A) Transect location from north boundary of the Iberian Peninsula to south boundary. Blue line corresponds to previous modeled transect in this thesis. Red line stands for the extended. The Iberian topography is plotted using the Etopo database. B) Initial and final stage of a transect between Africa and Iberia according to the kinematic model from Vergés & Fernàndez (2012).

authors describe the evolution of the Betic-Rif orogenic system along in a transect oriented SE-NW for the last 85 My with a kinematic model constrained by a good data of plate reconstructions, tectonic, sedimentary and metamorphic. They proposed a slow subduction of the Ligurian-Tethys to the south-east beneath Africa followed after middle Oligocene by a faster subduction to the east. Figure 4.17 represents the set-up of the transect. The geometry of the bodies in the northern sector (blue line) are the same as TM4 model from section 4.2 and the extended sector includes: A southern plate lithosphere analogue to African lithosphere, a transitional basin analogue to the Alboran basin, a Southern Range analogue to the Betics Range and a Southern Basin analogue to the Tagus basin. The input parameters are specified in Table 4.4 and the sublithospheric mantle has the same rheology as models from section 4.2. The rheology used is dry quarcite for all the new domains except for: i) The crustal viscosity of the Southern Plate (Africa) is multiplied by a factor of 3 to prevent a large deformation in that area (which is out of the scope of the present study). ii) The rheological behavior of the lithospheric mantle of the Southern Plate is of a dry olivine power law. iii) The domain named Transitional crust analogue to the Alboran crust in our model, at Cretaceous time was part of an oceanic regime which it has a denser crust than continental densities; it is a viscoplastic rheology with a viscosity cut-off of 10^{23} Pa·s that follow the Byerlee plastic criteria. iv) The Transitional lithospheric mantle is denser to force subduction dipping southwards and is twice viscous than the Iberian lithospheric mantle. In Figure 4.17 C and D we show how density and viscosity change with depth with a strain rate of 10^{-15} s^{-1}. Black triangles above the crust in Figure 4.17A are used to control the shortening between domains.

The boundary conditions consist of: free slip at the top and bottom walls of the domain and periodic in the vertical boundaries ensuring mantle and sticky air flow. The sticky air layer which has a lower viscosity of 10^{18} Pa·s. Other assumptions are:

- Distance between the Southern Plate (analogue to the African plate) and the Intermediate (Iberian) Plate main lands is 300 km. Previous works suggest

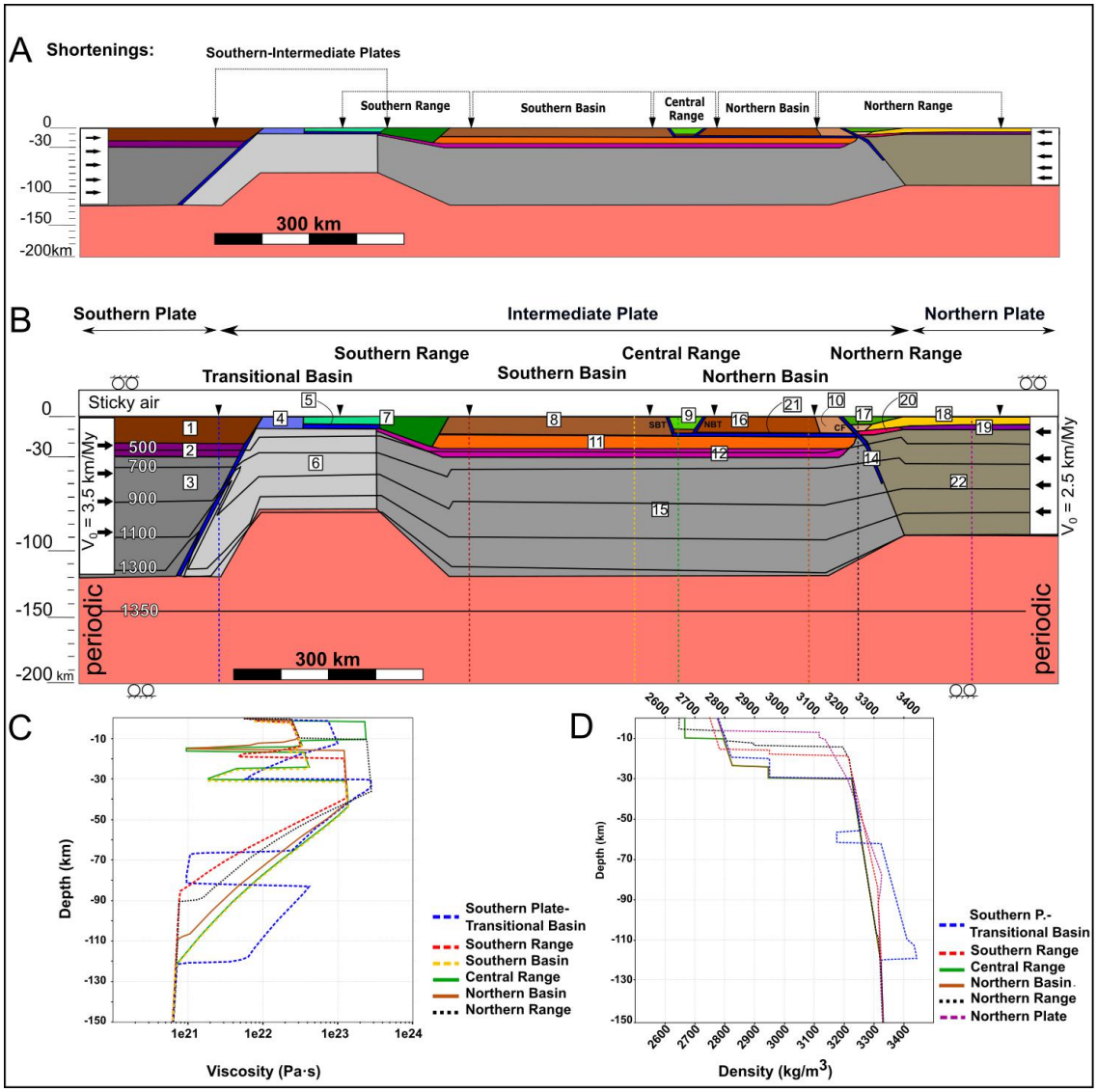

Figure 4.17. A) Scheme with scale 1:1 to follow the shortenings for the different domains. B) Material layering set up for the thermomechanical model which transect is in Figure 4.16 A. Black lines correspond to the initial temperature field. The model is divided in 7 domains, from south to north: Southern lithosphere analogue to the African lithosphere, the transitional lithosphere analogue to the Alboran lithosphere, the southern range analogue to the Betics, the southern basin analogue to the Tagus Basin, the Central Range analogue to Central System, the Northern basin analogue to the Duero Basin and the Northern Range analogue to the Cantabrian Range. Black triangles over the crust are the markers to control the shortening in A. The properties for each body are listed in Table 4.4. C) Viscosity vertical profiles when a constant strain rate second invariant of 1e-15 s^{-1} is applied to the model. D) Density profiles.

350-400 km of separation from Iberia and Africa (e.g., Rosenbaum 2002a; Capitanio & Goes, 2006) the modeled transect is more north-south oriented (red line Fig 4.16 A).

- A décollement is introduced under the Southern Range domain (analogue to the Betic domain) and in the Transitional basin acting as a Keuper material with low viscosity and cohesion (body 5).
- A northward velocity of 3.5 mm/yr is imposed to the lithosphere of the Southern Plate, and a southward velocity of 2.5 mm/yr to the Northern Plate (analogue to Europe) (white boxes with arrows inside in Figure 4.17A and B). Both velocity zones are localized far from the collision zones to not interfere with anomalous high values of strain rate. Vergés and Fernàndez (2012) suggested for their model an initial convergence value of 2.0 mm/yr in the first 55 My of convergence between Africa and Iberia and at mid-Oligocene times an increment up to 4.8 mm/yr in concordance with most of previous studies, so the chosen velocity will be the average velocity to ensure more than 250 km of convergence between the both plates in the model.
- A weak zone is imposed between the Southern Plate lithosphere and the Transitional lithospheric mantle as a suture zone low viscosity (10^{18}Pa·s) with low cohesion (1MPa·s), high temperature and with a 45° dipping angle. This is simulating an asthenosphere upwelling between the slab and the southern mantle in a roll-back process.

The model is 2800 km long and 660 km depth. With 1536 x 448 cells that makes a resolution of 1.82 km horizontal and 1.47 km vertical. Initially, the model has 15 particles per cell, with a total of 10,32 million particles.

This model attempts to address the hypothesis that south Iberian compression due to Africa north convergence may have transmitted stresses to the inner parts of the Iberian Peninsula during the Cenozoic compression and modified the shortening in Central System. Thus, we do not aim at modeling the full south geodynamic evolution and structural distribution of the geological units in the Betics, and Alboran domains, but instead we incorporate this region only as a way to force shortening in the continental scale. The evolution of the Betic-Rif is still under debate nowadays and there are still a lot of unknowns. Therefore, the

interest in this section is to analyze the intraplate deformation of a small plate with a southward subduction and under compression between two bigger plates. I will analyze the shortenings between the different intraplate basins and ranges.

Results for the TM5 model set up at 25 My are shown in Figure 4.18. It illustrates where the deformation is being accommodated during this first stage. The maximum strain rate locates in the Transitional lithosphere (Alboran) along all the weak zones from the Keuper material (body 5, Table 4.4) below the Southern Range domain (Betics) and the imposed weak zone between the Southern Plate (Africa) and Transitional mantle. The Transitional lithospheric mantle decouples from the Southern Plate lithosphere allowing subduction. In addition, the Transitional Crustal domain and Southern Range crust have high concentrations of strain rate and deformation. The Transitional crust also is being dragged by the slab. The Southern Basin (Tagus), Central Range (Central System) and Northern Basin (Duero) suffer tectonic extension during this period (black arrows in Fig 4.18A). This extension is due to the subduction dipping southwards of the Transitional lithospheric mantle below the Southern Plate. However, in the northern margin of the Intermediate Plate there is tectonic compression, which is reflected in the accumulation of strain rate in the Northern Range zone (Cantabrian Range). A detachment level is activated connecting the lower crust of the Northern Range with the mid-crustal detachment from the Northern Basin. Some deformation locates also in the junction of the Northern and the Intermediate Plates (analogue to the Eurasian and Iberian plates) (Figure 4.18B).

Subduction of the transitional lithospheric mantle continues during the next 15 My, dragging part of the Iberian lithospheric mantle with it (Figure 4.19A). The asthenosphere flux, together with its higher density, gradually thin and finally break the slab below the transitional basin instead of rolling back with an upwelling between the southern plate and the transitional lithospheric mantle. Vergés and Fernández (2012), kinematic model first shows a slow subduction below Africa, then a roll back of the slab SE-NW, and a final faster subduction. In the TM5 model, the transitional crust keeps subducting as well as the Keuper material.

Bodies	Analogue geological domain (for comparison only)	ρ_0 ($kg \cdot m^{-3}$)	Creep Parameters				Plastic Criteria	
			Lithology	n	A ($MPa^{-n} \cdot s^{-1}$)	E ($kJ \cdot mol^{-1}$)	C_0 (MPa)	Law
1	Southern plate crust (Africa)	2780	3*dry quarcite	2,4	$6,7\ 10^{-6}$	156	30	Byerlee-Dislocation
2	Southern plate Lower Crust (Africa)	2950	3*dry quarcite	2,4	$6,7\ 10^{-6}$	156	30	Byerlee-Dislocation
3	Southern plate Mantle (Africa)	3300	Dry olivine	3,5	$2,4\ 10^{-6}$	540	48	Byerlee-Diffusion
4	Transitional Crust (Alboran)	3000	-	-	-	-	30	Byerlee-Dislocation
5	Transitional detachment (Keuper material)	3000	-	-	-	-	1	Byerlee $\propto C_0$
6	Transitional Mantle (Alboran)	3350	2* Wet olivine	1 & 3,5	10^6 & 90	335 & 480	30	Diff & Disl
7	Southern range (Betics)	2750	Dry quarcite	2,4	$6,7\ 10^{-6}$	156	30	Byerlee-Dislocation
8	Southern Basin Crust (Tagus)	2780	Dry quarcite	2,4	$6,7\ 10^{-6}$	156	30	Byerlee-Dislocation
9	Central Range (Central System)	2670	dry granite	3,2	$1,8\ 10^{-9}$	123	48	Byerlee-Dislocation
10	Upper Crust	2780	Wet quarcite	4	$1,1\ 10^{-4}$	223	30	Byerlee-Dislocation
11	Middle Crust	2800	Quartzdiorite	2,4	$1,3\ 10^{-3}$	219	30	Byerlee-Dislocation
12	Intermediate Plate Lower Crust	2950	Felsic Granulite	3,1	$8\ 10^{-3}$	243	5	Byerlee-Dislocation
13	C. System Faults	2780	Dry granite	-	-	-	5	Byerlee $\propto C_0$
14	Cantabria Weak Zone	3300	-	-	-	-	1	Byerlee $\propto C_0$
15	Intermediate Plate Mantle	3300	Wet olivine	1 & 3,5	10^6 & 90	335 & 480	30	Diff & Disl
16	Northern Basin Crust (Duero)	2780	Hydrated Quartz	2,3	$3,2\ 10^{-4}$	154	30	Byerlee-Dislocation
17	Mesozoic Sediments	2650	Wet quarcite	4	$1,1\ 10^{-4}$	223	5	Byerlee-Dislocation
18	Northern plate Crust (Eurasia)	2860	Wet quarcite	4	$1,1\ 10^{-4}$	223	30	Byerlee-Dislocation
19	Northern plate Lower Crust (Eurasia)	3120	Wet quarcite	4	$1,1\ 10^{-4}$	223	30	Byerlee-Dislocation
20	Northern Range Lower Crust (Cantabria)	2900	Wet quarcite	4	$1,1\ 10^{-4}$	223	30	Byerlee-Dislocation
21	Mid-Crustal Detachment	2800	-	-	-	-	1	Byerlee $\propto C_0$
22	Northern plate Mantle (Eurasia)	3300	Dry olivine	3,5	$2,4\ 10^{-6}$	540	48	Byerlee-Diffusion

Table 4.4. Bodies properties for the thermomechanical model of the setup in the Figure 4.17. Creep Parameters are chosen from Karato & Wu, 1993; Gleason & Tullis, 1995; Fernàndez & Ranalli, 1997; Martín-Velazquez et al. (2012); and Pedreira et al (2015). Densities reference values are from Álvarez-Marron et al. (1996); Gómez-Ortiz et al. (2005) and Carballo et al. (2015). Byerlee $\propto C_0$ indicates the non-dependence of the frictional coefficient and depth por the plasticity criteria.

A clear thinning of the southern Intermediate Plate lithosphere can be observed due to the drag of the slab southwards. Consequently, the extension sustained in the entire Iberian crust, even in the northern basin. The convergence between the Southern plate (Africa) and the Southern Range of the Intermediate Plate lithosphere reaches 266 km in this 40 My. Strain rate (Figure 4.19B) reveals the high concentration of deformation in the Transitional and Southern Range crusts due to both processes, subduction of the lithosphere and the convergence between Southern and Intermediate Plates. The Southern Basin's extension is now

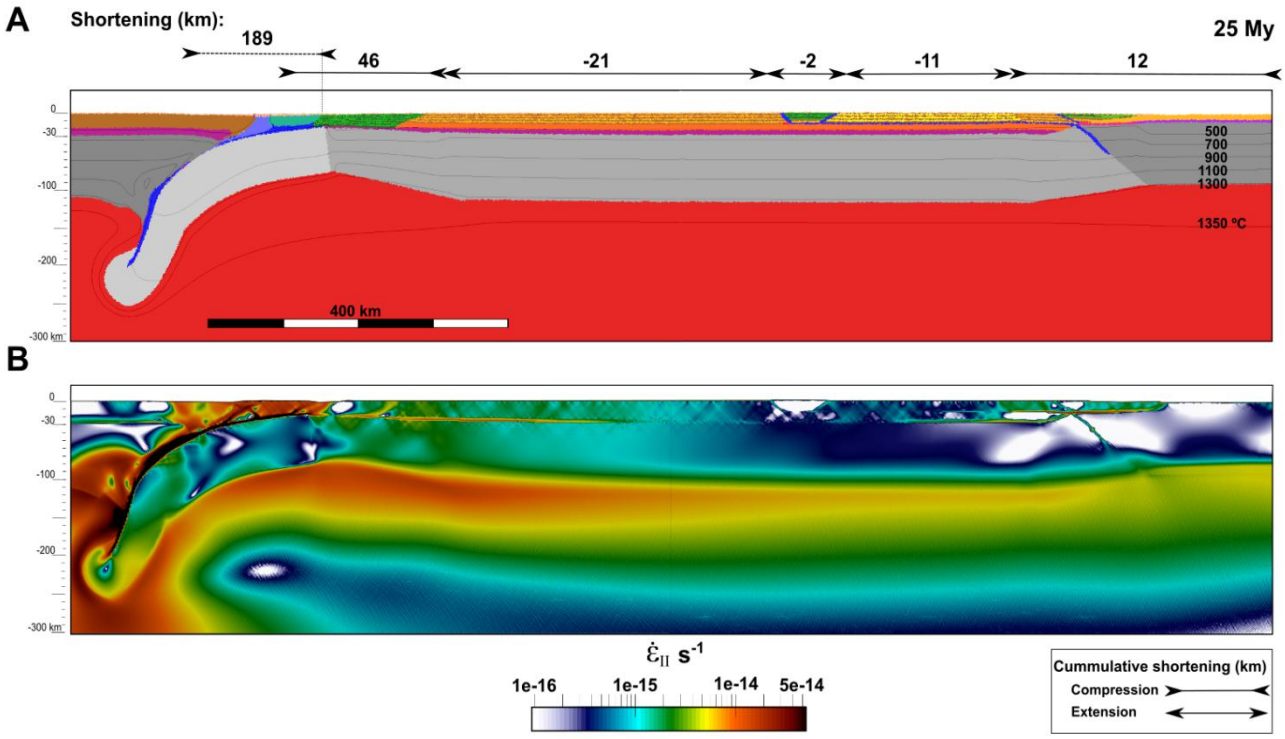

Figure 4.18. Results for TM5 model set up at 25 My. A) Material layer distribution after 25 My of geodynamic modeling. Grey thin lines correspond to the temperature isotherms. Cumulative shortening values are shown above each domain (Note the clarification box). B) Strain rate second invariant.

located in the northern part of this domain, reaching 67 km of extension. During this period a clear activation of the weak zone in the junction of the Northern Plate (Eurasian plate) and the Intermediate Plate lithosphere can be observed. The strain rate is practically null in this region.

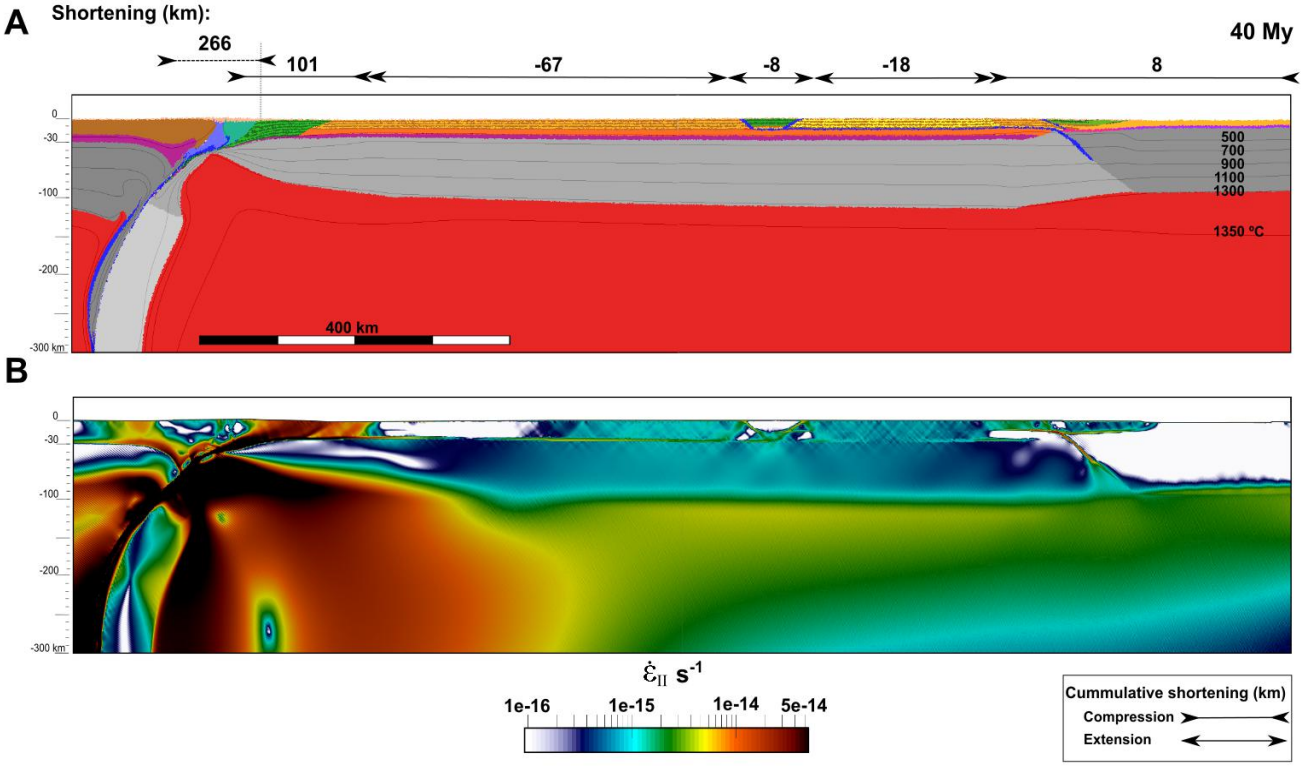

Figure 4.19. Results for TM5 model at 40 My time step. A) Material layer distribution after 40 My of geodynamic modeling. Grey thin lines correspond to the temperature isotherms. Cumulative shortening values are shown above each domain (Note the clarification box). B) Strain rate second invariant.

After 55 My (Figure 4.20), the slab has been broken and sunk into the asthenosphere. While the temperature is decreasing in the Transitional crust, part of it and the Keuper material (body 5, Table 4.4) that were subducted previously, accretes upwards. The convergence between the Southern Plate and the Southern Range changes from 266 km to 258 km, which is considered as an extension in the Transitional crust of 8 km. During this period the tectonic regime changed in the Southern Basin from extension to compression with 33 km of upper crust shortening (Figure 4.20 A). The Northern Range shortening increase up to 24 km while there was a southwards underthrusting of the Northern Plate on top the

Intermediate Plate. The deformation is accommodated in the Cantabrian Fault and in the lower crust, decoupling crust and lithospheric mantle.

The strain rate indicates that most of the shortening in the Intermediate Plate is taking place in the Southern Range and some in the Southern Basin. The lower crust is acting as a crust-mantle decoupling level from the Southern Range to the Southern Basin transmitting strain rates to the north of the basin. Additionally, some shear bands have been developed between the Southern Range domain and the Southern Basin domain. During this period the Central Range and Northern Basin do not have high concentrations of strain rates (Figure 4.20B). All the deformation of the north Iberian crust takes place in the Northern Range.

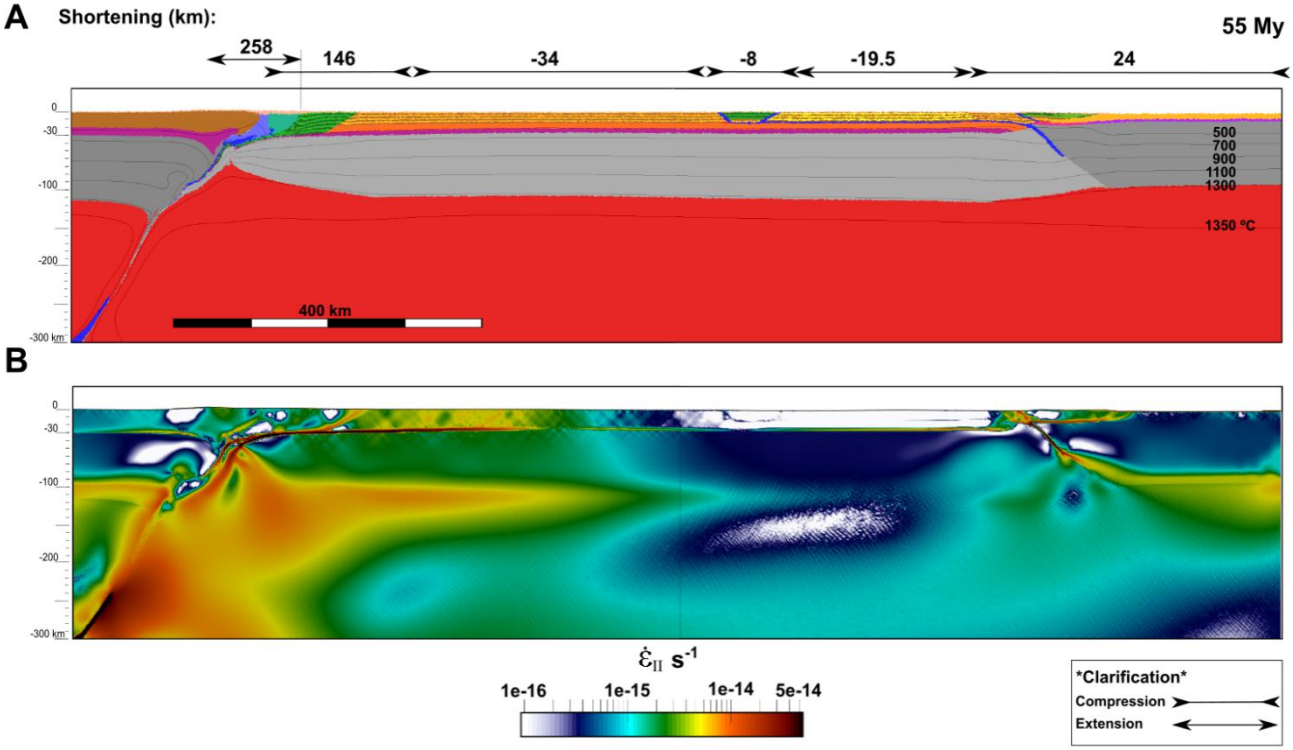

Figure 4.20. Results for TM5 model at 55 My time step. A) Material layer distribution after 55 My of geodynamic modeling. Grey thin lines correspond to the temperature isotherms Cumulative shortening values are shown above each domain (Note the clarification box). B) Strain rate second invariant.

After 72 My, the convergence between the Southern Plate and the Intermediate plate has stopped, both plates are now attached (Figure 4.21 A). The strain rate concentration in the collision crust between the Southern and Intermediate Plate is very low (Figure 4.21B). Most of the shortening occurred in

the crust of the Southern Basin with 45 km during this period and 3 km in the Central Range. The shortening accommodated in the Northern Basin crust is less than 3 km. In the northern zone most of the shortening is located in the Northern Range, reaching 52 km. The southwards underthrusting of the Northern Plate lithospheric mantle is still active. The underthrusting of the denser lower crustal body was complemented by the beginning of its indentation into the margin. This forced the beginning of subduction of the Intermediate lower crust dipping northwards. The SBT of the Central Range activates, accommodating some deformation The strain rate increases in the Northern Basin domain, obtaining some shortening (black arrows Fig 4.21 A vs. Fig 4.22 A). In the Northern Range and Northern Plate, the decoupling between crust and lithospheric mantle still exists and strain rate increments in the Eurasian side of the Northern Range, indicating that part of the shortening is generated offshore the margin.

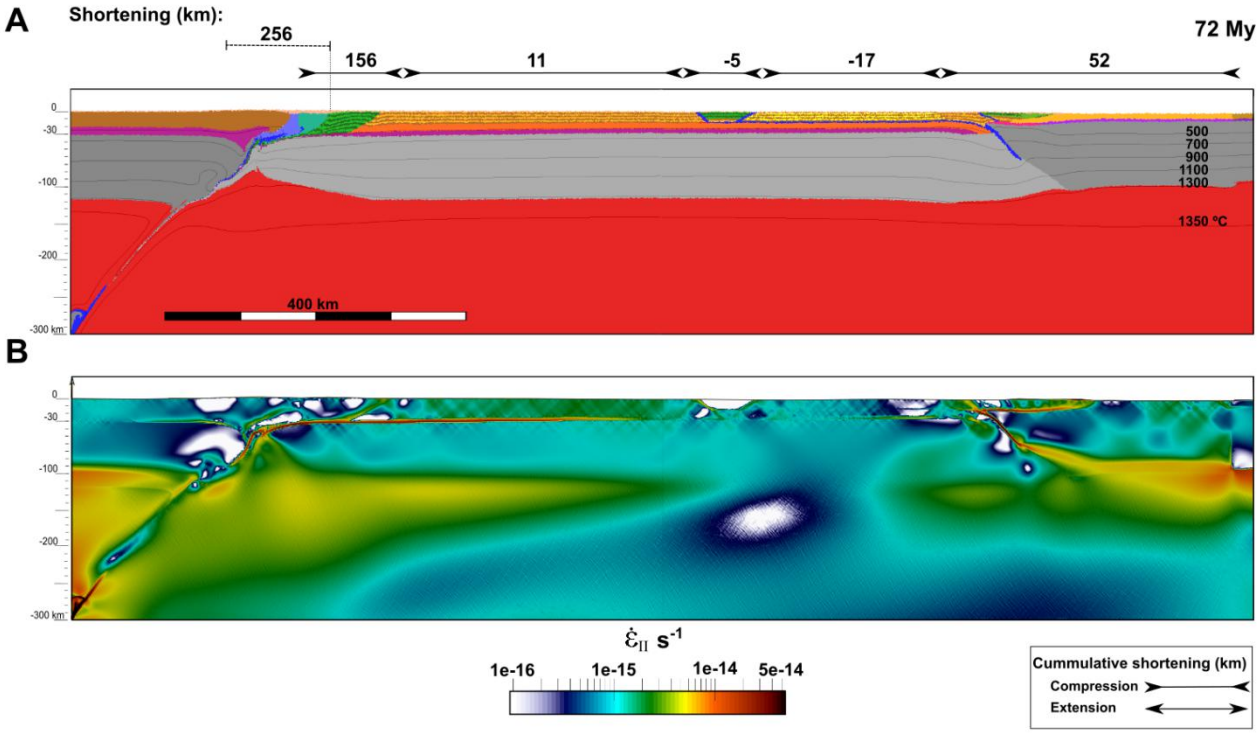

Figure 4.21. Results for TM5 model at 72 My time step. A) Material layer distribution after 72 My of geodynamic modeling. Grey thin lines correspond to the temperature isotherm. Cumulative shortening values are shown above each domain (Note the clarification box). B) Strain rate second invariant.

After 87 My of convergence (Figure 4.22), the shortening decrease in the Southern Basin reaching 31 km, but shortening increase to the north. The north dipping subduction of the lower crust Intermediate Plate is more incipient during this period (Figure 4.22A). Noticeable is the activation of a main shear band between the Southern Range and the Southern Basin during this period. The southern Iberian lower crust is accumulating strain rate transmitting stresses from the south boundary to inner parts of the Southern Basin domain (Figure 4.22B). Both faults in the Central Range are active during this period and root to the base of the crust.

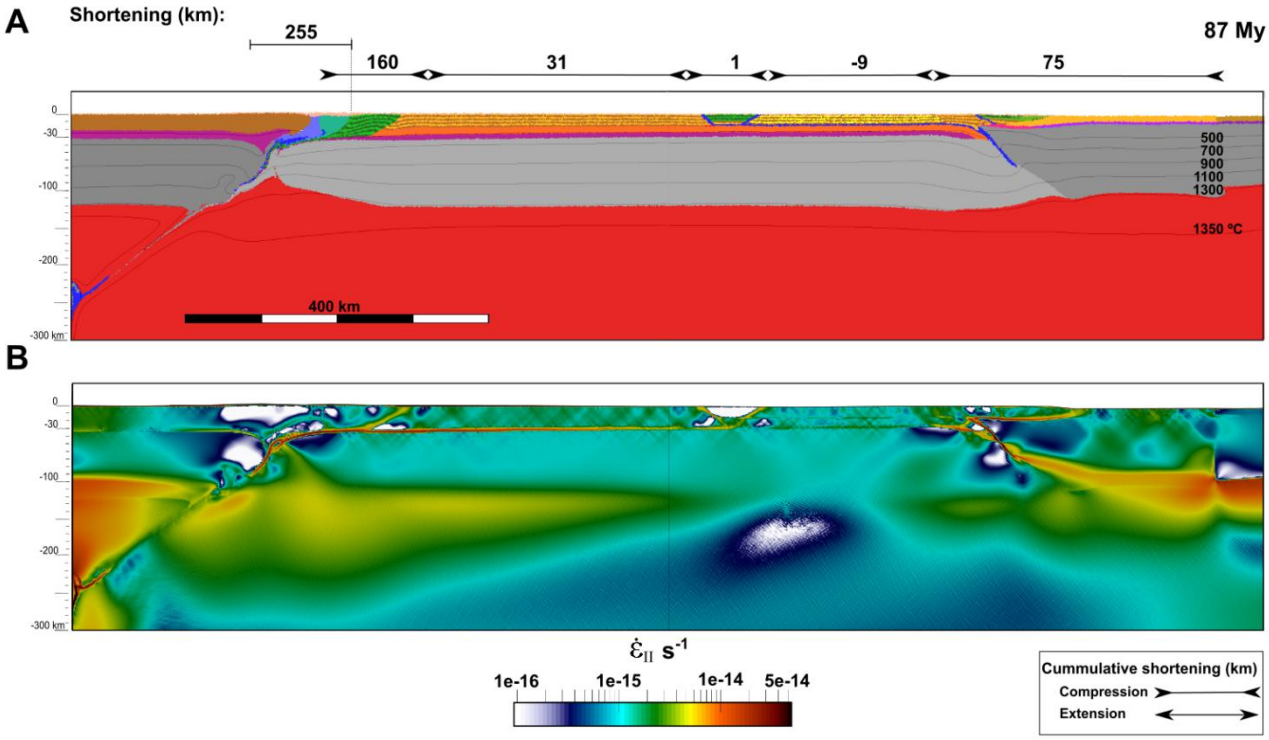

Figure 4.22. Results of TM5 model at 100 My time step. A) Material layer distribution after 87 My of geodynamic modeling. Grey thin lines correspond to the temperature isotherms. Cumulative shortening values are shown above each domain (Note the clarification box). B) Strain rate second invariant.

During the last millions of years of geodynamic evolution the Intermediate Plate crust shortening incremented in all the domains, reaching 97 km of total shortening in the northern margin (Figure 4.23A). The middle-lower crust of the Intermediate Plate is still subducting during this period. In this period, the lower

crust of the southern region of the Intermediate Plate still concentrates high concentrations of strain rate (Figure 4.23B). In the Central Range, the south boundary thrust (SBT) roots to the base of the crust, while the northern one (NBT) reaches to the mid-crustal detachment.

The extensional and compressional periods for each domain are clearly shown in Figure 4.24. The convergence between the Southern Plate (Africa) and the Intermediate Plate (Iberia) has two differentiated phases. First 40 My a fast convergence while the slab was subducting, and a stabilization phase where no convergence exists between both lithospheres. Except for a slight initial extension period, the Southern Range has three different phases (blue line). Between 8 to 38 My a shortening rate of 2.67 km/My, followed by a faster period during the slab break off with rates of 7.14 km/My, and a final slow rate of 0.64 km/My for the last 55 My of the geodynamic evolution. The Southern Basin, has an extensional

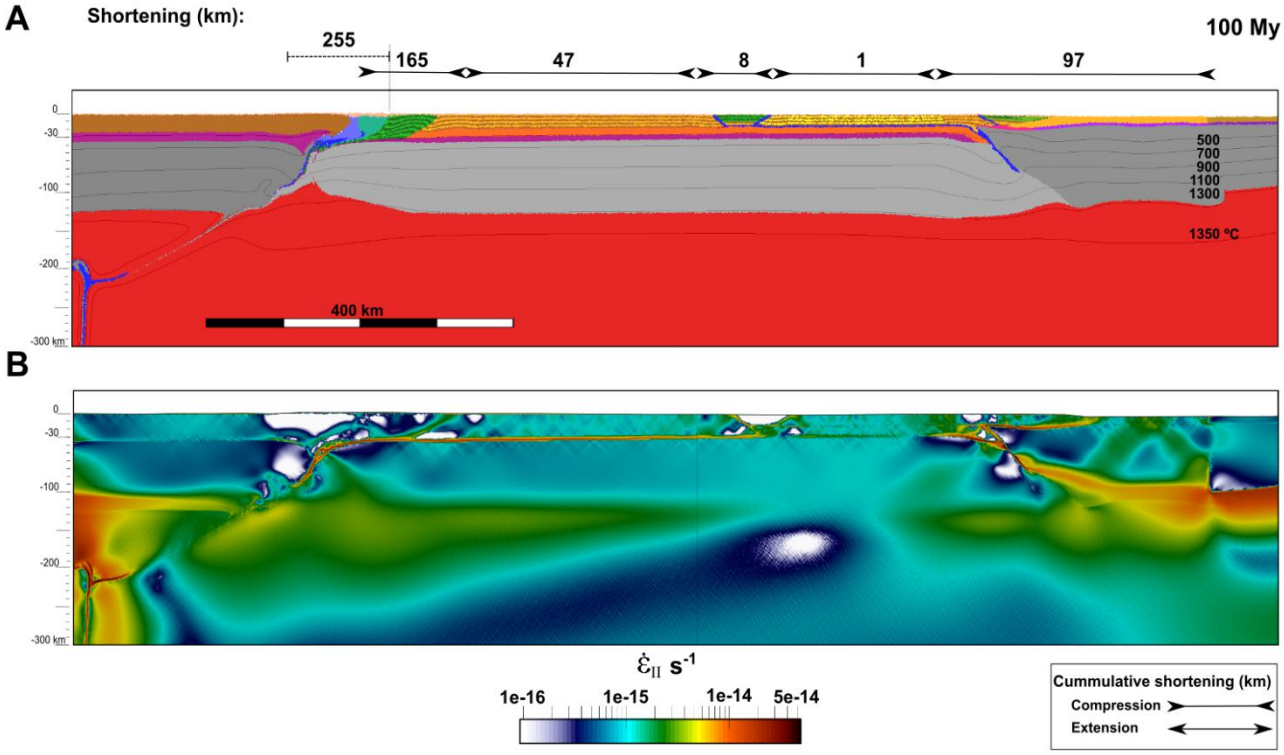

Figure 4.23. Results of TM5 model at 100 My time step. A) Material layer distribution after 100 My of geodynamic modeling. Grey thin lines correspond to the temperature isotherms. Cumulative shortening values are shown above each domain (Note the clarification box). B) Strain rate second invariant.

period of 1 km/My the first 30 My, then its suffers a high extensional rate of 4 km/My. It is the domain which suffers most extension, reaching 70 km in the second phase. Then it has two compressive phases, a faster one between 40 to 65 My of 2.8 km/My and a slower for the last 30 My of 1.33 km/My. The tendency of the Central Range and Northern Basin are similar. The Central Range does not have extension neither shortening the first 30 My, similar to the Northern Basin. Both undergo a fast period of extension between 30-40 My. The total accumulated shortening in the Central Range is 17 km in the last 45 My of the model. The Northern Range has first phase of compressional, with a slow rate of 0.67 km/My, a short extensional period and finally a compressional period with constant shortening rate of 1.5 km/My (~90 km of shortening).

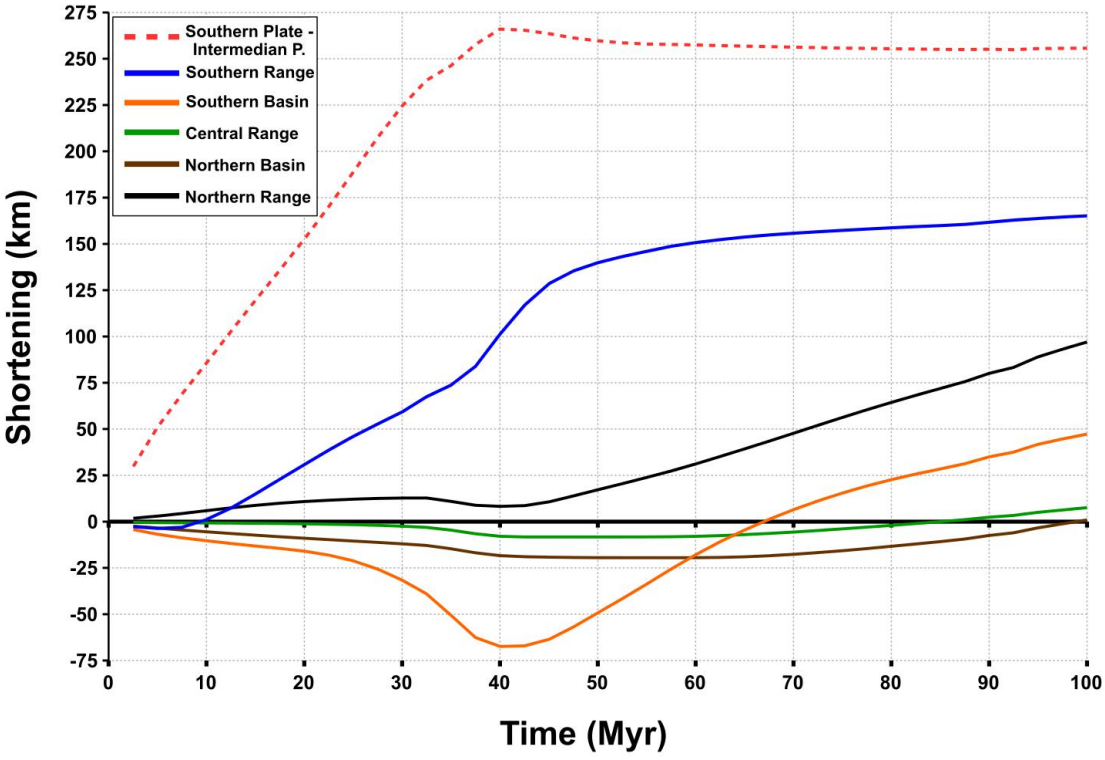

Figure 4.24. Shortening for the different domains. Red dashed line corresponds to the convergence between the Southern Plate (analogue to Africa) and the Intermedian Plate. A negative slope is considered as an extensional period, and a positive slope a compressional period.

Figure 4.25 displays the stress distribution for model TM5, showing the extensive and compressive periods between 10 and 55 My in the Intermediate

Plate. After the slab break up (from 40 My), stress changes from extension to compression in most of the plate. When the southern subduction is active, the slab

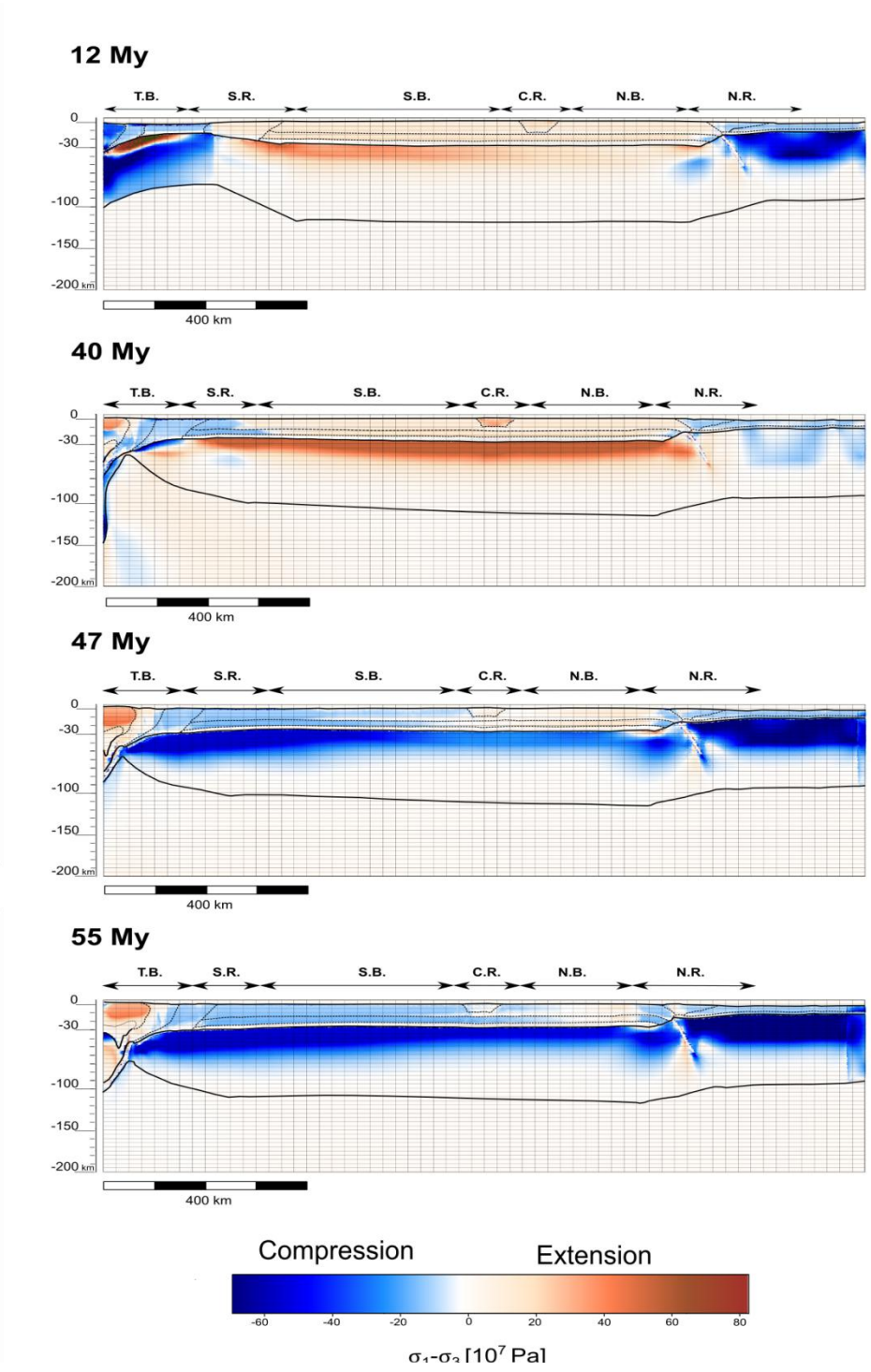

Figure 4.25. Differential stress distribution along the Intermediate Plate (analog to Iberia) of the model in section 4.3 (TM5), at four time steps. Negative values indicate tectonic compression (blue shading) and positive values mean extension (brown shade). Note the overall change from extension to compression triggered by the slab break-off at t = 40 My.

pulls the intermediate plate, bringing it under extension in spite of the overall convergence between the two surrounding plates (Africa and Eurasia).

Figure 4.26 displays the modelled elevation. The elevation is defined by markers located in a sediment layer (500 m thick) between the sticky air and the crust. The basin formed on top of the south subduction is about 0.5-1 km below the 0 level. The elevation decreases from the Southern Range to the Central Range. The crust of the Intermediate Plate is thickened in the Southern Range due to the huge compression in the zone, and the crust become thinner to the north. The Central Range average elevation is 400 m, and it is 500 m higher than the minimum value in the Northern Basin. In the Northern Range two clear peaks can be observed being the northern one the highest. Then the continental slope deeps fast to 3 km

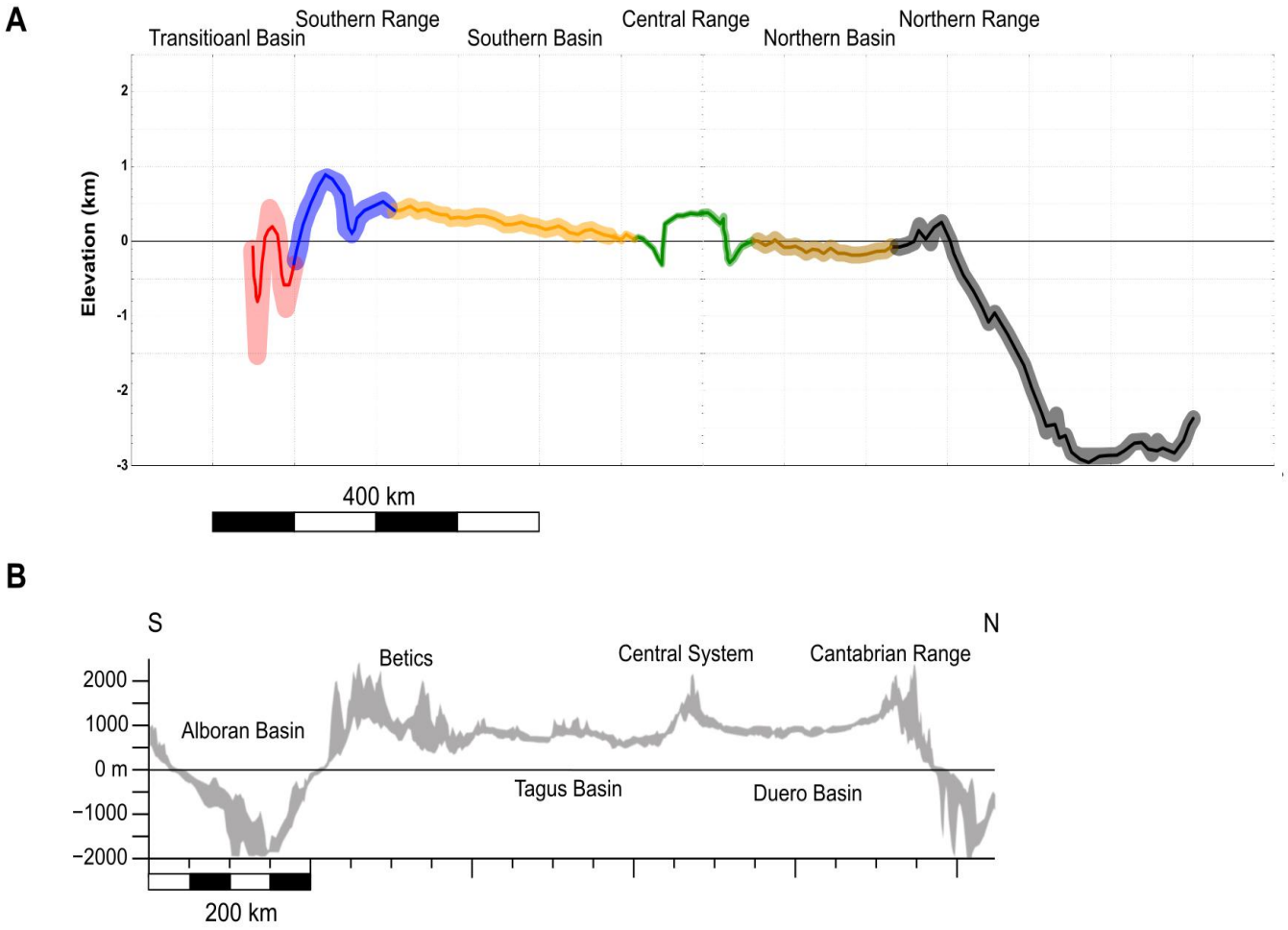

Figure 4.26. A) Elevation of the crust for the different domains of the numerical model with an error band due to dispersion of the markers for each domain. B) Etopo database topography projection from a 50 km band for the transect in Figure 4.16 A.

depth. Although the overall elevation of the model is less than the observed in Iberia, the distribution of the different geographical features can be identified.

Although the results of the shortening and elevation displays similarities with the observations and data from Iberia, the timings of the several stages are arbitrary. This model helps us to understand the deformation within a plate submitted to several processes as tectonic convergence, slab subduction and slab break off. Each stage affects in a different way the intraplate deformation, having periods under extension and compression, and localizing the deformation on different zones. The model presents some limitations, related to crustal and mantle rheology, or to processes that can affect the composition of materials and the distribution of temperature, such as, material phase change, melting, porosity, fluid transport, etc. Other processes that affect the evolution and the elevation are the surface processes, like the erosion and sedimentation. The accumulation of sediment in endorheic basins has been proven to be a mechanism contributing to topography flattening and significant elevation increase in the Ebro and the Duero Basins (e.g., García-Castellanos & Larrasoaña, 2015; Rodríguez-Rodríguez et al., 2020).

Chapter 5

Discussion

5.1 Double vergence vs. crustal folding

Far-field (intraplate) deformation has been the target for numerical modeling since the earliest earth-science computer modeling in te 80s. Lithospheric folding theories started pointing out the relevance of the viscosity contrast between lithospheric layers in order to generate folding with different wavelengths (Biot, 1961; Smith, 1975). The linear analysis for the wavelength of folding in the 60s was not enough for many different small scales crustal folds. The main reason was not considering gravity and friction and, the rheology was pressure -, strain - and temperature-independent. Non-linear rheologies can support regular folding cases and non-regular folding, such as, biharmonic folding where the crust presents a dominant wavelength and lithospheric mantle presents a larger one (e.g., Burov et al., 1993; Cloetingh et al., 1999). Pioneer modeling studies of continental deformation found for most lithospheric-scale folding cases that the ratio between the folding's wavelength (λ) and the thickness of the folded layer (h) ranges between 4 to 6 (after Burov et al., 1993). Burov et al. (1993) found a relationship between the ratio λ/h and the ratio of the crustal layer viscosities (μ_2/μ_1) according to which, when high strain localize in a region, the effective viscosities ratio (η_2/η_1) controls the non-dimensional growth rate of the vertical undulations

or folds. After this study, effective viscosities are assumed to have a contrast at least of two orders of magnitude in order to present folding for elasto-visco-plastic rheology in the majority of cases (e.g., Gerbault et al., 1999; Vanderhaeghe et al., 2003). Hunt et al. (1996) suggested the importance of elasticity in large amount of shortenings, generating aperiodic folding, and indicated the relevance of the viscous effects for the wavelength distribution over time. Cloetingh et al. (1999) corroborated the idea of lithospheric-scale folding as a response to tectonic compression, the importance of the gravity force to form megafolds and the necessity of strong rheology to preserve folds over long time periods (more than 20 My).

In Chapter 3 section 1, I address a continental collision scenario where shortening is initially facilitated by an inherited weakness dipping towards the upper plate and triggering underthrusting. The models encompass the whole lithosphere and extends enough down into the sublithospheric mantle to avoid bottom boundary effects. These Underworld-based models are naturally isostatically compensated, in the sense that lateral pressure gradients at the asthenosphere are naturally homogenized as a result of the depth-viscosity distribution adopted. This is in contrast with models with prescribed velocity subduction boundary conditions applied to the base of the crust or S-point models (e.g., Willet et al., 1993; Beaumont et al., 1994, 1996 & 2000; Willet, 1999, Pfiffner et al., 2000; Vanderhaeghe et al., 2002). This type of models need incorporating arbitrary subcrustal loads to simulate the negative slab buoyancy (Boonma et al., 2019). The methodology employed, allows to explicitly model subduction and study the role of subducting lithospheric in the topographic evolution and crustal deformation in the overriding plate. The models presented in Chapter 3 do not include any oceanic or transitional lithosphere between the two continental ones. Many studies incorporate this to study the crustal deformation and later evolution of the continental lithospheric plates (Schmalholz et al., 2009; Sokoutis & Willingshofer, 2011; Jammes & Huismans, 2012; Burov et al., 2014; Liao & Gerya, 2017). In these studies, sediments and the content of water in minerals subducting plays an important role in the subduction channel and influence the viscosity

contrast between both continental lithospheric plates. The models from Chapter 3 have disregarded this for the sake of simplicity and with the goal of focusing on the propagation of deformation upon collision.

The results showed in Chapter 3 are consistent with the two orders of magnitude of minimum viscosity contrast between a strong upper crust and a weak lower crust required by Burov et al. (1993) and Cloetingh et al. (1999) to obtain crustal folding. Figure 5.1A compares the initial viscosity ratio (horizontal axis) vs. the cohesion ratio (vertical axis) between the upper crust and the lower crust layers for all the models. Colours represent the relieve, the difference between the maximum orogen elevation (h_{max}) and the average elevation at 200 km from the orogen (h_{distal}) divided by the maximum elevation (h_{max}) (see Figure 5.1B for clarification). Models that develop a double vergence orogeny after 100 km of crustal shortening have relieve value above 0.9 (brown to yellow in Figure 5.1A). Models that develop folding have values below number 1 (dark brown to dark purple). Double vergence models have an initial viscosity ratio equal to 100 or less and less than 6 for the effective viscosity ratio.

Vanderhaeghe et al. (2002) stated that a two orders of magnitude differences between the viscosity of the upper crust and the basement are enough to pass from the double vergence model to a plateau. This transition takes place when a full basal decoupling occurs. The main shear bands characteristic of double vergence orogens become more and more set-apart with time with the transmission of deformation through the basement. However, models presented suggest another mechanism allowing to switch from double vergence orogens to a distributed deformation that allows for upper crustal folding: The cohesion must be low enough in the lower crust, in order to allow the strain propagation and decrease viscosities in the lower crust towards the distal parts of the orogen. When the viscosity contrast between lower and upper crust is higher than the two orders of magnitude, deformation tends to propagate within the crust. Models from Chapter 3 do not evolve into a plateau, instead, new shear bands are localized and transmitted farther from the initial collision zone while basal decoupling grows with distance, generating well-developed folds within the crust. Not only with an

cohesion ratio between 4 and 6 appears the crustal folding model behavior, but also when there is a combination of two orders of magnitude in the initial viscosity ratio and a cohesion ratio higher than 6, or when the viscosity ratio is three orders of magnitude.

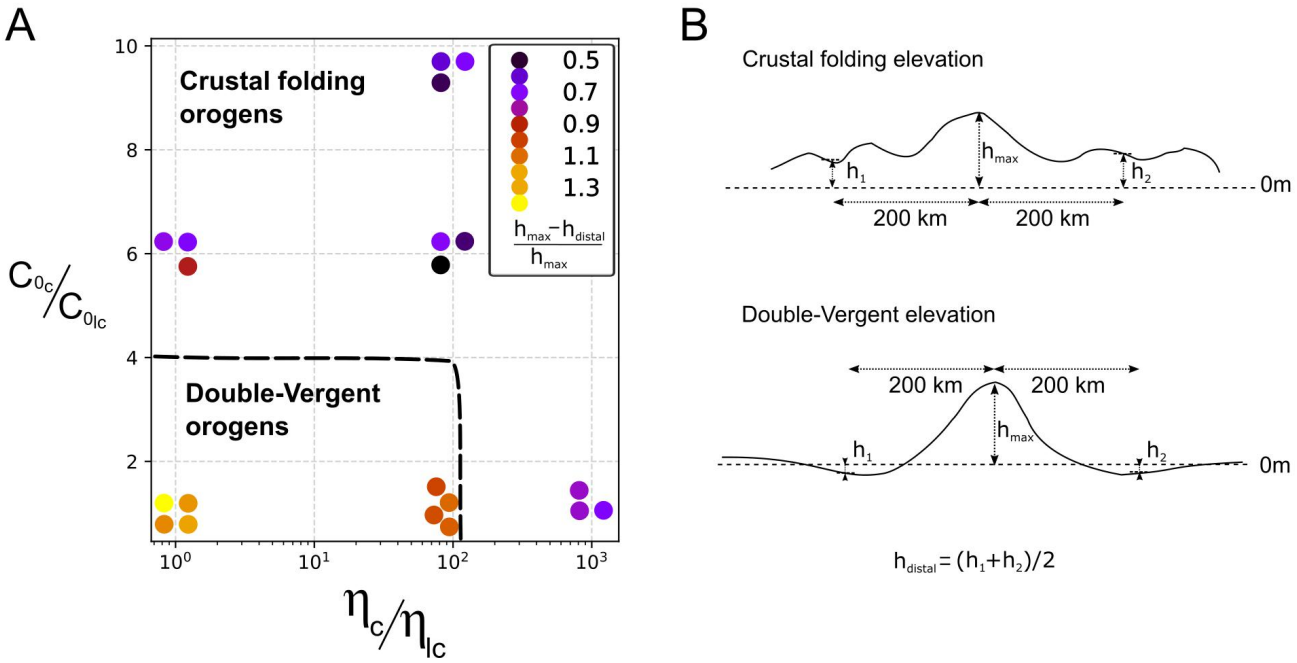

Figure 5.1. A) Overview of all models comparing crust and lower crust cohesion ratio vs. initial viscosity ratio when reaching 100 km of crustal shortening. The colour scale represents relieve: the difference between the maximum and the average value of a distal elevation divided by the maximum elevation of the orogen. Doble-vergent (DV) models correspond to values above 1. B) Schematic clarification to calculate the relieve shown in colours in A. h1 and h2 are the average (among the particles inside a cell) elevations at 200 km from the center of the orogen (higher elevation).

These results point out the need to consider how the deformation accommodates through time in a continental collision scenario. Burov et al. (2014) explore a variety of continental subduction scenarios and suggested the relevance of the convergence velocity and tectonic heritage which modifies the way of deformation of the mountain belts. Ruh et al. (2012) demonstrated that increasing the frictional angle in the basal layer makes thrust sheets longer, reducing the width of the orogen and the slope angle of the orogen increments (Figure 6; Ruh et

al., 2012). When the tectonic compression continues incorporating more materials above the weak layer, high strain rates and stresses are dispersed throughout the layered sequence. If the lower weak layer has a small frictional angle, cohesion decreases while the strain localizes in the layer. Consequently, the location of the deformation front occurs far from the backstop leading to the formation of wide fold and thrust belts as Zagros.

Jammes and Huismans (2012) also conclude that in contractional settings a weaker crustal rheology generates wider orogens with lower topography (like the Zagros Mountain Range) whereas a strong upper crust partially decouple of the lower crust lead to Alpine-style orogeny (like in Eurasian Alps or Pyrenees). This is reflected in Figure 5.1 where the crustal folding models imply wider orogens (considering the folds part of the orogenic system) and less topography than in the double-vergent models. In this sense, the difference between the maximum topography and the minimum in folding system is less than the difference between the maximum topography and the pro- and retro-basins of the double vergence models.

Duretz et al. (2013) explored the slab detachment during a continental collision and how it affects the crustal rheology in the later lithosphere structure. Although their models have an oceanic lithosphere between the two continental ones, they reach to similar results for the topography evolution: strong crustal rheology facilitates mechanical coupling generating narrow double-vergent orogens (<200km) with high topography. Weak crustal rheology provides decoupling at Moho, and the crust develops a series of folds. The models from this thesis are in concordance with this results without including the oceanic lithosphere in between the continental lithospheres, which may indicated that oceanic lithosphere subduction between two continental lithosphere is not a main factor controlling the type of orogen in the first stages of the geodynamic evolution.

From the modeling results presented in this thesis, it can be noted that the lower crust is subducting when it is weak enough to be decoupled from the upper crust while at the same time it remains coupled to the lithospheric mantle. Liao and Gerya (2017), analyzed the effect of the temperature at the base of the crust.

Temperatures values between 300 to 600 °C generate enough crustal decoupling to have crustal folding with part of the upper and lower crust subducting within the mantle and has a gentle curve. Crustal folding models from this thesis generate a gentle slab curve where high strain localizes between the lithospheric domains, remaining flat the overriding lithospheric mantle. On the contrary, double-vergent models develop steeper subduction angles, the strain rates are disperse in the overriding plate, and there is no localization of strain in the slab. In those cases, the lithospheric mantle presents a long-wavelength (~300 km) harmonic deformation. Analogously, Vogt et al. (2018) showed when a weaker lithosphere subducts under a strong lithosphere, the lower plate accumulates shortening and have a gentle subduction angle. Calignano et al. (2015) suggested that continental asymmetric subduction occur when a strong upper lithospheric mantle controls localization of deformation and exists a strong crust-mantle coupling. Song and Simons (2003) and Heuret et al. (2012) showed that there is a relationship between the topography of the forearc region and different parameters in which they include the dip subduction angle. Gerya and Meilick (2011) or Tan et al. (2012) showed that is the interface between the lithospheres, i.e., the subduction channel, that controls the lithosphere structure when subducting and therefore the dip angle of the incoming plate. They vary the viscosity of this subducting interface by different mechanism like changing the pore fluid pressure, the frictional strength or the thickness of serpentinized layer in the mantle wedge. In nature, studies like King (2001) or Schellart et al. (2008) demonstrated the lack of correlation between subduction dip angle and slab geometry, overriding plate shortening, and in general lithosphere structure during the subduction process. However, numerous authors explained the differences in crustal deformation in continental collision scenarios according to the length of oceanic crust subducted and its rheology, or depending on whether hydrated sediment has been subducted along with the crust (Gerya & Meilick, 2011; Dymkova et al., 2016; Andrić et al., 2018).

When the lower crust is strong enough to inhibit high contrast viscosity within the crust (not decoupled), the strain tends to localize near the suture zone producing two main shear bands and building up the orogeny as a double vergent

style. As there is no decoupling between crustal layers, most of the strain rate shift to the upper mantle, weakening and folding. This is in concordance with many studies suggesting that the degree of coupling in the collision zone is a major factor controlling the slab subduction, architecture, deformation of plates and orogen evolution (e.g., Faccenda et al., 2009; Luth et al., 2010; Tan et al., 2012; Willingshofer et al., 2013).

5.2 Role of inherited structures

Ziegler et al. (1998) suggested that pre-existing crustal faults decrease the strength of the crust being an important factor in localizing compressional intraplate structures at far distance from the center of the collision zone. Oblique and horizontal weak layers inherited can accommodate deformation and transmit stresses to distances up to 1600 km far from the collision (for instance, by the Paleocene deformation of the northern Alpine foreland or in the foreland Appalachian-Ouchita-Maratonn orogen in the Rocky Mountains). Our results from Chapter 3 support this hypothesis, specially for settings where crustal folding develops. Whenever a weak-horizontal layer at middle crust levels accommodates part of the deformation, or whenever it is the lower crust that plays the role of detachment level, high stresses tend to propagate via these layers to farther distances from the collision zone.

Other studies also suggest that differences in lateral variations of crustal strength can modify the way orogens evolve, which affects how the incoming plate subducts, the development of décollements, the accretion and intrusion of material from the lower crust or the mantle upwards to the upper crust, etc (e.g., Sokoutis & Willingshofer, 2011; Jamieson & Beaumont, 2013; Calignano et al., 2015; Vogt, et al., 2018). Jammes and Huismans (2012) and Jammes et al. (2013), apply this concept to explain the differences in crustal shortening between the western and eastern Pyrenees. In the eastern part, there is at least 65 km (40%) more shortening than in the western Pyrenees due to a weaker crust related to a Jurassic

hyperextension (for example, Teixell, 1998). This eastern part was a Cretaceous basin with marine sediments between the Eurasian and Iberian plates whereas the western basin has more exhumated mantle. The authors concluded that during the Cenozoic compression of the chain, the eastern basin was weaker than the western generating bigger deformation and higher topography towards the east.

In the Pyrenees-style deformation models showed in Chapter 3, we included a horizontal layer at the middle crust level acting as a Triassic salt. In models where this salt extends further than the subducting plane or weak dipping zone, the lower crust of the incoming plate subducts with the lithospheric mantle instead of being accreted upwards to the overriding plate (Figure 5.2). Various studies have shown the importance of a lower viscosity layer in between two colliding plates, which facilitates the subduction of lower crust into the mantle (Ziegler, 1995; Ellis et al., 1999; Luth et al., 2010; Willingshofer et al., 2013). In addition, a retro shear develops when this weak lower crust extends beyond the center of the collision zone. This is in concordance with models from Beaumont et al. (2000) which include inherited weak layers to decouple the lower crust from the mantle. The decoupling generates initially the retro shear and a pro-shear where crust material is accreted. This first thrust unit evolves into a compressed structure or eventually into a pop-up structure with more lateral transported crust. Therefore, the pro-shears form because of the decoupling imposed initially, and also due to the subduction of the lower crust.

Shallower detachment levels generate a crustal folding with a shorter wavelength as suggested by numerous previous studies where folding formation is related to the total thickness of the weak layer plus layers above and the relative thickness of the detachment to the cover layers (e.g., Simpson, 2009; Yamato et al., 2011). Including a salt layer in the Pyrenees style deformation models at 5 km depth validates this hypothesis. The location of these materials within the crust can vary the lateral shortening in a chain. The inherited location of weaker rocks and the inheritance of a faulted crust from the previous extensional event has been proven to shape the crustal evolution for the Pyrenees Chain (e.g., Beaumont et al., 2000; Jammes & Huismans, 2012; Erdös et al., 2014; Grool et al., 2019). In nature,

remarkable examples of crustal folding have been identified, such as the Zagros Mountain Belt located in Iraq. The shallower salt layer generates upper crustal folding in the Gachsaran upper mobile group (Vergés et al., 2011). This folding triggers crustal shortening in the pro-side of the imbricated zone and the Main Zagros Thrust (MTZ). It is well documented the different phases of the Eurasian Alps and Apennines evolution with episodes of thrusting and crustal-scale folding (e.g., Beaumont et al., 1996; Pififfner & Ellis, 2000; Schmid et al., 2017; and references there in). Some studies (f.e. Rosenberg and Kissling,, 2013), suggested than the upper plate also concentrates deformation when it has a decoupling between upper and lower crust in the upper plate (western Alps). This is comparable to the Figure 5.2Ia, when a weak zone decouples the upper crust and the lower crust in the retro-crust. Figure 5.2Ib, the weak zone is located only in the

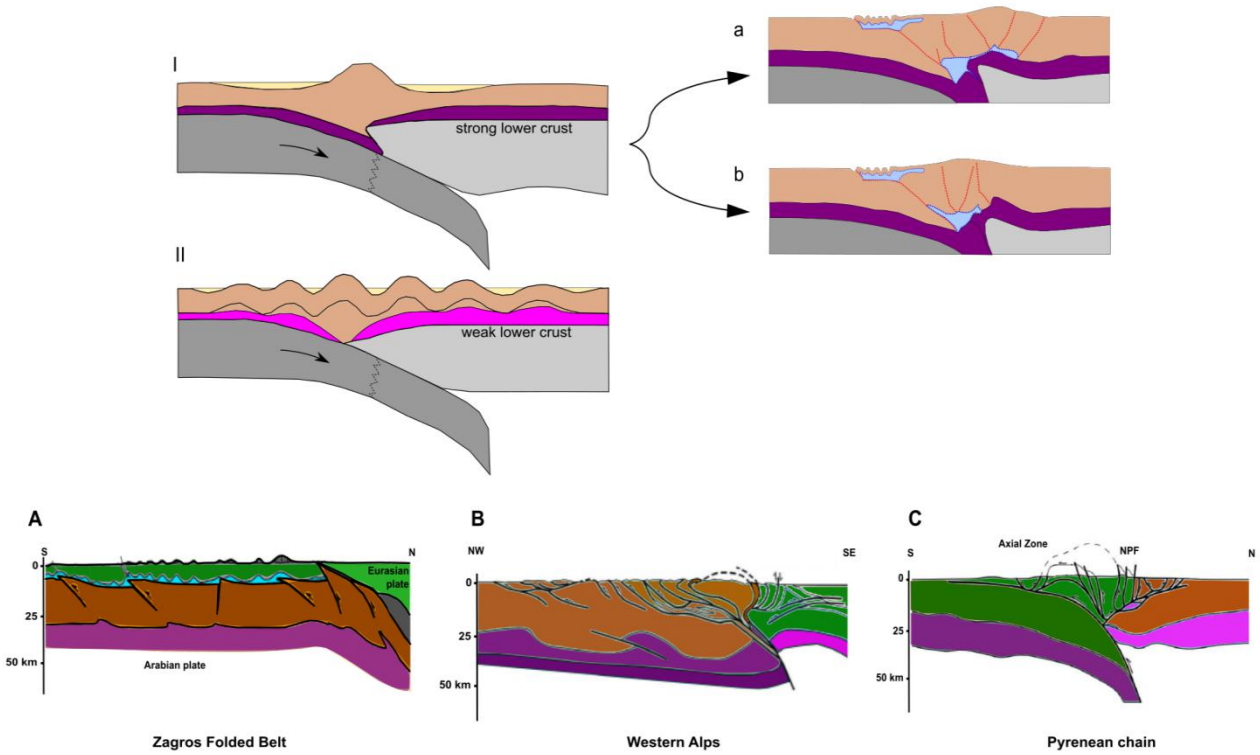

Figure 5.2. Summary of the end-member models steaming out of this work. I) Double-vergent orogeny model. a) Extended décollement. b) Not-extended décollement. II) Crustal folding orogeny model. A) Schematic cross section of Zagros folded belt (modified from Mouthereau et al., 2007). B) Crustal cross section across Western Alps (modified from Pfiffner, 2016). C) Crustal cross section accross the Pyrenean chain (modified after Muñoz, 1992)..

incoming plate, and the upper plate remains undeformed. In the Central Alps with the Ivrea body acting as a strong backstop, the deformation concentrates in the lower plate. Vogt et al., (2017), suggested that the strong coupling between crust and mantle for the incoming plate generates double-vergent orogens, whereas an intra-crustal décollement leads to lower topography, deformation of the upper-plate and thickening crustal thickenning. Figure 5.2 is in agreement with those results.

5.3 Accommodation of deformation between the Central System and the Cantabrian Mountains during the Cenozoic

As described in the previous section, many previous studies showed that inherited structures from past tectonic events modify the later response of a geological domain to tectonic boundary forces. This becomes also clear in the geodynamical models for the northern part of the Iberian microplate when introducing a weak zone down going to the lithospheric mantle beneath the Cantabrian ancient margin. Without this structure or weak zone, the Iberian lower crust cannot subduct, and the lithospheric mantle does not develop a root below the Cantabrian Mountains (Figure 4.7, Chapter 4). An inherited weak zone below the Cantabrian Mountains is needed to trigger a localization of deformation of the lithosphere during the compression. It also defines the subduction polarity and the orientation of the lower crust dipping northwards and impacting on the shortening values on the different domains of the Iberian Peninsula, the Central System and Duero Basin. Such weak zone must be inherited from past events. In the case of the Cantabrian Mountains, this is supported by geological restorations based on

structural geology and seismic receiver functions (Gallastegui, 2000; Tugend et al., 2014; Quintana et al., 2015; Pedreira et al., 2015; Pedrera, et al., 2017), showing a double wedge indentation below the Cantabrian Mountains. Most of the shortening occurred offshore and in an imbricated structure of Tertiary sediments that were accumulated in a 6 km thick sedimentary basin (Gallastegui et al., 2002). Although surface processes are not included in our model, the topography and thrust structures agree reasonably well with real topography and previous geological studies (Figure 5.3) if the model includes: a hyperthinned oceanic crust in the Eurasian part, a thin layer of Mesozoic sediments in the Cantabrian margin, a

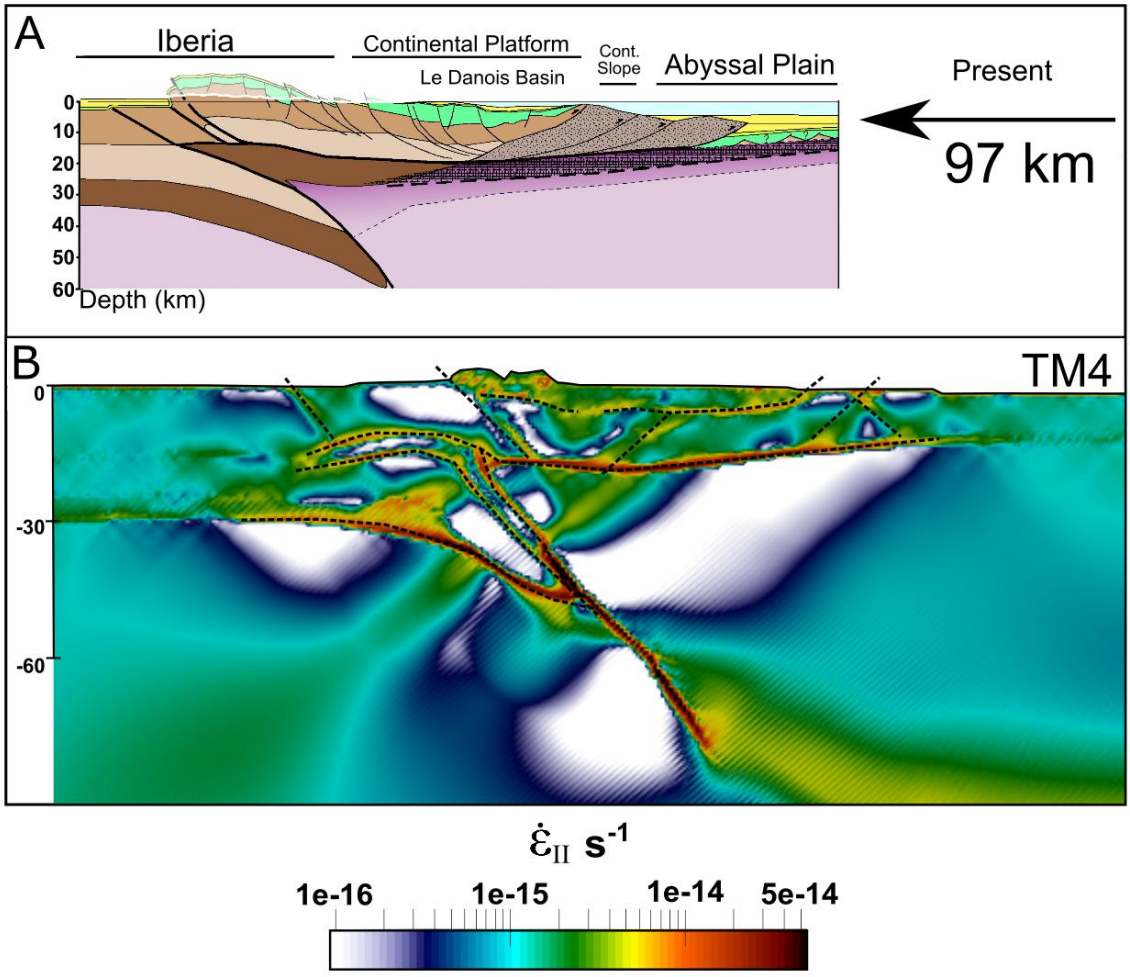

Figure 5.3. Comparison of the observed geostructural section of Cantabrian Range and predicted by model TM4. A) Thrust structure of a section crossing the Bay of Biscay and the Cantabrian Mountain after 98 km of total shortening starting in the Latest Paleocene and during the Cenozoic modified from Pedreira et al., 2015. B) Second invariant of the strain rate, from Figure 4.13-I, model TM4.

denser lower crust between the Iberian and the Eurasian lower crust, and a hardening of the Duero basin crust southwards with a fault of 45°.

All models present an oceanic crustal folding that resemble the submarine mountain known as Le Danois Bank in the Asturias-Cantabrian coast (location in Figure 4.14 from Chapter 4). The double wedge indentation transmits stresses from the boundary to the interior through a mid-crustal detachment in the Duero basin crust which corresponds to a layer between the Cenozoic new basin and the Variscan basement. When the weak zone is active below the Cantabrian Mountains, strain localizes more there and in the mid-crustal detachment, as a consequence, there is less shortening in the Duero basin and more in the Cantabrian and Central System Mountains. Moreover, when this transmission occurs the Iberian lower crust easily subducts northwards with a low dipping angle, otherwise the lower crust can hardly subduct at higher angles.

Considering a harder rheology for the Duero Crust, a mid-crustal detachment in North Iberia connected with the Cantabrian Fault down into the mantle, then, it is activated a low subduction angle for the lower crust into the Cantabrian margin. The model reaches 98 km of shortening in the Cantabrian Zone, as suggested by previous studies for the last 60 My (e.g., Gallastegui, 2000; Pedreira et al., 2015). Without a mid-crustal detachment in the Duero basin, the crust thickens excessively and accumulates unrealistic high quantities of shortening. When a mid-crustal detachment level is included connecting the north boundary with the Central System, shortening and crustal thickening are reduced in the Duero Basin. Moreover when the mid-crustal detachment is active accommodating deformation from the north boundary to inner parts, the shortening in the Central System increments 30%. Models with lateral variations in rheology in the Central System exceed the maximum values of 22-24 km calculated in geological studies for the Central System during the Cenozoic (de Vicente & Vegas, 2009; de Vicente & Muñoz-Martín, 2013). However, Banks and Warburton (1991) and Quintana et al. (2015) envisaged the possibility of up to 50 km shortenings in the Central System, accommodating part of the shortening between Iberia and the Betics through a mid-crustal detachment level crossing the entire southern half of the Peninsula.

They justify the 50 km of shortening in the Central System taking into account both compressional boundaries of the Iberian plate, one in the north where the Cantabrian Mountains built up transmitting stresses to the interior, and another one during Oligocene, as the African plate approached Iberia and the internal Betics uplifted.

The present-day crustal thickness in the Duero Basin obtained in the models varies between 31 to 33 km, and from seismic profiles and receiver functions they suggested 31-35 km (Mancilla & Diaz, 2015) and from potential-field models 32-36 km (Torne et al., 2015; Carballo et al., 2015). The Moho below the Central System presents a root with a minimum value below the southern part of the chain at 35 km depth (Suriñach et al., 1988; Stapel et a.l, 1999; Gómez-Ortiz, 2005a; Díaz et al., 2009a, Mancilla & Díaz, 2015), from gravitational and geoid fields method they also inferred a crustal root of ~35 km (Carballo et al., 2015; Torne et al., 2015). Tectonic compression in our models rises the area analogue to the Duero Basin up to 500 meters on average. This value is insufficient to the match the observed average 800 meters. A relevant point is that we do not take into account the erosion of the Central System and Cantabrian Mountains and posterior sedimentation in the Duero Basin, which would have increased the topography in the Duero domain, the highest alpine intra-mountain basins of this size in Europe. According to the sedimentary basin map elaborated by Fernández-Lozano and Gutiérrez-Alonso (2015) along our transect, the Duero basin basement has an average depth of -1000 m which reveals the amount of sediment deposited during the Cenozoic and its implications to the actual topography of the basin.

According to the results obtained in section 4.2, models with harder rheology in the Central System domain present less shortening than models with softer rheology. Most shortening occurs in the main transform faults located at the northern and southern boundaries. But deformation also accommodates in the inner parts of the Central System (Figure 5.4). The softer rheology and accommodation of deformation along the main faults results with a base of the crust modified. The deformation accommodation and the Moho depths are also influenced by the angles of the main faults. These angles accumulate most of

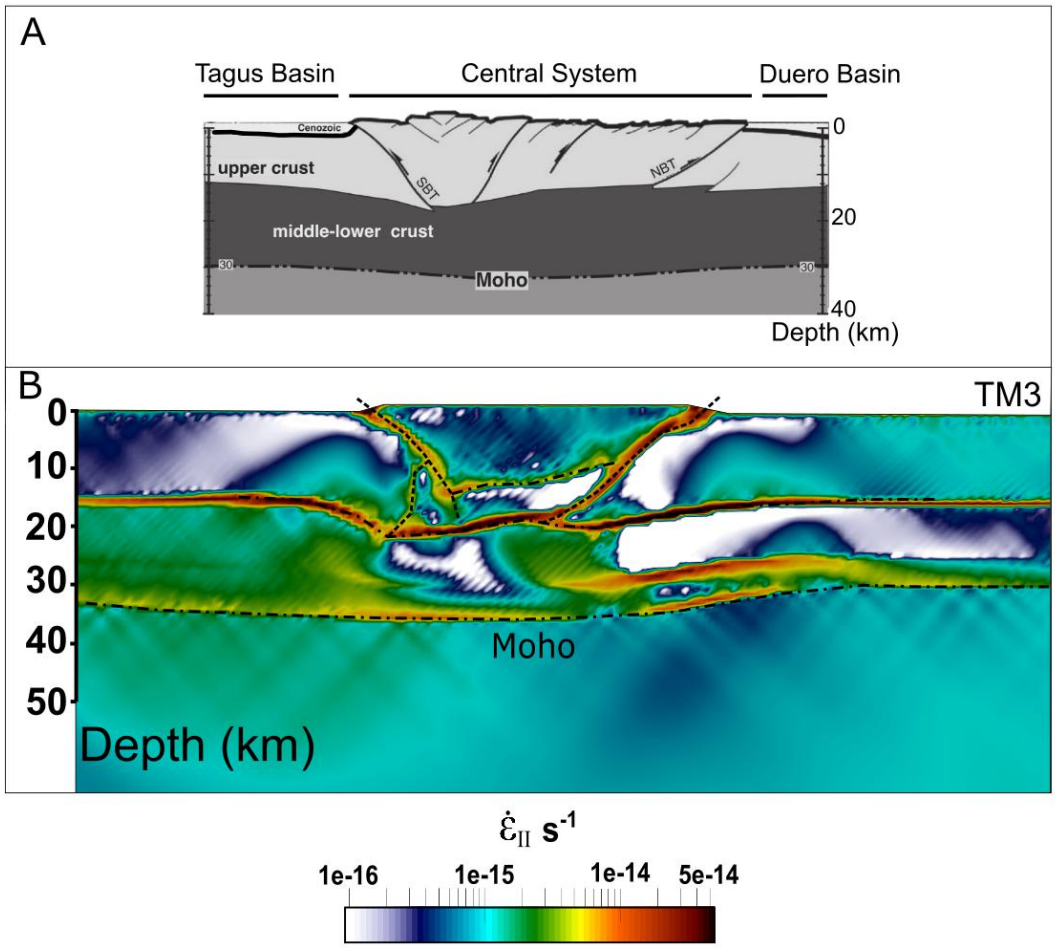

Figure 5.4. Comparison of observed thrust structure section of Central System and predicted by the TM3 model. A) Thrust structure of a section crossing the Duero Basin, Central System and Tagus Basin modified from de Vicente et al., 2007. B) Zoom to Figure 4.12-I from TM3 model where the initial rheology of the granitoid block is the softest between all the models. Note the agreement with the SBT and NBT configuration, Moho discontinuity and mid-crustal detachment level.

shortening in the Central System, being higher in the southern part of the orogen than in the northern part. Only when a lateral contrast in rheology is prescribed, models develop a single crustal root under the Central System pop-up structure. This is in concordance with Martín-Velázquez, et al. (2012) where they introduce lateral thermomechanical contrast to explain the crustal root under the Central System mountains, the maximum heights Tertiary sediments in the adjacent basins and the ~20% of crustal shortening.

The 1300°C asthenosphere-lithosphere boundary is similar for all of our thermomechanical models with average values of 120-130 km depth for the

Iberian lithosphere (in agreement with present-day lithospheric structure studies based on potential fields and isostasy; Carballo et al., 2015, Kumar et al., 2020). All the models lead to the formation of a lithospheric root beneath the Cantabrian Mountains due to north dipping lower crustal subduction reaching ~145 km depth. This crustal subduction beneath Cantabria in the models reaches 50 km depth. Values from receiver-functions and seismic-profiles (see Carballo at al., 2015) give similar values for the north dipping crustal subduction. Although the values coincide for the crustal root, the lithospheric root that this thesis predicts is shallower than previous studies based on geophysical-petrological modeling of the lithosphere suggested (Carballo et al., 2015; Pedreira et al., 2015). Pedreira et al. (2015) analyze two possible models to explain the geometry beneath the Cantabrian Mountains. One model has a crustal root down to ~90 km depth, coinciding with Gallastegui's (2000) interpretations. A second model with a crustal root to 60 km depth is favored, because this number agrees better with the seismic experiments in the area and the tomographic models. Both models predicts a deeper lithospheric root reaching values of 160 km depth. Carballo et al., (2015) also employed the crustal root of 60 km depth to adjust the geoid anomalies and obtained a lithospheric root reaching 160 km depth.

All the models have a similar accommodation of the deformation through time. During the first 5-10 My shortening is accommodated in the Cantabrian region, later the deformation is transmitted to the Central System, and from 10-15 My we obtain some minor shortening also in the Duero Basin (up to 12 km). This timing of the deformation agrees with several studies, where they propose shortening first in the northern margin at Cretaceous-Paleocene times and 10 to 15 My later during the Eocene in the Central System (e.g., Álvarez-Marron et al., 1996; Gallastegui et al., 2002; de Vicente et al., 2007; de Vicente & Muñoz-Martin, 2012; Macchiavelli et al., 2017).

5.4 Insights on the mechanics of deformation of the Iberian microplate

Once the structure and rheology of the northern area of the Iberian microplate had been constrained, I tested the role of the plate convergence in the southern edge of the Iberian microplate. The models in Chapter 4.3 included a second subduction towards an additional plate representing the Nubian (African) plate. This Southern Plate moves northwards towards the southern part of the Iberian microplate, with the lithospheric structure inspired by the kinematic model of Vergés and Fernàndez, 2012 (Figure 4.16). The initial structure consists of a partially subducted oceanic domain between the African and Iberian plates, and a continental lithosphere of 400 km long that assembles to the previous modeled northern part. The objective was to obtain a the shortening at the Cantabrian Margin (~98km) and the Central System (~25 km) plus the total shortening of the Iberian plate (between 267 km and 292 km according to Quintana et al., 2015, and references therein) and about 145 km in the Betics domain according to previous studies. One last objective was to examine if the intraplate deformation during the Cenozoic in the Iberian microplate is best explained by a lithospheric folding (Cloetingh et al., 2002) or by tectonic compression that thickened the lithosphere and the deformation was accommodated via detachment levels (Banks and Warburton, 1991).

Previous studies have suggested that the Iberian and African plates were around 350-450 km separated in the NW-SE direction ca. 85 Ma (e.g., Rosenbaum et al., 2002a; Vergés & Feràndez, 2012). The onset of the subduction of the Tethys Ocean in between started in the Late Cretaceous or Paleocene (Zeck et al., 1996; Puga et al., 1999; Casas-Sainz & Faccena, 2001, Quintana et al., 2015). Followed by the continental subduction which would produce finally the Betic–Rif Chain during the Oligocene–Miocene. At the same time an extensional event developed oceanic crust in the western Mediterranean and the result was the development of the Alboran basin (e.g., Royden, 1993). In Tortonian times, a new tectonic compression

took place (e.g., Lonergan & White, 1997; Platt & Vissers, 1989; Vergés & Fernàndez, 2012).

Although the results of the 2D thermomechanical model presented in last section of chapter 4 (TM5) are synthetic and their quantitative comparison with the southern Iberia must be done cautiously, some features of the model behaviour can shed some light on the region's geodynamic evolution. In the numerical model, the oceanic subduction occurs in the first 40 My, followed by inflow of the asthenosphere from the north, i.e., from the Iberian sublithospheric mantle. In the following 10 My, the slab breaks off and sinks into the sublithospheric mantle, starting a continental collision (Figure 4.19). During this first ~50 My, the domains representing south Iberia and Africa undergo a total convergence of 265 km. Machiavelli et al. (2017) calculated a first stage of 80 km of shortening from Cretaceous times to Oligocene times followed of 150 km shortening until present between the northern coast of the African plate and southern Iberia. Van Hinsbergen et al. (2014) gives even higher values from 45 Ma until present by the consumption of the area between Africa and Iberia by the NW-Africa S-Iberia convergence.They fixed the African-Iberia convergence using Central Atlantic reconstructions from Müller et al. (1999) and North Atlantic and Bay of Biscay from Visser and Meijer (2012), pointing out that in the North Balearic Transform Zone (NBTZ) the total amount of convergence was ~280 km since 85 Ma (150 km the last 30Ma) in the Gibraltar area the maximum value for the convergence is 120 km. For the sake of economizing computer resources, the timing of our convergence model between Africa and Iberia is not precise. But we do force the total quantity of shortening to be comparable to observations. In the southern part of the numerical model (representing the Betics), the total shortening of 165 km is satisfactory: Banks and Warburton (1991), calculated a total Betics' shortening of 150 km. Platt et al. (2003) suggested a minimum value of 122 km and a maximum of 260 km. Quintana et al. (2015) also estimated 145 km of total shortening. The succession of compressional and extensional events in the Betics is not captured by the model. This is because the 2D nature of the model prevents incorporating the migration of the slab and its tearing under the Betics in the direction

perpendicular to the modeled section, besides, the premature break up of the slab in the model, with the impossibility of a slab roll back. It is during the slab roll back northwards, when the Betic domain suffered the extensional period. Previous studies suggested that the initiation of the slab rupture and sinking to the asthenosphere started at ~22 Ma (e.g., Zeck et al., 1996) and then propagated westwards (Garcia-Castellanoss & VIllaseñor, 2011). Recent studies suggest that the lithospheric slab detachment happens first under theeastern Betics and later in the central part of the Betics, that means that there is a lateral slab tearing starting from eastern Betics. The western Betics still preserve an attached slab (Casas-Sainz & Faccena, 2001; Platt et al., 2013; Marín-Lechado et al., 2017; Spakman et al., 2018). Due to its 2D nature, our model cannot reproduce the slab dragging force and the slab retreat proposed in the area. One interesting prediction of the model is the upwelling of crustal material that subducted during the first stages of the geodynamic evolution of the model in the Transitional lithosphere (analogue to Alboran domain). During the first 25 My, part of material from the transitional crust is dragged by the southwards subduction (Figures 4.18-4.19), later part of this material is embedded in the lower crust of the transitional crust (Figures 4.20-4.23). This material movement is in concordance with several papers of material exhumation in the Alboran basin and the Betics (e.g., Platt et al., 2006; Rossetti et al., 2005; Jolivet et al., 2003; Vergés & Fernàndez, 2012).

The total compression is overestimated for the region Tagus Basin (Southern Basin) in our model. Although part of that shortening might actually belong to the External Betics, there is no evidence for shortening in the Tagus basin. The majority of our shortening in the basin occurs in the latest 60 My while previous authors propose that the External Betics have some earlier compressional phases (e.g., de Jong, 1990). The first compressional event in the Prebetic domain is dated 83 Ma (Chacón, 2002), and the most noticeable compressional event in the Prebetic occurred in the Paleocene (De Ruig, 1992; Geel & Roep, 1998). There were also several different shortening phases during Eocene and Oligocene times (e.g., Martín-Chivelet & Chacón, 2007).

In my model, there is no significant shortening in the Cantabrian domain at the north margin of Iberia before the southern slab breaks off. Africa and the Iberian microplate are attached and move towards the Eurasian plate until the slab detaches from Iberia. It is well documented that the shortening in Iberia initiates in the northern margin in the Pyrenean chain and Basque-Cantabrian chain, followed by intraplate deformation in the Iberian Range and Central System, and finally the deformation migrates to the southern margin in the Betic chain (e.g., Vergés & Fernàndez, 2012; Quintana et al., 2015; Machiavelli et al., 2017; and references therein). In the model shown in Chapter 4.3, the deformation concentrates first in the southern margin until the slab breaks during the first 40 My of the geodynamic model and later the deformation migrates to the north. Finally, to illustrate the limitations in matching model and geological observations, while the model shortening lasts until 0 Ma, there is a consensus that the shortening at the northern margin of the Peninsula stopped 30-20 Ma.

20 My after the initiation of the shortening in the Cantabrian Margin, the shortening of the Central System starts, and continues up to the end the model. This agrees with previous studies suggesting the transmission of stress from the margins modifying where the deformation accommodates in the different domains of the Iberian Peninsula during the Cenozoic. Quintana et al. (2015) pointed out that there is a period between Oligocene and middle Miocene where all chains where simultaneously active. However, the total shortening obtained in the Central System is less than the 2D thermomechanical models for the northern part of Iberia (section 4.2) and far from the maximum estimated values of 22-24 km (de Vicente & Vega, 2009; de Vicente & Muñoz-Martin, 2013). The preferred model in section 4.3 also reproduces the Iberian lower-middle crust subduction below the Cantabrian Mountains and the southwards indentation of the Eurasian mantle with the Cantabrian lower crust. What is not well captured is the lithospheric bulge at LAB depth in the Cantabrian margin (Figure 4.23). The whole Iberian lithosphere thickens in response to the tectonic compression, but there is no lithosphere folding in that model, in contrast to what Cloetingh et al. (2002) obtained. Neither the material nor the 1300 °C isotherm reveals any characteristic wavelength of

300-400 km. The strain rate second invariant is uniformly distributed in the lithospheric mantle with no evidence for mega shear bands or which can generate megafolds.

The topography of the model has a similar pattern than the actual topography of Iberia but with a lower mean elevation (Figure 5.5). The southern part of the Iberian topography is higher than the northern one. This results from a larger shortening in the south relative to the north, and the larger crustal thickness in the south, which is overestimated. Mancilla and Díaz (2015) Moho map shows the crustal thickenning for Iberia, revealing that the crustal thickness under the Betic Chain has equivalent values to those obtained for the Cantabrian Mountains. The transitional crust analogue to the Alboran basin domain overpasses the sea level due to folding of this area. Maximum topography is located in the Betics domain, which includes a mini internal basin (see black profile from Figure 5.5) that seems consistent with the formation of the Guadix-Baza basin during the Neogene. The Southern Basin (analogue to Tagus Basin) goes from ~500 m over sea level to ~0 m nearby the Central System. The analogue Central System behaves as a double vergence pop-up structure, which uplifted in the first 5 My due to the difference in density with the surrounding crust and later, during the compressional period (last 60 My). In this model, no maximum peaks are observed in this Central Range at the north and south transform faults, but it has a mean elevation of ~500 m compared to the Duero basin, which is in concordance with the actual relief. The Cantabrian Range develops two peaks with its maximum height at the north. The continental slope descends to 3 km depth with a topographic bulge at 1 km depth, roughly comparable to the Le Danois Bank.

Initially, the average topography elevates up to about 1 km (Fig 5.5). Then, during the first 40 My of oceanic subduction, the mean elevation is around in 500 m. During the next 10 My, when the slab breaks, a sudden 400 m decrease in the mean elevation occurred. At the same time, the compression in the south rises the Betics, and stops at 70 My with 1 km of elevation. Tagus Basin also presents an increment in the mean topography of 1 km the last 50 My due to the thickening of

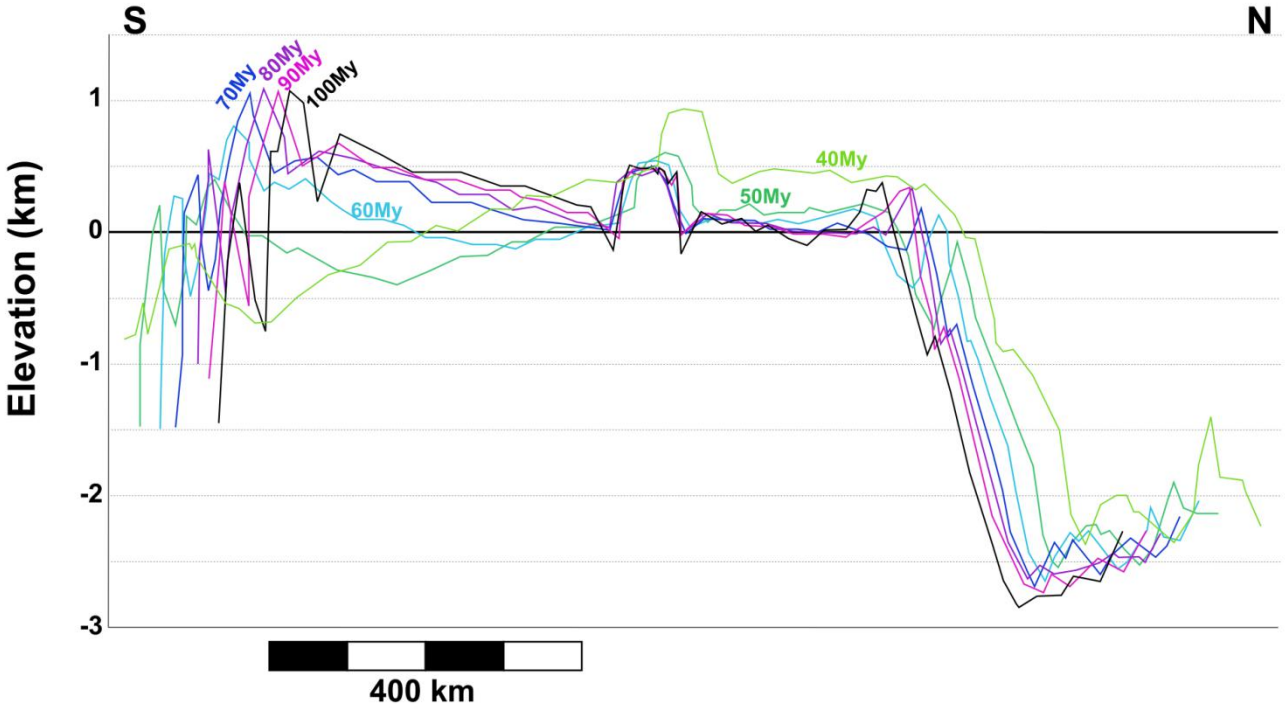

Figure 5.5. Elevation evolution of the N-S thermomechanical model (TM5) for the analogue Iberian Peninsula described in Chapter 4.3. Plots every 10 My, from 40 to 100 My of the evolution.

the crust. Meanwhile, at the northern margin, when the compression started, there was an increment in elevation of almost 1 km of maximum elevation. At 60 My, the mean elevation increases slowly, while the crust between the Duero basin and the formation of the Cantabrian Mountains undergoes subsidence. In the last 40 My (from t=60 to t= 100 My in Figure 5.5), the depocenter disappeared while the Cantabrian Range builds up. The modifications of our topography are due to compression, thickening or reactivation of weak zones. The average elevation from the northern topography of the model is close to the 0 m level which does not fit with the observed mean topography of around 800 m in the Duero basin. However, the main mountain ranges and relative high between them and the adjacent basin fits relatively well with the present topography. Some explanations for the lower mean elevation of the model presented in this thesis could be the initial temperature field distribution or the reference column considered to calculate the isostatic elevation.

This work offers an additional source of topographic growth of Iberia relative to the hypothesis by Conway-Jones et al. (2019), who suggested an anomaly in the temperature of the sublithospheric mantle during the Neogene as the cause for uplift, and also an additional mechanism for uplift relative to the lithospheric folding during the Cenozoic, as proposed by Cloetingh et al. (2002).

Chapter 6

Conclusions

The present study was set to improve our understanding on what determines the styles of deformation and the accommodation of tectonic shortening during continental collision and orogenic growth, using a numerical modeling approach. We have identified two characteristic end-members cases for orogen formation during continental collision: The double-vergent orogen and the crustal-scale folding. We have then used the numerical modeling methodology to address unsolved questions about the Cenozoic geodynamic evolution, intraplate deformation, lithospheric structure and relief formation of the Iberian microplate. In this chapter, I summarize the main conclusions from this thesis following the order of the previous chapters: i) Crustal Folding vs. Double Vergence; the role of inherited structures (Chapter 3); ii) the deformation of North Iberia during the Cenozoic (Chapter 4); and, iii) the contribution to the North and Central Iberian intraplate deformation of the African plate converging against the south Iberian margin (Section 4.3). Finally, I suggest some for future plans or actions to continue the line of research of this thesis.

The synthetical numerical experiments of continental collision (Chapter 3) show that the evolution of orogens is sensitive to the viscosity contrast between crustal layers and the distribution of inherited weaknesses at crustal depths:

a) Based on results from synthethic modeling scenarios, I have identified two end-member scenarios developing during the first stages of the evolution of an orogen in a continental collision scenario, two end-members have been identified: Double-vergent orogen and Crustal folding orogen. The viscosity contrast between the crustal layers is the main parameter controlling the style of orogens deformation in a continental collision scenario.

b) The double-vergent style of the deformation requires a viscosity contrast of two orders of magnitude or less between the crustal layers and a low contrast (less than a factor 4 in the cohesion ratio) in terms of effective-viscosity. Crustal folding orogens can be generated when the viscosity contrast between the crustal layers is two orders of magnitude or less if the effective-viscosity contrast is higher enough to detach the lower crust from the upper crust. The latter is achieved when the cohesion ratio is greater than 6.

c) Decoupling the crust from the mantle with a weak lower crust acting as a detachment level favors a crustal folding response to continental collision. A weak lower crust concentrates strain and accommodates the deformation in the crust of both colliding plates, hindering the deformation of the lithospheric upper mantle of the upper plate. The occurrence of crustal folding proves that the deformation can be transmitted far from the initial collision zone generating folds with wavelengths of 50-60 km.

d) During the growth of double-vergent orogens, strain rate is distributed in a diffuse pattern far into the crust while generating long-lived shear bands near the axis of the collision zone. Strain tends to localize in the upper mantle of the overriding lithosphere favoring upper mantle folding with a large wavelength (~300 km).

e) The dip angle of subduction and the density of the crust play a minor role in controlling the style of orogenic deformation, relative to the aforementioned changes in viscosity.

f) The development of crustal folding is also related to the detachment level depth. Shallow décollement levels generate upper crustal folding with a short

wavelength of between 2 and 3 times the depth of the décollement. Examples include the Zagros Mountain Belt or the crustal folding in the Pyrenees related to Mesozoic salt layers in the upper crust. Décollements at mid-crustal levels or a weak lower crust acting as detachment generate crustal folding and can develop into more complex orogens shapes (e.g., developing big thrust seeds, antiformal stacks, plateaus, etc), for instance in the European Alps.

g) The size of the detachment level and its depths modifies the orogen deformation. If the detachment level extends beyond the subduction zone a main retro shear forms and pop-up structures are likely to develop.

Based on these conclusions, we applied the mechanical and thermomechanical models to the Iberian microplate, adopting geologically-based rheology distributions and accounting for weaknesses possibly inherited from the Variscan orogeny. We aimed at explaining the different Iberian crustal shortenings, the main geological constraint on our models. We then tried to reproduce the present lithospheric-scale geostructure and the high average elevation of the Iberian Peninsula. Based on the results and the discussion sections we can summarize:

h) North-Iberian mid-lower crustal subduction can only be explained by a mid-crustal detachment level that extends down to the lithospheric mantle, dipping northwards below the Cantabrian Range. I interpret this weak zone as inherited from the extensional crustal event during the Cretaceous. Crustal subduction, which goes deeper than 50 km, is an essential contributor to form a lithospheric root of 150-160 km depth, as derived from previous studies based on potential-field and thermal models. Only with this inherited weakness is possible to explain the difference in shortening between the upper and lower crust in the Cantabrian margin. The mid-lower crustal subduction is necessary to achieve the suggested shortening values for the area (85-98 km) between the late Cretaceous and the Eocene-Oligocene (Gallastegui, 2000; Pedreira et al., 2015; Quintana et al., 2015; Macchiavelli et al, 2017).

i) To achieve the present elevation of the Cantabrian chain, an initial angle of 30° is necessary, between the Duero Basin crust from the Cantabrian margin, which has undergone a previous hyper-extensive process. Besides, a less dense

lower crust is needed under the Cantabrian margin that together with the lithospheric mantle show a double wedge indentation to the south between the upper and middle crust of Iberia.

j) A mid-crustal detachment level is needed to transmit enough stress to the inner parts of Iberia and trigger shortening in the Central System 15 My later than the initiation of the compression in the northern margin. Also, hard rheology under the Duero Basin is necessary so that the deformation in that region is minimal and most of the stress is transmitted towards the Central System. Both mechanism allow reproducing the shortening values of 22 to 25 km in less than 40 My derived from previous structural studies.

k) A lateral change in rheology underneath the Central System at middle crust depths is needed to develop a small root reaching 35 km in depth and a slightly thicker upper crust in the Tagus Basin than in the Duero Basin near the SBT and NBT, respectively. Prescribing these two faults zones located on the southern and northern borders of the Central System is necessary to accommodate there a significant part of the deformation, raising the chain and generating a pop-up structure that roots down to levels of the lower crust.

Finally, I completed the numerical experiments by incorporating a Southern Plate analogue to the African plate converging northwards against the southern margin of the Iberian plate (Section 4.3). The main purpose of this model was to reproduce the timing of deformation and to reproduce previous estimations of the total shortening of the Iberian plate and the Betics domain along with the shortening of the northern part of Iberia. The conclusions are:

l) Intraplate deformation of the Iberian plate can be best explained as the result of stress transmission through mid-crustal detachment levels rather than through a lithospheric folding response to the Cenozoic Africa-Eurasia approaching. The whole Iberian lithosphere might have thickened by 14-21% during this process.

m) Deep subduction and slab break-up under the plate edge controls the migration of shortening within the upper plate. In the case of Iberia, the weight

of the subducted slab under the Gibraltar Arc and its later reduction after slab tearing seems crucial in transmitting shortening from the northern margin of Iberia to the intraplate area, and finally to the southern margin. When subduction occurs in the southern margin, without the subducting plate retreating and rolling-back, the entire Iberian plate is dragged away and extended by the subduction, hindering compression in the north. The modeling results suggest that upon subduction, the Africa-Iberia convergence is concentrated mostly in the southern margin, while as the slab breaks off, it reduces the downwards slab pull, hindering convergence in the south, and transmitting compression to the rest of the upper intermediate plate (the plate analogue to Iberia)

n) The designed model captures the documented amount of convergence between Africa and Iberia (~300 km during the Cenozoic) and the total shortening in the Betics of 165 km. The timing and shortening obtained for the Cantabrian domain (80 to 85 km from Late Cretaceous to the end of the Eocene) are consistent with previous studies. Although the timing of the shortening in the Central System is roughly correct (17 km during 45 My) the hard rheology employed for the granitoid block of the Central System impedes reaching the full 22 km of shortening estimated in previous structural studies. This model reproduces the basic patterns of the topography but seems insufficient to explain the high average elevation of the entire Iberian microplate, suggesting that mechanisms other than accounted for here (dynamic topography or sediment trapping in endorheic basins) are at least comparable in importance.

Future work

Better petrological constraints will be required in order to understand how strain rates propagate through the lower crust depending on its coupling state with the mantle and how it is transmitted further from the initial collision zone during the evolution. Many of the parameters involved in modeling are determined

only with large uncertainties (e.g., the rheological and thermal parameters). Additionally, to understand when stress is transmitted to the upper mantle generating lithosphere folding, different types of mantle should be tested using different rheologies like dry olivine or peridotite. Methodologically speaking an interesting feature to develop would be implementing melting process in the subducting mantle in response to slab tearing, as well as, compositional phase changes for rocks as function of the water content of hydrated materials dragged by the subduction into the lithospheric mantle, since recent studies (Sobolev & Brown, 2019, Nature) seem to indicate the importance of water-rich sediments for the lubrication of subducting plates. Also, something that should be explored is the level of affectation of the inherited weaknesses, whether they are only at crustal levels or extend into the upper mantle, and how they impact on the accommodation of the deformation.

Future thermomechanical models addressing the development of the elevation of the Iberian Peninsula, would beneficiate from incorporating surface processes and probably dynamic topography related to thermal/convection processes in the mantle. Another interesting open challenge is to explore different pre-Cenozoic temperature distributions in the mantle and how they may affect the overall elevation changes, and its contribution to rise the entire Iberian relief.

Finally, 3D numerical modeling will be needed in order to 1) account for lateral variations in rheology and 2) temperature and 3) lateral geotectonic movements that 2D models can not incorporate, to capture the complex 3D dynamics of the Iberia Peninsula between the Africa and the Eurasia plates. It would permit to study the movement of the mantle due to the subduction in the northern and southern margin of the Iberian microplate (e.g., Civiero et al., 2019; Peral, M., PhD Thesis 2020), how it changes the temperature distribution, and hence the lithosphere structure during the Cenozoic. Presently, however, 3D models consume too many computer resources and computational time, and simplifications and compromises will have to be done.

References

Afonso, J. C., Fernàndez, M., Ranalli, G., Griffin, W. L. and Connolly, J. A. D., 2008. Integrated geophysical-petrological modeling of the lithosphere and sublithospheric upper mantle: Methodology and applications. *Geochem. Geophys. Geosyst.,* 9, Q05008, doi:10.1029/2007GC001834.

Álvarez-Marron, J., Rubio, E., and Torne, M., 1997. Subduction-related structures in the North Iberian Margin*. Journal of Geophysical Research,* 102, B10, 22497-22511.

Andeweg, B., De Vicente, G., Cloetingh, S., Giner, J., and Muñoz Martin, A., 1999a. Local stress fields and intraplate deformation of Iberia: variations in spatial and temporal interplay of regional stress sources.*Tectonophysics, 305*, 153-164.

Andeweg, B., 2002 Cenozoic tectonic evolution of the Iberian Peninsula, the effects and causes of changing stress fields*, Ph.D. thesis*, 178 pp., Vrije Univ., Amsterdam.

Andrić, N., Vogt, K., Matenco, L., Cvetković, V., Cloetingh, S., & Gerya, T., 2018. Variability of orogenic magmatism during Mediterranean-style continental collisions: A numerical modelling approach. *Gondwana Research*, *56*, 119–134. https://doi.org/10.1016/j.gr.2017.12.007

Andrieux, J., Fontbote, J.-M. & Mattauer, M., 1971. Sur un modèle explicatif de l'arc de Gibraltar. *Earth Planet. Sci. Lett.*, 12, 191-198.

Artemieva, I., 2011. What is the lithosphere? In The Lithosphere: An Interdisciplinary Approach (pp. 1-14). *Cambridge: Cambridge University Press.* doi:10.1017/CBO9780511975417.003

Arthaud, F., Matte, P., 1975. Les décrochements tardi-herciniens du Sud-Ouest de l'Europe: geómetrie et essai de reconstruction des conditions de la deformation. *Tectonophysics*, 25, 139–171.

Asch, K., 2005: IGME 5000: 1 : 5 Million International Geological Map of Europe and Adjacent Areas. BGR (Hannover).

Balanyá, J.C., García-Dueñas, V., Azañón, J.M., Sánchez-Gómez, M., 1997. Alternating contractional and extensional events in the Alpujarride nappes of the Alboran domain (Betics, Gibraltar arc). *Tectonics* 16, 226–238.

Banks, C.J. and Warburton, J., 1991. Mid-crustal detachment in the Betic system of southeast Spain. *Tectonophysics*, 191, 275-289.

Baumgardner, J. R., 1985. Three-dimensional treatment of convective flow in the Earth's mantle. *Journal of Statistical Physics*, 39, 501–11.

Beaumont C., Fullsack P., Hamilton J., 1992. Erosional control of active compressional orogens. In: McClay K.R. (eds) Thrust Tectonics. Springer, Dordrecht, https://doi.org/10.1007/978-94-011-3066-0_1

Beaumont, C., P. Fullsack, and J. Hamilton, 1994. Styles of crustal deformation in compressional orogens caused by subduction of the underlying lithosphere. *Tectonophysics* ,232, 119-132.

Beaumont, C., Ellis, S., Hamilton, J., Fullsack, P., 1996. Mechanical model for subduction-collision tectonics of Alpine-type compressional orogens. *Geology, 24*(8), 675-678.

Beaumont, C., Muñoz, J. A., Hamilton, J., & Fullsack, P., 2000. Factors controlling the Alpine evolution of the central Pyrenees inferred from a comparison of observations and geodynamical models. *Journal of Geophysical Research: Solid Earth*, *105*(B4), 8121–8145. https://doi.org/10.1029/1999JB900390

Biot, M.A., 1961. Theory of Folding of Stratified viscoelastic media and its implications in tectonics and orogenesis. *Geological Society of American Bulletin, 72 (11)*, 1595-1620. https://doi.org/10.1130/0016-7606(1961)72[1595:TOFOSV]2.0CO;2

Bois, C., Pinet, B., Gariel, O., 1997. The sedimentary cover along the ECORS Bay of Biscay deep seismic reflection profile. A comparison between the Parentis basin and other Eurasian rifts and basins. *Soc. Géol. Fr. Mém.* 171, 143–165.

Bonini, M., 2003. Detachment folding, fold amplification, and diapirism in thrust wedge experiments. *Tectonics*, 22(6), n/a–n/a. doi:10.1029/2002tc001458

Bouillin, J., Durand Delga, M., Olivier, P., 1986. Betic–Rif and Tyrrhenian distinctive features, genesis and development stages. In: Wezel, F.C. (Ed.), The Origin of Arcs. *Elsevier*, pp. 281–304.

Boonma, K., Kumar, A., Garcia-Castellanos, D. *et al.* Lithospheric mantle buoyancy: the role of tectonic convergence and mantle composition. *Sci Rep* 9, 17953 (2019). https://doi.org/10.1038/s41598-019-54374-w

Bourrouilh, R., Richert, J. P., Zolnai, G., 1995. The North Pyrenean Aquitaine Basin, France: Evolution and hydrocarbons. *The American Association of Petroleum Geologist Bulletin, 79*(6), 831-853

Brandon, M.T., Roden-Tice, M.K., and Garver, J.I., 1998, Late Cenozoic exhumation of the Cascadia accretionary wedge in the Olympic Mountains, northwest Washington State: Geological Society of America Bulletin, v. 110, p. 985–1009, doi:10.1130/0016-7606 (1998)110<0985:LCEOTC>2.3.CO;2.

Brun, J-P, Sokoutis, D., Tirel, C., G., van den Driessche, J., et al., 2018. Crustal versus mantle core complexes. *Tectonophysics*, *Elsevier*, 2018, 746, pp.22-45. 10.1016/j.tecto.2017.09.017. insu-01610186

Brun, J-P., 2002. Deformation of the continental lithosphere: Insights from brittle-ductile models. *Geological Society, London, Special Publications, 200*(1), 355–370. https://doi.org/10.1144/GSL.SP.2001.200.01.20

Bullard, E.C., Everett, J.E. & Smith, A.G., 1965. The fit of the continents around the Atlantic: a symposium on continental drift. *Phil. Trans. R. Soc. Lond. A,* 258(1088), 41–51.

Burg, J. P., & Podladchikov, Y., 1999. Lithospheric scale folding: Numerical modelling and application to the Himalayan syntaxes. *International Journal of Earth Sciences*, *88*(2), 190–200. https://doi.org/10.1007/s005310050259

Burov, E., Lobkovsky, L., I., Cloetingh, S. & Nikishin, M.,A., 1993. Continental lithosphere folding in Central Asia (Part II): constraints from gravity and topography. *Tectonophysics, 226*, 73-87.

Burov, E.B., François, T., Agard,P., Le Pourhiet, L., Meyer,B., et al., 2014. Rheological and geodynamic controls on the mechanisms of subduction and HP/UHP exhumation of crustalrocks during continental collision: Insights from numerical models. *Tectonophysics*, *Elsevier*, 631, pp.212-250. 10.1016/j.tecto.2014.04.033. insu-01065788

Byerlee, J., 1978. Friction of rock. *Pure and Applied Geophysics,* 116, 615 – 626.

Calignano, E., Sokoutis, D., Willingshofer, E., Guedan, F., Cloetingh, S., 2015. Asymmetric vs. symmetric deep lithospheric architecture of intra-plate continental orogens. *Earth and Planetary Science Letters,* 424, 38–50. http://dx.doi.org/10.1016/j.epsl.2015.05.022

Capitanio, F.A., Goes, S., 2006. Mesozoic spreading kinematics: consequences for Cenozoic Central and Western Mediterranean subduction. Geophysical Journal International 165, 804–816.

Capitanio, F. A., and A. Replumaz, 2013. Subduction and slab breakoff controls on Asian indentation tectonics and Himalayan western syntaxis formation, Geochem. Geophys. Geosyst., 14, 3515–3531, doi:10.1002/ggge.20171.

Capitanio, F. A., 2014. The dynamics of extrusion tectonics: Insights from numerical modeling, Tectonics, 33, 2361–2381, doi:10.1002/2014TC003688.

Carballo. A., Fernandez, M., Jiménez-Munt, I., Torne, M., Vergés, J., Melchiorre, M., Pedreira,D., Afonso, J.C., Garcia-Castellanos, D., Díaz, J., Villaseñor, A., Pulgar J.A., Quintana, L., 2015. From the North-Iberian Margin to the Alboran Basin: A lithosphere geo-transect across the Iberian Plate. *Tectonophysics* 663, 399–418 http://dx.doi.org/10.1016/j.tecto.2015.07.009

Carry, N., Gueydan, F., Brun, J. P., & Marquer, D., 2009. Mechanical decoupling of high-pressure crustal units during continental subduction. *Earth and Planetary Science Letters*, *278*(1–2), 13–25. https://doi.org/10.1016/j.epsl.2008.11.019

Casas-Sainz, A.M., Faccenna, C., 2001. Tertiary compressional deformation of the Iberian plate. *Terra Nova*, 13, 281-288, 2001

Casas-Sainz, A.M., de Vicente, G.. 2009. On the tectonic origin of Iberian topography, *Tectonophysics*. doi:10.1016/j.tecto.2009.01.030

Casciello, E., Fernàndez, M., Vergés, J., Cesarano, M., Torné, M., 2015. The Alboran domain in the western Mediterranean evolution: the birth of a concept. *Bull. Soc. géol. France*, 2015, t. 186, no 4-5, pp. 371-384

Chacón, B., 2002. Las sucesiones hemipelágicas del final del Cretácico e inicio del Paleógeno en el SE de la Placa Ibérica: Estratigrafía de eventos y evolución de la cuenca. Ph.D. Thesis. Universidad Complutense, Madrid 1–439.

Chapman, David, S., and Pollack, Henry, N., 1977. Component parts of the World Heat Flow Data Collection. *PANGAEA*, https://doi.org/10.1594/PANGAEA.803867

Civiero, C., Custódio, S., Rawlinson, N., Strak, V., Silveira, G., Arroucau, P., and Corela, C. 2019. Thermal nature of mantle upwellings below the Ibero-western Maghreb region inferred from teleseismic tomography. Journal of Geophysical Research: Solid Earth, 124, 1781–1801. https://doi.org/10.1029/2018JB016531

Cloetingh, S., Burov, E., & Poliakov, A., 1999. Lithosphere folding: Primary response to compression? (from central Asia to Paris basin). *Tectonics*, *18*(6), 1064–1083. https://doi.org/10.1029/1999TC900040

Cloetingh, S., Burov, E., Beekman, F., Andeweg, B., Andriessen, P.A.M., Garcia Castellanos, D., de Vicente, G., Vegas, R., 2002. Lithospheric folding in Iberia. *Tectonics* 21. 5, 1041, doi:10.1029/2001TC901031

Cloetingh, S., Burov, E., 2011. Lithospheric folding and sedimentary basin evolution: a review and analysis of formation mechanisms. *Basin Research 23*, 257–290. http://dx.doi.org/10.1111/j.1365-2117.2010.00490.x

Choukroune, P., 1989. The ECORS Pyrenean deep seismic profile reflection data and the overall structure of an orogenic belt. *Tectonics* 8, 23-39.

Conway-Jones, B. W., Roberts, G. G.,Fichtner, A., & Hoggard, M., 2019. Neogene epeirogeny of Iberia. *Geochemistry, Geophysics, Geosystems*, *20*, 1138–1163. https://doi.org/10.1029/2018GC007899

Crameri, F., Schmeling, H., Golabek, G. J., Duretz, T., Orendt, R., Buiter, S. J. H., … Tackley, P. J., 2012. A comparison of numerical surface topography calculations in geodynamic modelling: an evaluation of the "sticky air" method. *Geophysical Journal International, 189(1), 38–54.* http://dx.doi.org/10.1111/j.1365-246x.2012.05388.x

Davy, P., Cobbold, P.R., 1991. Experiments on shortening of a 4-layer model of the continental lithosphere. *Tectonophysics* 188 (1–2), 1–25.

De Bruijne, C.H., and Andriessen, P.A.M., 2002. Far field effects of Alpine plate tectonism in the Iberian microplate recorder by fault-related denudation in the Spanish Central System. *Tectonophysics*, 349, 161-184.

de Jong, K., 1990. Alpine tectonics and rotation pole evolution of Iberia. *Tectonophysics,* 184, 279–296.

De Ruig, M.J., 1992. Tectono-sedimentary evolution of the Prebetic fold belt of Alicante (SE Spain): a study of stress fluctuations and foreland basin deformation. Ph.D. Thesis, Vrije Universiteit Amsterdam, 1–207.

de Vicente, G., Vegas, R., Muñoz Martín, A., Silva, P.G., Andriessen, P., Cloetingh, S., González Casado, J.M., Van Wees, J.D., Álvarez, J., Carbó, A., Olaiz, A., 2007. Cenozoic thick-skinned deformation and topography evolution of the Spanish Central System. *Global and Planetary Change* 58, 335-381. doi:10.1016/j.gloplacha.2006.11.042.

de Vicente, G., Muñoz-Martín, A., 2012. The Madrid Basin and the Central System: A tectonostratigraphic analysis from 2D seismic lines. *Tectonophysics* 602, 259-285. doi:10.1016/j.tecto.2012.04.003.

de Vicente, G. and Vegas, R., 2009. Large-scale distributed deformation controlled topography along the western Africa-Eurasia limit: Tectonic constraints. *Tectonophysics* 474, 124-143. doi:10.1016/j.tecto.2008.11.026.

de Vicente, G., Vegas, R., Muñoz Martín, A., Silva, P.G., Andriessen, P., Cloetingh,S., González Casado, J.M., Van Wee, J.D., Álvarez, J., Carbó, A., Olaiz, A., 2017. Cenozoic thick-skinned deformation and topography evolution of the Spanish Central System*. Global and Planetary Change* 58, 335–381.

de Vicente, G., Cunha, P. P., Muñoz-Martín, A., Cloetingh, S. A. P. L., Olaiz, A., & Vegas, R. (2018). The Spanish-Portuguese Central System: An example of intense intraplate deformation and strain partitioning. Tectonics, 37, 4444–4469. https://doi.org/10.1029/2018TC005204

Dercourt, J., Zonensshain, L.P., Ricou, L.E., Kazmin, V.G., Le Pichon, X., Knipper, A.L.,Grandjacquet, C., Sbortshikov, I.M., Geyssant, J., Leprevier, C., Pechersky, D.H.,Boulin, J., Sibuet, J.C., Savostin, L.A., Sorokhtin, O., Westphal, M., Bazhenov, M.L.,Lauer, J.P., Biju-Duval, B., 1986. Geological evolution of the Tethys belt from the Atlantic to the Pamir since the Lias. *Tectonophysics* 123, 241–315.

Dewey, J. F., and Bird, J. M., 1970, Mountain belts and the new global tectonics, *J. Geophys. Res.*, 75(14), 2625– 2647, doi:10.1029/JB075i014p02625.

Díaz, J., Villaseñor, A., Gallart, J., Morales, J., Pazos, A., Córdoba, D., Pulgar, J., García-Lobón,J.L., Harnafi, M., the TopoIberia Seismic Working, 2009a. The IBERARRAY broadband seismic network: a new tool to investigate the deep structure beneath Iberia*. Orfeus Newsl*. 8, 2.

Doblas, M., López-Ruiz, J. & Cebriá, J.M., 2007. Cenozoic evolution of the Alboran domain: A review of the tectonomagmatic models. *In: L. BECCALUVA, G.*

Duretz, T. and Gerya. T., 2013. Slab detachment during continental collision: Influence of crustal rheology and interaction with lithospheric delamination. *Tectonophysics*, 602, 124–140. https://doi.org/10.1016/j.tecto.2012.12.024

Dymkova, D., Gerya, T., & Burg, J. P., 2016. 2D thermomechanical modelling of continent-arc-continent collision. *Gondwana Research*, *32*, 138–150. https://doi.org/10.1016/j.gr.2015.02.012

Ellis, S., C., Beaumont, and O.A., Pfiffner, 1999. Geodynamic models of crustal-scale episodic tectonic accretion and underplating in subduction zones. *J. Geophys. Res.*, 104, 15,169-15,190.

Faccenda, M., Gerya, T.V., Chakraborty, S., 2008. Styles of post-subduction collisional orogeny: influence of convergence velocity, crustal rheology and radiogenic heat production. *Lithos* 103 (1–2), 257–287.

Faccenda, M., Minelli, G., Gerya, T.V., 2009. Coupled and decoupled regimes of continental collision: Numerical modeling. *Earth and Planetary Science Letters*, 278, 337–349.

Fernàndez, M., Ranalli, G., 1997. The role of rheology in extensional basin formation modelling. *Tectonophysics* 282, 129±145.

Fernàndez, M., Marzán, I., Correia, A., and Ramalh, E., 1998. Heat flow, heat production, and lithospheric thermal regime in the Iberian Peninsula,*Tectonophysics*, 291, 29–53, doi:10.1016/S0040-1951(98)00029-8.

Fernández-Lozano, J., Gutiérrez-Alonso, G., 2015. Evolución dinámica de la cuenca del Duero (Long-term evolution of Duero Basin). *Geogaceta*, 58, 87-90. ISSN: 2173-6545

Fernández-Lozano, J., D. Sokoutis, E. Willingshofer, S. Cloetingh, and G. de Vicente, 2011. Cenozoic deformation of Iberia: A model for intraplate mountain building and basin development based on analogue modeling. *Tectonics*, 30, TC1001, doi:10.1029/2010TC002719.

Fernández-Lozano, J., Sokoutis, D., Willingshofer, E., Dombrádi, E., Martín, A. M., de Vicente, G., and Cloetingh, S., 2012. Integrated gravity and topography analysis in analog models: Intraplate deformation in Iberia, *Tectonics*, 31, TC6005, doi:10.1029/2012TC003122.

Fernández-Viejo, G., & Gallastegui, J., 2005. The ESCI-N project after a decade: A synthesis of the results and open questions. *Trabajos de Geología*, Universidad de Oviedo, 25, 9–25.

Galindo-Zaldívar, J., Azzouz, O., Chalouan, A., Pedrera, A., Ruano, P., Ruiz-Constán, A., et al., 2015. Extensional tectonics, graben development and fault terminations in the eastern Rif (Bokoya-Ras Afraou area). *Tectonophysics*, *663*, 140–149. https://doi.org/10.1016/j.tecto.2015.08.029

Gallastegui, J., 2000. Estructura cortical de la cordillera y margen continental cantábricos: Perfiles ESCI-N, *Trab. Geol*., 21, Univ. de Oviedo, Spain, 231 pp.

Gallastegui, J, Pulgar, J A; Gallart, J., 2002. Initiation of an active margin at the North Iberian continentocean transition. *Tectonics*, vol.21, no.4, 14 pp.

García-Castellanos, D., M. Fernández, and M. Torne, 2002. Modelling the evolution of the Guadalquivir foreland basin southern Spain. *Tectonics*, 21(3), 1018, doi:10.1029/2001TC001339.

García-Castellanos, D. & S. Cloetingh, 2012. Modeling the interaction between lithospheric and surface processes in foreland basins. In: *Tectonics of Sedimentary Basins: Recent Advances*, C. Busby & A. Azor (eds.). Blackwell Pub. Ltd., 152-181, doi:10.1002/9781444347166.ch8

García-Castellanos, D., Larrasoaña, J.C., 2015. Quantifying the post-tectonic topographic evolution of closed basins: The Ebro basin (northeast Iberia). *Geology*, doi:10.1130/G36673.1

García-Mondéjar, J., 1990. The Aptiane Albian carbonate episode of the Basque-Cantabrian Basin (northern Spain): General characteristics, controls and evolution. In M. E. Tucker, et al. (Eds.), *Carbonate Platforms: Facies, Sequences and Evolution, Special Publication International Association of Sedimentologists* (Vol. 9, pp. 257–290).

Geel, T., Roep, T.B., 1998. Oligocene to middle Miocene basin development in the eastern Betic Cordilleras, SE Spain (Vélez Rubio Corridor–Espuña): reflections of West Mediterranean plate-tectonic reorganizations. *Basin Research* 10, 325–344.

Gerbault, M., Burov, E. B., Poliakov, A. N. B., & Daignières, M., 1999. Do faults trigger folding in the lithosphere? *Geophysical Research Letters*, *26*(2), 271–274. https://doi.org/10.1029/1998GL900293

Gerya, T. V., Fossati, D., Cantieni, C., & Seward, D., 2009. Dynamic effects of aseismic ridge subduction: numerical modelling. Eurasian Journal of Mineralogy, 21(3), 649–661. doi:10.1127/0935-1221/2009/0021-1931

Gerya, T. V., & Meilick, F. I., 2011. Geodynamic regimes of subduction under an active margin: Effects of rheological weakening by fluids and melts. *Journal of Metamorphic Geology*, *29*(1), 7–31. https://doi.org/10.1111/j.1525-1314.2010.00904.x

Glatzmaiers, G., Roberts, P., 1995. A three-dimensional self-consistent computer simulation of a geomagnetic field reversal. *Nature* 377, 203–20. https://doi.org/10.1038/377203a0

Gleason, G. C., and Tullis, J., 1995. A flow law for dislocation creep of quartz aggregates determined with the molten salt cell. *Tectonophysics*, 247, 1–23, doi:10.1016/0040-1951(95)00011-B.

Gómez, M., Vergés, J., Riaza, C., 2002. Inversion tectonics of the northern margin of the Basque Cantabrian Basin. *Bull. Soc. Geol. Fr.* 173 (5), 449–459.

Gómez-Ortiz, D., R. Tejero-López, R. Babín-Vich, and A. Rivas-Ponce, 2005. Crustal density structure in the Spanish Central System derived from gravity data analysis (Central Spain), *Tectonophysics*, 403, 131–149, doi:10.1016/j.tecto.2005.04.006.

Gong, Z., Langereis, C.G., and Mullender, T.A.T., 2008. The rotation of Iberia during the Aptian and the opening of the Bay of Biscay. *Earth and Planetary Science Letters*, 273, 80-93.

Gràcia, E., Grevemeyer, I., Bartolomé, R. et al., 2019. Earthquake crisis unveils the growth of an incipient continental fault system. *Nat Commun* 10**,** 3482. https://doi.org/10.1038/s41467-019-11064-5

Grool, A.R., Huismans, R.S., Ford, M., 2019. Salt décollement and rift inheritance controls on crustal deformation in orogens. *Terra Nova*; 31: 562–568. https://doi.org/10.1111/ter.12428

Harlow, F.H., 1955. A Machine Calculation Method for Hydrodynamic Problems. Los Alamos Scientific Laboratory. LAMS-1956, 94p, New Mexico.

Hess, H.H., 1959a. Nature of the great oceanic ridges [abstract], in Sears, M. [ed.], Preprints of the 1st International Oceanographic Congress [August 31-September 12, 1959, New York], American Association for the Advancement of Science, Washington, D.C., p. 33-34.

Hessami, K., Koyi, H.A., Talbot, J., Tabasi, H., & Shabanian, E., 2001. Progressive unconformities within an evolving foreland fold-thrust belt, Zagros Mountains. *Journal of the Geological Society, 158*, 969-981.

Heuret, A., C. P. Conrad, F. Funiciello, S. Lallemand, and L. Sandri (2012), Relation between subduction megathrust earthquakes, trench sediment thickness and upper plate strain, *Geophys. Res. Lett.*, 39, L05304, doi:10.1029/2011GL050712.

Hirth, G., & Kohlstedf, D., 2003. Rheology of the upper mantle and the mantle wedge: A view from the experimentalists. *Geophysical Monograph-American Geophysical Union*, *138*, 83-106.

Hunt, G., H. Muhlhaus, B. Hobbs, and A. Ord, 1996. Localized folding of viscoelastic layers. *Geol. Rundsch, 85*, 58-64, 1996.

Jamieson, R. A., & Beaumont, C., 2013. On the origin of orogens. *Bulletin of the Geological Society of America*, *125*(11–12), 1671–1702. https://doi.org/10.1130/B30855.1

Jammes, S., Manatschal, G., Lavier, L., & Masini, E., 2009. Tectono sedimentary evolution related to extreme crustal thinning ahead of a propagating ocean: Example of the western Pyrenees. *Tectonics,* 28, TC4012. https://doi.org/10.1029/2008TC002406

Jammes, S. and Huismans, R. S., 2012. Structural styles of mountain building: Controls of lithospheric rheologic stratification and extensional inheritance. *Journal of Geophysical research,* vol. 117, B10403, doi:10.1029/2012JB009376

Jammes, S., Huismans, R. S., & Muñoz, J. A., 2013. Lateral variation in structural style of mountain building: controls of rheological and rift inheritance. *Terra Nova*, *26*(3), 201–207. https://doi.org/10.1111/ter.12087

Jolivet, L., Faccenna, C., Goffé, B., Burov, E., Agard, P., 2003. Subduction tectonics and exhumation of high-pressure metamorphic rocks in the Mediterranean orogens. *American Journal of Science* 303, 353–409.

Karato, S., & P. Wu. 1993. Rheology of the upper mantle: A synthesis. *Science*, 260(5109), 771–778, doi:10.1126/science.260.5109.771.

Kenter, J.A.M., Reijmer, J.J.G., Van der Straaten, H.C., and Peper, T., 1990. Facies patterns and subsidence history of the Jumilla-Cieza region (southeast Spain). *Sedimentary Geology, 67*, 263-280.

King S. D., 2001. Subduction zones: observations and geodynamic models. *Physics of the Earth and Planetary Interiors,* 127, 9–24. https://doi.org/10.1016/S0031-9201(01)00218-7

Kumar, A., Fernàndez, M., Jiménez‐Munt, I., Torne, M., Vergés, J., & Afonso, J. C., 2020. LitMod2D_2.0: An improved integrated geophysical‐petrological modeling tool for the physical interpretation of upper mantle anomalies. *Geochemistry, Geophysics, Geosystems,* 21, e2019GC008777. https://doi.org/10.1029/2019GC008777

Lallemand, S., Heuret, A., and Boutelier, D., 2005. On the relationship between slab dip, back-arc stress, upper plate absolute motion, and crustal nature in subduction zones. *Geochemistry, Geophysics, Geosystems,* v. 6, Q09006, https://doi:10.1029/2005GC000917

Le Pichon, X., and F. Barbier, 1987. Passive margin formation by low angle faulting within the upper crust, the northern Bay of Biscay margin, Tectonics 6, 133-150.

Lewis, C.J., Vergés, J., Marzo, M., 2000. High mountains in a zone of extended crust: Insights into the Neogene-Quaternary topographic development of northeastern Iberia. Tectonics 19, 86–102.

Liao, J., and T. Gerya, 2017. Partitioning of crustal shortening during continental collision: 2-D thermomechanical modeling, *J. Geophys. Res. Solid Earth*, *122*, 592–606, https://doi.org/10.1002/2016JB013398

Lonergan, L., White, N., 1997. Origin of the Betic–Rif mountain belt. *Tectonics* 16, 504–522.

Luth, S., Willingshofer, E., Sokoutis, D., & Cloetingh, S., 2010. Analogue modelling of continental collision: Influence of plate coupling on mantle lithosphere

subduction, crustal deformation and surface topography. *Tectonophysics*, *484*(1–4), 87–102. https://doi.org/10.1016/j.tecto.2009.08.043

Macchiavelli, C., Vergés, J., Schettino, A., Fernàndez, M., Turco, E., Casciello, & E., Tunini, L., 2017. A new southern North Atlantic isochron map: Insights into the drift of the Iberian plate since the Late Cretaceous. *Journal of Geophysical Research: Solid Earth*, *122*. https://doi.org/10.1002/2017JB014769

Mancilla, F.L., Díaz, J., 2015. High resolution Moho topography map beneath Iberia and Northern Morocco from receiver function analysis. *Tectonophysics* 663, 203–211. https://doi.org/10.1016/j.tecto.2015.06.017

Marín-Lechado, C., A. Pedrera, J. A. Peláez, A. Ruiz-Constán, A. González-Ramón, and J. Henares, 2017. Deformation style and controlling geodynamic processes at the eastern Guadalquivir foreland basin (Southern Spain), *Tectonics*, 36, 1072–1089, https://doi.org/10.1002/2017TC004556

Martín-Chivelet, J., Chacón, B., 2007. Event stratigraphy of the upper Cretaceous to lower Eocene hemipelagic sequences of the Prebetic Zone (SE Spain): record of the onset of tectonic convergence in a passive continental margin. *Sedimentary Geology* 197, 141–163.

Martín-Velázquez, S., and de Vicente, G., 2012. The role of lithospheric heterogeneities in the location of the Cenozoic intraplate deformation of Iberia from finite element modeling. *Tectonics*, 31, TC1009, doi:10.1029/2011TC002954

Martinod, J., Davy, P., 1994. Periodic instabilities during compression or extension of the lithosphere: 2. Analogue experiments*. Journal of Geophysical Research* 99 (B2), 12057–12069.

Mauffret, A., Ammar, A., Gorini, C., Jabour, H., 2007. The Alboran sea (western Mediterranean) revisited with a view from the Moroccan margin. – *Terra Nova*, 19, 195-203.

Michard, A., Chalouan, A., Feinberg, H., Goffé, B., Montingny, R., 2002. How does the Alpine belt end between Spain and Morocco. *Bulletin de la Société Géologique de France* 173, 3–15.

Minear, J. W., Toksöz, M. N.,1970. Thermal regime of a downgoing slab and new global tectonics. *Journal of Geophysical Research*, 75, 1397–419.

Moresi, L., Muhlhaus, H.-B., Dufour, F., 2001. Viscoelastic formulation for modelling of plate tectonics. In: Muhlhaus, H.-B., Dyskin, A., Pasternak, E. (Eds.), *Bifurcation and Localization in Soils and Rocks*. Balkema, Rotterdam, pp. 337–344.

Moresi, L., Dufour, F., & Mühlhaus, H. B., 2003. A Lagrangian integration point finite element method for large deformation modeling of viscoelastic geomaterials. *Journal of Computational Physics*, *184*(2), 476–497. https://doi.org/10.1016/S0021-9991(02)00031-1

Moresi, L., Quenette, S., Lemiale, V., Mériaux, C., Appelbe, B., & Mühlhaus, H. B., 2007. Computational approaches to studying non-linear dynamics of the crust and mantle. *Physics of the Earth and Planetary Interiors*, *163*(1–4), 69–82. https://doi.org/10.1016/j.pepi.2007.06.009

Mouthereau, F., Lacombre, O., & Meyer, B., 2006. The Zagros folded belt (Fars, Iran): Constraints from topography and critical wedge modelling. *Geophysical Journal International, 165*(1), 336-356

Mouthereau, F., Tensi, J., Bellahsen, N., Lacombe, O., De Boisgrollier, T., & Kargar, S., 2007. Tertiary sequence of deformation in a thinskinned/thick-skinned collision belt: The Zagros folded belt (Fars, Iran), *Tectonics, 26*, TC5006, doi:10.1029/2007TC002098.

Müller, R. D., J.-Y. Royer, S. C. Cande, W. R. Roest, and S. Maschenkov, 1999. New constraints on the Late Cretaceous-Tertiary plate tectonic evolution of the Caribbean, in Caribbean Basins, edited by P. Mann, pp. 33–57, *Elsevier*, Amsterdam.

Muñoz, J. A., 1992. Evolution of a continental collision belt: ECORS-Pyrenees crustal balanced cross-section. In *Thrust Tectonics* (pp. 235–246). https://doi.org/10.1007/978-94-011-3066-0_21

Muñoz, J.A., 2002. Alpine tectonics I: the Alpine system north of the Beltic Cordillera: The Pyrenees. *En: The Geology of Spain* (W. Gibbons y T. Moreno, Eds.) Geological Society, London: 370-385.

Olivet, J-L., 1996. La cinèmatique de la plaque Ibèrique, *Bull. Cent. Rech.Explor. Prod. Elf Aquitaine*, 20, 131-195

Parsons, B. and Sclater, J.G., 1977. An Analysis of the Variation of Ocean Floor Bathymetry and Heat Flow with Age. *Journal of Geophysical Research*, 82, 803-827. https://doi.org/10.1029/JB082i005p00803

Pedreira, D., Ph.D. Thesis, 2004. Estructura cortical de la zona de transición entre los Pirineos y la Cordillera Cantábrica. Universidad de Oviedo.

Pedreira, D., Afonso, J. C., Pulgar, J. A., Gallastegui, J., Carballo, A., Fernàndez, M., et al., 2015. Geophysical-petrological modeling of the lithosphere beneath the Cantabrian Mountains and the North-Iberian margin: Geodynamic implications. *Lithos*, *230*, 46–68. https://doi.org/10.1016/j.lithos.2015.04.018

Pedrera, A., García-Senz, J., Ayala, C., Ruiz-Constán, A., Rodríguez-Fernández, L. R., Robador, A., & González Menéndez, L., 2017. Reconstruction of the Exhumed Mantle Across the North Iberian Margin by Crustal-Scale 3-D Gravity Inversion and Geological Cross Section. *Tectonics*, *36*(12), 3155–3177. https://doi.org/10.1002/2017TC004716

Peral Millán, M. Ph.D. Thesis 2020, Dynamics of subduction systems with opposite polarity in adjacent segments: application to the Westernmost Mediterranean. Universidad de Barcelona, (ICTJA-CSIC).

Pfiffner O.A., 1993. The Structure of the Alps: An Introduction. In: *von Raumer J.F., Neubauer F. (eds) Pre-Mesozoic Geology in the Alps. Springer,* Berlin, Heidelberg. https://doi.org/10.1007/978-3-642-84640-3_1

Pfiffner O., A., and Ellis, S., 2000. Collision tectonics in the Swiss Alps: Insigth from geodynamic modelling . *Tectonics, vol. 19-6, 1065-1094.*

Pfiffner, O., 2016. Basement-involved thin-skinned and thick-skinned tectonics in the *Alps. Geol. Mag.* 153 (5–6), 1085–1109.

Platt, J.P., Anczkiewicz, R., Soto, J.-I., Kelley, S.P., Thirlwall, M., 2006. Early Miocene continental subduction and rapid exhumation in the western Mediterranean. *Geology* 34, 981–984.

Platt, J. P., Allerton, S., Kirker, A., Mandeville, C., Mayfield, A., Platzman, E. S. & Rimi, A. 2003. The ultimate arc: differential displacement, oroclinal bending, and vertical axis rotation in the External Betic-Rif arc. *Tectonics*, 22(3), 1017, doi: 10.1029/ 2001TC001321.

Platt, J., Vissers, R., 1989. Extensional collapse of thickened continental lithosphere: a working hypothesis for the Alboran Sea and Gibraltar arc. *Geology* 17, 540–543.

Platt, J. P., W. M. Behr, K. Johanesen, and J. R. Williams, 2013, The Betic-Rif arc and its orogenic hinterland: *A review, in Annual Review of Earth and Planetary Sciences,* edited, pp. 313-357.

Puigdefàbregas, C., Muñoz, J.A., Vergés, J., 1992. Thrusting and foreland basin evolution in the southern Pyrenees. In: McClay, K. (Ed.), *Thrust Tectonics*. Chapman & Hall, London, pp. 247–254.

Puga, E., Nieto, J.M., Díaz de Federico, A.,Bodinier, J.L. and Morten L., 1999. Petrology and metamorphic evolution of ultramaphic rocks and dolerite dykes of the Betic Ophiolitric Association (Mulhacén complex, SE Spain): evidence of Neo-Alpine subduction following an ocean floor metasomatic process. *Lithos*, 49, 23-56.

Pulgar, J.A., Alonso, J.L., Espina, R.G., Marín, J.A., 1999. La deformación alpina en el basamento varisco de la Zona Cantábrica. *Trab. Geol.* 21, 283–294.

Quintana, L., 2012. Extensión e Inversión Tectónica en el sector central de la Región Vasco-Cantábrica (Cantabria-Vizcaya, norte de España) (Tesis Doctoral), vol. I. Universidad de Oviedo (560 pp.).

Quintana, L., Pulgar, J. A., & Alonso, J. L., 2015. Displacement transfer from borders to interior of a plate: A crustal transect of Iberia. *Tectonophysics*, *663*, 378–398. https://doi.org/10.1016/j.tecto.2015.08.046

Ranalli, G., 1995. Rheology of the Earth. *Chapman and Hall*, London.

Ranalli, G., 2000. Rheology of the crust and its role in tectonic reactivation. *Journal of Geodynamics, 30*,3-15.

Ranalli, G., & Murphy, D. C., 1987. Rheological stratification of the lithosphere. *Tectonophysics, 132(4), 281–295.* doi:10.1016/0040-1951(87)90348-9

Rodríguez-Rodríguez, L., L. Antón, Á. Rodes, R. Pallàs, D. García-Castellanos, I. Jiménez-Munt, L. Struth, L. Leanni, ASTER Team, 2020. Dates and rates of endo-exorheic drainage development: Insights from fluvial terraces (Duero River, Iberian Peninsula). *GloPlaCha*, 193. doi.org/10.1016/j.gloplacha.2020.103271.

Roest, W. R., & Srivastava, S. P., 1991. Kinematics of the plate boundaries between Eurasia, Iberia, and Africa in the North Atlantic from the Late Cretaceous to the present. *Geology*, 19(6), 613–616. https://doi.org/10.1130/0091-7613(1991)019<0613:KOTPBB>2.3.CO;2

Rosenbaum, G. & Lister, G.S. 2004. Formation of arcuate orogenic belts in the western Mediterranean region. – *Geol. Soc. Amer. Sp. Paper*, 383, 41-56.

Rosenbaum, G., Lister, G.S., Duboz, C., 2002a. Reconstruction of the tectonic evolution of the western Mediterranean since the Oligocene. *Journal of the Virtual* Explorer 8, 107-130.

Rosenbaum, G., Lister, G. S., & Duboz, C., 2002b. Relative motions of Africa, Iberia and Europe during Alpine orogeny. *Tectonophysics*, *359*(1-2), 117–129. https://doi.org/10.1016/S0040-1951(02)00442-0

Rosenberg, C. L., and E. Kissling, 2013. Three-dimensional insight into Central-Alpine collision: Lower-plate or upper-plate indentation? *Geology*, *41*(12), 1219–1222, doi:10.1130/G34584.1

Rossetti, F., Faccenna, C., Crespo-Blanc, A., 2005. Structural and kinematic constraints to the exhumation of the Alpujarride Complex (Central Betic Cordillera, Spain). *Journal of Structural Geology* 27, 199–216.

Roure, F., Choukroune, P., Beràstegui, X., Muñoz, J. A., Villien, A., Matheron, P., Déramond, J., 1989. ECORS deep seismic data and balanced cross sections: Geometric constraints on the evolution of the Pyrenees. *Tectonics*, 8(1), 41–50. https://doi.org/10.1029/TC008i001p00041

Royden, L.H., 1993. The tectonic expression slab pull at continental convergent boundaries. *Tectonics* 12, 303–325.

Ruh, J.B., Kaus, B. J. P., Burg, J-P., 2012. Numerical investigation of deformation mechanics in fold-and-thrust belts : Influence of rheology of single and multiple décollements. *Tectonics*, vol. 31, TC3005, doi :10.1029/2011TC003047

Ruh, J. B., T. Gerya, and J.-P. Burg, 2013. High-resolution 3D numerical modeling of thrust wedges: Influence of décollement strength on transfer zones. *Geochem. Geophys. Geosyst.*,14, 1131–1155, doi:10.1002/ggge.20085.

Ruh, J. B., L. Le Pourhiet, P. Agard,E. Burov, and T. Gerya, 2015. Tectonics licing of subducting oceanic crust along plate interfaces: Numerical modeling, *Geochem. Geophys. Geosyst.,*16, 3505–3531, doi:10.1002/2015GC005998.

Savostin, L A., Sibuet, Jean-Claude, Zonenshain, Lev P , Le Pichon, Xavier; Roulet, Marie-Jose, 1986. Kinematic evolution of the Tethys belt from the Atlantic Ocean to the Pamirs since the Triassic. *Tectonophysics*, 123, no.1-4, pp.1-35.

Schellart, W.P., 2002. Analogue modelling of large-scale tectonic processes: an introduction. *Journal of the Virtual Explorer*, 7, 1 - 6

Schellart, W.P., 2008. Overriding plate shortening and extension above subduction zones: A parametric study to explain formation of the Andes Mountains. *GSA Bulletin*, v. 120; no. 11/12; p. 1441-1454; doi:10.1130/B26360.1

Schellart, W. P., & Moresi, L., 2013. A new driving mechanism for backarc extension and backarc shortening through slab sinking induced toroidal and poloidal mantle flow: Results from dynamic subduction models with an overriding plate. *Journal of Geophysical Research: Solid Earth*, 118(6), 3221–3248. doi:10.1002/jgrb.50173

Schettino, A. and Turco, E., 2011, Tectonic history of the western Tethys since Late Triassic. *GSA Bulletin*, 123, no. ½, 89-105, doi:10.1130/B30064.17

Schmalholz , S. M. , Boris J.P. Kaus, Jean-Pierre Burg, 2009. Stress-strength relationship in the lithosphere during continental collision. *Geology*; 37 (9): 775–778. doi: https://doi.org/10.1130/G25678A.1

Schmid, Stefan M.; Fügenschuh, Bernhard; Kissling, Eduard; Schuster, Ralf, 2004. "Tectonic map and overall architecture of the Alpine orogen". *Eclogae Geologicae Helvetiae*. 97 (1): 93–117. doi:10.1007/s00015-004-1113-x

Schmid, Stefan M., Kissling, E., Diehl, T., van Hinsbergerm, J. J., Molli, G., 2017. Ivrea mantle wedge, arc of the Western alps, and kinematic evolution of the Alps.-Apenines orogenic system. *Swiss Geologica Society,* 110:581–612 DOI 10.1007/s00015-016-0237-0

Sibuet, J. C., Srivastava, S. P., & Spakman, W., 2004. Pyrenean orogeny and plate kinematics. *Journal of Geophysical Research*, 109, B08104. https://doi.org/10.1029/2003JB002514

Simpson, G. D. H., 2006. Modelling interactions between fold-thrust in fold belts. *Basin Research*, *18*,125-143.

Simpson, G. D. H., 2009. Mechanical modelling of folding versus faulting in brittle-ductile wedges. *Journal of Structural Geology*, *31*(4), 369–381. https://doi.org/10.1016/j.jsg.2009.01.011

Smith, R.B., 1975. Unified theory of the onset of folding, boundinage and mullion structure, *Geological Society of America Bulletin, 88*. 1601-1609.

Sobolev, S.V., Brown, M, 2019. Surface erosion events controlled the evolution of plate tectonics on Earth. *Nature* 570**,** 52–57. https://doi.org/10.1038/s41586-019-1258-4

Sokoutis, D., & Willingshofer, E., 2011. Decoupling during continental collision and intra-plate deformation. *Earth and Planetary Science Letters*, 435-444. [305]. https://doi.org/10.1016/j.epsl.2011.03.028

Solé Sabarís, L., 1983. Morfología general de la Península Ibérica. In: *Comba, J.A. (Ed.), Geología de España. Libro Jubilar J.M. Ríos*, 2. IGME, Madrid, pp. 589–605.

Solomatov, V.S. & Moresi, L.N., 1997. Three regimes of mantle convection with non-Newtonian viscosity and stagnant lid convection on the terrestrial planets, *Geophys Res Lett*, 24, 1907–1910.

Song, T. R. A., and M. Simons, 2003. Large trench-parallel gravity variations predict seismogenic behavior in subduction zones, *Science*, 301, 630 – 633, doi:10.1126/science.1085557.

Spakman, W., Chertova, M. V., van den Berg, A., & van Hinsbergen, D. J. J., 2018. Puzzling features of Western Mediterranean tectonics explained by slab dragging. *Nature Geoscience*, *11*, 211–216. https:// doi.org/10.1038/s41561-018-0066-z

Spakman, W. & Wortel, R., 2004. A tomographic view on western Mediterranean geodynamics. *In*: W. Cavazza, F. Roure, W. Spakman, G.M.Stampfli & P. Ziegler, Eds., The TRANSMED Atlas. The Mediterranean region from crust to mantle. – *Springer*, Berlin Heidelberg, 31-52.

Srivastava, S. P., Schouten, H., Roest, W. R., Klitgord, K. D., & Kovacs, L. C., 1990. Iberian plate kinematics: A jumping plate boundary between Eurasia and Africa. *Nature*, 344(6268), 756–759. https://doi.org/10.1038/344756a0

Suriñach, E., Vegas, R., 1988. Lateral inhomogeneities of the Hercynian crust in central Spain. *Phys. Earth Planet. Inter.* 51 (1–3), 226–234. https://doi.org/10.1016/0031-9201(88)90049-0

Stampfli, G., Hochard, C., Plate tectonics of the Alpine realm. 2009. Geological Society, London, Special Publications, 327, pp. 89-111

Stampfli, G., Borel, G., Marchant, R., & Mosar, J., 2002. Western Alps geological constraints on western Tethyan reconstructions. *Journal of the Virtual Explorer*, 8, 77–106.

Stapel, G., 1999. The nature of isostasy in West Iberia. And its bearing on mesozoic and cenozoic regional tectonics. PhD Thesis. VU Amsterdam. 148pp.

Tan, E., Lavier, L. L., Van Avendonk, H. J. A., & Heuret, A., 2012. The role of frictional strength on plate coupling at the subduction interface. *Geochemistry, Geophysics, Geosystems*, *13*(10). https://doi.org/10.1029/2012GC004214

Teixell, A., 1998. Crustal structure and orogenic material budget in the west central Pyrenees. *Tectonics,* 17(3), 395-406.

Tejero, R., and J. Ruiz, 2002. Thermal and mechanical structure of the central Iberian Peninsula lithosphere, *Tectonophysics*, 350, 49–62, doi:10.1016/S0040-1951(02)00082-3.

Torné, M., Banda, E., Fernàndez, M., 1996. The Valencia Trough: geological and geophysical constraints on basin formation models. In: Ziegler, P.A., Horvàth, F. (Eds.), *Peri-Tethys Memoir 2: Structure and Prospects of Alpine Basins and Forelands. Mémoires Muséum National d'Histore Naturelle*, 170, pp. 103–128.

Torne M., M. Fernàndez, J. Vergés, C. Ayala, M.C. Salas, I. Jiménez-Munt, G.G. Buffet, J. Díaz, 2015. Crust and mantle lithospheric structure of the Iberian Peninsula deduced from potential field modeling and thermal analysis, *Tectonophysics*, 663, 419-433, http://dx.doi.org/10.1016/j.tecto.2015.06.003

Tugend, J., Manatschal, G., Kusznir, N. J., Masini, E., Mohn, G., & Thinon, I., 2014. Formation and deformation of hyperextended rift systems: Insights from rift domain mapping in the Bay of Biscay-Pyrenees. *Tectonics*, 33, 1239–1276. https://doi.org/10.1002/2014TC003529

Turcotte, D. L. and Schubert, G. 2002. Geodynamics, 2nd ed. xv + 456 pp. Cambridge, New York, Melbourne: Cambridge University Press. Price £75.00, US $110.00 (hard covers); £29.95, US $45.00 (paperback). ISBN 0 521 66186 2; 0 521 66624 4 (pb). https://doi.org/10.1017/S0016756802217239

van Hinsbergen, D. J. J., R. L. M. Vissers, and W. Spakman, 2014. Origin and consequences of western Mediterranean subduction, rollback, and slab segmentation, *Tectonics*, 33, 393-419, doi:10.1002/tect.20125.

van Hinsbergen, D.J.J., Torsvik,T.H., Schmid,S.M., et al., 2019. Orogenic architecture of the Mediterranean region and kinematic reconstruction of its tectonic evolution since the Triassic. *Gondwana Research*, https://doi.org/10.1016/j.gr.2019.07.009

Vanderhaeghe, O., Medvedev, S., Fullsack, P., Beaumont, C., and Jamieson, R. A.,(2003). Evolution of orogenic wedges and continental plateaux: insightsfrom crustal thermal–mechanical models overlying subducting mantle lithosphere. *Geophys. J. Int.* 153, 27–51. https://doi.org/10.1046/j.1365-246X.2003.01861.x

Vázquez Hoehne, A., 1992. Superficies aplanadas en la paramera de Sigüenza. *Anales de Geografía de la Universidad Complutense* 11, 207–214.

Vegas, R., Vázquez, J.T., Suriñach, E., Marcos, A., 1990. Model of distributed deformation, block rotations and crustal thickening for the formation of the Spanish Central System. *Tectonophysics,* 184, 367-378. doi:10.1016/0040-1951(90)90449-I.

Vergés, J., Millan, H., Roca, E., Muñioz, J. A., & Marzo, M., 1995. Eastern Pyrenees and related foreland basins: Pre-, syn-and post-collisional crustal-scale cross-

sections. *Marine and Petroleum Geology*, 12(8), 903–915. https://doi.org/10.1016/0264-8172(95)98854-X

Vergés, J., and Fernàndez, M., 2006. Ranges and basins in the Iberian Peninsula: their contribution to the present topography. *Eurasian Lithosphere Dynamics.* Geological Society, London, Memoirs, 32, 223-234.

Vergés, J., Goodarzi, M. G. H., Ernani, H., Karpuz, R.,, Efsathiou, J., & Gillespie, P., 2011. Multiple detachment folding in Pusht-e Kuh arc, Zagros: Role of mechanical stratigraphy, in K. McClay, J.H. Shaw, and J. Suppe, eds, Thrust fault-related folding: *American Association of Petroleum Geologist Memoir 94*, 69-94, https://doi.org/10.1306/1325133M942899

Vergés, J., & Fernàndez, M., 2012. Tethys–Atlantic interaction along the Iberia–Africa plate boundary: The Betic–Rif orogenic system. *Tectonophysics,* 579, 144–172. https://doi.org/10.1016/j.tecto.2012.08.032

Vissers, R.L.M., and Meijer, P. Th., 2012a. Mesozoic rotation of Iberia: Subduction in the Pyrenees? *Earth-Science Reviews*, 110, 93-110.

Vissers, R. L. M., & Meijer, P. T., 2012b. Iberian plate kinematics and Alpine collision in the Pyrenees. *Earth-Science Reviews*, *114*(1-2), 61–83. https://doi.org/10.1016/j.earscirev.2012.05.001

Vogt, K., Matenco, L., & Cloetingh, S., 2017. Crustal mechanics control the geometry of mountain belts. Insights from numerical modelling. *Earth and Planetary Science Letters*, *460*, 12–21. https://doi.org/10.1016/j.epsl.2016.11.016

Vogt, K., Gerya, T.V., 2014. From oceanic plateaus to allochthonous terranes: numerical modelling. *Gondwana Res*.25 (2), 494–508.

Vogt, K., Willingshofer, E., Matenco, L., Sokoutis, D., Gerya, T., & Cloetingh, S., 2018. The role of lateral strength contrasts in orogenesis: A 2D numerical study. *Tectonophysics*, *746*, 549-561. https://doi.org/10.1016/j.tecto.2017.08.010

Wegener, A. (1924). The origin of continents and oceans, trans. *JGA Skerl. Dutton and Co., New York*.

Willet, S.D., Beaumont, C., & Fullsack, P., 1993. Mechanical model for the tectonics of double-vergent compressional orogens. *Geology, 21*,371-374.

Willett SD. 1999. Orogeny and orography: The effects of erosion on the structure of mountain belts. Journal of Geophysical Research: Solid Earth 104(B12): 28957–28981.

Willingshofer, E., & Sokoutis, D., 2009. Decoupling along plate boundaries: Key variable controlling the mode of deformation and the geometry of collisional mountain belts. *Geology*, *37*(1), 39–42. https://doi.org/10.1130/G25321A.1

Willingshofer, E., Sokoutis, D., Luth, S. W., Beekman, F., & Cloetingh, S., 2013. Subduction and deformation of the continental lithosphere in response to plate

and crust-mantle coupling. *Geology*, *41*(12), 1239–1242. https://doi.org/10.1130/G34815.1

Yamato, P., Kaus, B. J. P., Mouthereau, F., & Castelltort, S., 2011. Dynamic constraints on the crustal-scale rheology of the Zagros fold belt, Iran. *Geology*, *39*(9), 815–818. https://doi.org/10.1130/G32136.1

Zeck, H., 1996. Betic–Rif orogeny: subduction of Mesozoic Tethys lithosphere under eastward drifting Iberia, slab detachment shortly before 22 Ma, and subsequent uplift and extensional tectonics. *Tectonophysics* 254, 1–16.

Ziegler, P.A., 1988. Evolution of the Arctic–North Atlantic and Western Tethys. *Am. Assoc. Pet. Geol., Mem*. 43, 198 pp.

Ziegler, P. A., Cloetingh, S, & Van Wees, J. D., 1995. Dynamics of intra-plate compressional deformation: The Alpine foreland and other examples. *Tectonophysics*, 252,7–59.

Ziegler, P. A., Van Wees, J. D., & Cloetingh, S., 1998. Mechanical controls on collision-related compressional intraplate deformation. *Tectonophysics*, 300(1–4), 103–129. https://doi.org/10.1016/S0040-1951(98)00236-4

Zlotnik, S., Jiménez-Munt, I., Fernàndez, M., 2014. Coupled mantle dripping and lateral dragging controlling the lithosphere structure of the NW-Moroccan margin and the Atlas Mountains: A numerical experiment, *Lithos*,1 89, 16-27,https://doi.org/10.1016/j.lithos.2013.10.016.

CSIC
Consejo Superior de Investigaciones Científicas

GEO3BCN
Geosciences Barcelona - CSIC

Universitat de Barcelona